THE INFLUENCE OF BLOCKAGE AND CAVITATION ON THE HYDRODYNAMIC PERFORMANCE OF ICE CLASS PROPELLERS IN BLOCKED FLOW

By

Daniel Lloyd Norris Walker, B. Eng., P. Eng.

A thesis submitted to the School of Graduate Studies

In partial fulfilment of the requirements for the degree of

Doctor of Philosophy

Faculty of Engineering and Applied Science

Memorial University of Newfoundland

August, 1996

St. John's, Newfoundland, Canada

ABSTRACT

Ships operating in ice in Canadian waters normally use open or ducted marine screw propellers for propulsion. The operation of the vessel in an ice cover, especially during icebreaking operations, often results in the submergence of broken ice pieces at the bow, and along the length, of the vessel. As the vessel moves through the ice field, the propeller approaches the submerged piece or pieces of ice and contact or non-contact interference between the ice and the propeller occurs.

This work examines the effects of blockage and cavitation on the hydrodynamic loads associated with non-contact propeller ice interaction. A series of experiments were done in medium sized cavitation tunnels with two 200 mm open propeller models and two 200 mm ducted propeller models. Tests were also conducted in a towing tank with one of the open propellers. The tests were conducted in uniform flow and in blocked flow using simulated ice blockages installed upstream of the propeller. Measurements were made of mean and instantaneous propeller thrust and torque, duct thrust in uniform flow, block drag load and blade pass pressure on the face of the block adjacent to the propeller. Effects of blockage, cavitation and proximity of the ice piece were examined.

Blockage of a propeller resulted in increased mean levels of thrust and torque over uniform flow values. Furthermore the blockage increased the oscillation of the loads about their mean. Cavitation reduced the mean loads associated with blockage but further increased oscillation about the mean. The development of severe sheet and cloud cavitation posed the risk of both fatigue and erosion to the propeller.

DEDICATION

This work is dedicated to my parents, Lloyd and Ena Walker. Without their love, support, and encouragement, I would have had neither the opportunity nor the perseverance to receive an education. My work, life and love are for Sharon, Jane and Ian, who have inspired and motivated me. It was their sacrifice that made this possible.

ACKNOWLEDGMENTS

Sincere appreciation is extended to: Dr. Neil Bose, a great supervisor and friend; Dr. Stephen Jones and Professor Hajime Yamaguchi, whose assistance and guidance over the past five years were invaluable; Dr Mahmoud Haddara and Dr. Don Bass and; the technical personnel of the Memorial University of Newfoundland, the Institute for Marine Dynamics and the University of Tokyo.

Funding for the research was provided by the Natural Sciences and Engineering Research Council, the National Research Council of Canada, the Canada-Newfoundland Offshore Development Fund, the Memorial University of Newfoundland, the Canadian Council of Professional Engineers and the Maritime Awards Society of Canada.

CONTENTS

LIST OF FIGURES

LIST OF TABLES

LIST OF SYMBOLS, ABBREVIATIONS AND ACRONYMS

A_D	Developed blade area
A_O	Propeller disk area
c	Blade chord length
$c_{0.7}$	Chord length At 0.7D
D	Propeller diameter
F	Block force
Fn	Froude number $V_S/(gD)^{0.5}$
G	Gap between propeller and adjacent ice block surface
G/D	Gap diameter ratio
g	Acceleration due to gravity, 9.81 m/s^2
H	Maximum spanwise penetration of propeller into ice piece (Cut Depth)
H/D	Cut depth propeller diameter ratio
J	Propeller advance coefficient V_A/nD
J_S	Ship advance coefficient V_S/nD
K_B	Coefficient of block load $F/\rho n^2D^4$
K_Q	Coefficient of torque $Q/\rho n^2D^5$
K_{TD}	Coefficient of duct thrust $T_D/\rho n^2D^4$
K_T	Coefficient of open propeller thrust $T/\rho n^2D^4$
N	Propeller rotational speed (rpm)
n	Propeller rotational speed (rps)
P	Propeller pitch

P/D	Pitch diameter ratio
P_A	Ambient pressure
P_{ATM}	Atmospheric pressure
P_c	Pressure at which cavitation occurs
P_V	Vapour pressure of water at ambient temperature
Q	Propeller torque
Rn	Reynolds number $c_{0.7}U/\upsilon$
s.d.	Standard deviation
T	Propeller thrust
T_D	Duct thrust
U	Blade section velocity
V_S	Ship speed
V_A	Propeller advance speed
w_T	Taylor thrust wake fraction
w_Q	Taylor torque wake fraction
α_S	Saturated gas content at atmospheric pressure
α	Gas content at atmospheric pressure
ϕ	Angular position of key blade
η_o	Propeller efficiency $(JK_T/2\pi K_Q)$
$\underline{\sigma}$	Standard deviation
σ_{nD}	Cavitation number $(P_A - P_V)/0.5\rho(nD)^2$

σ_V	Cavitation number $(P_A - P_V)/0.5\rho V_A^2$
ρ	Density of water
υ	Kinematic viscosity of water
ω	Blade pass frequency
ω_n	Natural frequency of system
CCG	Canadian Coast Guard
CPP	Controllable pitch propeller
EG/AD/S	Ethylene Glycol Ammonia Detergent Sugar
HDPE	High density polyethylene
IMD	Institute for Marine Dynamics
JRPA	Joint Research Project Arrangement
MUN	Memorial University of Newfoundland
NSERC	Natural Sciences and Engineering Research Council Canada
NRCC	National Research Council Canada

1. INTRODUCTION

1.1 Background

Ships operating in ice covered Canadian waters normally use marine screw propellers for propulsion. The propellers may be open, as with the R-Class Icebreakers used by the Canadian Coast Guard (CCG), or ducted, as is the case with the *M/V Robert Lemeur*, a vessel owned and operated by Canadian Marine Drilling Co. (Canmar) in the Beaufort Sea. The operation of a vessel in an ice cover, especially during breaking operations, often results in the submergence of broken ice pieces at the bow of the vessel. As the vessel moves through the ice field, the propeller approaches the submerged piece or pieces of ice and interference between the ice and the propeller occurs, resulting in the imposition of extreme loads on the propeller.

Such loads can be divided into three categories. Impacts result from initial contact of ice blocks with the propeller. Milling loads are developed when a propeller cuts its way through a block that is too large to pass through the propeller disk. Extreme hydrodynamic loads stem from the operation of a propeller in the wake of, and in close proximity to, nearby ice bodies. The relative magnitude of the three loading mechanisms is primarily governed by the configuration of the propeller. An open propeller is exposed to impact by larger ice pieces and more prolonged milling events than is a ducted propeller. On the other hand, a ducted propeller is more regularly exposed to higher levels of extreme hydrodynamic loadings associated with blockage caused by ice pieces lodged on the duct and very near to the operating propeller. Results from full scale trials with the *M/V Robert Lemeur* (Laskow et al., 1986) and tests in an ice tank, (Keinonen and

Browne, 1990) show that the magnitude of the non-contact hydrodynamic loads for a ducted propeller is similar to those that arise from milling and impacts. Additionally, the duration of the event for a ducted propeller is affected by the configuration of the propulsion system of the vessel: a vessel propelled by a single ducted propeller, such as the *M/V Arctic* would be likely to have a lower duration of blockage than that of the configuration of the *M/V Robert Lemeur*, a vessel with twin ducted propellers. During breaking operations of the former, blockage of the single propeller could result in a substantial loss of propeller thrust, forcing the vessel operators to take action to clear the blocked propeller. In the latter case, the blockage of one of the propellers could result in an insufficient level of propulsion loss to require remedial actions on the part of the crew.

In an attempt to establish the magnitude of the loading regime during propeller ice interaction, with a goal of updating the Canadian Arctic Shipping Pollution Prevention Regulations and the Swedish-Finnish Rules for Baltic Navigation, the governments of Canada and Finland entered into a Joint Research Project Arrangement (JRPA-6). The responsibility of estimating the magnitude of non-contact loadings was given to the Institute for Marine Dynamics (IMD) of the National Research Council of Canada (NRCC). IMD subsequently contracted the Faculty of Engineering and Applied Science of the Memorial University of Newfoundland (MUN) to measure the effects of cavitation on the hydrodynamic loads on a propeller operating in ice-blocked flows. The research carried out in fulfilment of that contract illustrated the complicated nature of the flow regime during propeller-ice interaction. Full investigation would require substantially more effort than was justified by the terms of the contract between MUN and IMD. The

range of the research was subsequently expanded when Dr. Neil Bose of MUN and Dr. Stephen Jones of IMD successfully applied for a Strategic Grant from the Natural Sciences and Engineering Research Council (NSERC) to investigate the operation of marine propellers in ice blocked flow. This thesis forms a part of that research.

1.2 Objectives

The work of this thesis aims to improve the understanding of the way in which cavitation affects the loads on an ice-class propeller operating in the immediate wake of an ice block and the effects on propeller blade performance of such a loading regime. Tests on model ice-class propellers were done at both atmospheric pressure in a towing tank and a cavitation tunnel and at reduced pressure in two cavitation tunnels. Measurements of mean and dynamic loads during simulated interactions were done. Dynamic measurements were corroborated with numerical work conducted by Neil Bose using a panel method (Bose, 1996) for similar conditions. The work that forms the basis of this thesis includes:

- cavitation tunnel tests of open and ducted propeller models over a range of propeller conditions and cavitation numbers;
- tests on an open propeller model in the MUN towing tank over a range of uniform flow and simulated ice-blocked conditions;
- comparison of experimental results from the cavitation tunnel and tank in blocked and unblocked flow over a range of cavitation numbers;
- comparisons between experimental and numerical results and;
- an assessment of the meaning and relevance of the results to the total propeller loading regime during propeller-ice interaction.

What follows is an assessment of the way in which cavitation affects the total loading regime on a propeller during propeller-ice interaction. Chapter Two outlines previous work done in the area of propeller-ice interaction, both in terms of hydrodynamic loads and loads resulting from contact between the propeller and an ice piece. Chapter Three gives details of the experimental program from which the results were developed; the experimental program was conducted both at the Institute for Marine Dynamics and the University of Tokyo. Chapter Four describes results of blockage and cavitation on open and ducted propellers, including: mean and dynamic loads; cavitation patterns; and numerical comparisons. Finally, Chapter Five provides a discussion of the results of the comprehensive test program and outlines the conclusions of the research.

The thesis presents the results of an experimental research program which focuses on one aspect of the loading regime: hydrodynamic loads including the effects of cavitation. The program was necessarily experimental for two reasons: numerically modeling a cavitating propeller operating in the shear flow behind a simulated ice blockage would represent new and substantial work in itself and; to date, there has been no experimental data against which to compare such numerical predictions and prior to undertaking numerical work it is necessary to have a fundamental understanding of the physics of the interaction. The program was restricted to non-contact loading for a practical reason: there was no cavitation tunnel available in which measurements of ice contact loads could be made at low ambient pressure. Any estimate of the total propeller-ice interaction loading regime based on experimental data incorporating the effects of

cavitation must be made by superposition of independently measured contact and non-contact loads.

The work was undertaken to examine whether cavitation of the flow around a propeller had any effect on the loading regime to which ice class propellers are exposed. The thesis shows that the magnitude of hydrodynamic loads associated with propeller ice interaction, which are a significant proportion of the propeller loading regime, are dramatically changed by cavitation and predictions of full-scale loads associated with propeller-ice interaction from model scale data should therefore take into account the effects of cavitation. Cavitation results in a reduction of mean forward directed hydrodynamic loads associated with propeller ice interaction and can increase the aftwards directed total load by as much as thirty percent. Furthermore, cavitation results in an increase in the oscillatory nature of the hydrodynamic loads, exposing the propulsion system to a risk of possible fatigue. Prior to this research, no other work has been done which quantitatively showed such effects of cavitation.

2. LITERATURE REVIEW

Research on the interaction of ice with propellers has historically concentrated on contact loads between propeller blades and ice. Prior to the mid 1980's there had been little published work on the hydrodynamic loads induced on the propeller as a result of an irregular blockage upstream of the propeller disc. Even less information is available on the effects of propeller cavitation on such loads. The following section presents an overview of work conducted in both the areas of contact and non-contact propeller-ice interaction, in order to provide a context in which propeller-ice interaction occurs.

2.1 Cavitation During Propeller Ice Interaction

Lindroos and Björkestam (1986) published one of the earliest works on modelling of hydrodynamic loads associated with the blockage of a propeller duct with ice in which the cavitation effects during blockage were addressed. The program was initiated by Valmet Shipyard in Helsinki to investigate any advantages of ducted propellers in ice conditions in order to develop a more efficient propulsion system for use in ice covered waters.

The tests were done in the 1200 mm cavitation tunnel at Marintek in Norway using a propeller in an NSMB type 19A duct. The four bladed 250 mm diameter propeller had an expanded area ratio (A_E/A_0) of 0.55, a pitch to diameter ratio (P/D) of 0.90 and a modified Kaplan type blade. The effects of ice blockage on the propeller were simulated using a flat plate mounted on a hinged bracket in front of the duct.

Tests were made at various advance coefficients, cavitation numbers, propeller speeds, blockage ratios and blockage geometries. For each test, measurements of several

parameters were taken: shaft torque, shaft thrust, shaft bending moment, blade root bending moment, blade spindle torque and perpendicular and lateral blade forces. Cavitation was not recorded in any rigorous manner but some qualitative discussions were presented.

The authors noted that considerable difficulties arose in measuring and analysing quickly changing dynamic forces and recommended caution in the interpretation of their results. Notwithstanding that recommendation, tests at maximum blockage factors exhibited increases in the mean values of most parameters of around 2.5 times open water values. The only exceptions were blade spindle torque, which exhibited an increase of eight times open water results, and chordwise, in plane, blade force, which dropped to near zero. Peak values displayed considerably larger variations than did mean values. In all cases, peak values were increased by the worst case blockage condition, but there was no consistent level of elevation. Peak values varied from twice open water values for thrust to as high as 35 times open water values for blade spindle torque.

The authors noted that blockage resulted in heavy pulsing cloud cavitation. The worst cavitation resulted in increased mean values of measured shaft loads to twice the values measured in tests at atmospheric conditions; this is opposite to the normal effect due to cavitation, which is to reduce mean values. No graphical or photographic record was made of the cavitation. Neither was there any discussion of likely scale effects from parameters such as dissolved gas content, or cavitation nuclei.

The least significant effects on the loading regime were from blockage geometry and speed of advance. It was suggested that blockage geometry had no effect on the

measured loads. While this may be true for a flat plate blockage, Keinonen and Browne (1990) have suggested that the flow around a flat plate is not representative of the flow around an ice block and the measurements taken during the course of the experiments may not be representative of full scale performance.

The above conclusions are of interest since the work appears to be the first experimental work dealing with the cavitation effects of a propeller in the wake of a simulated blockage. Unfortunately, the lack of authors' confidence in the data acquisition and the inadequacy of information about the form and effects of cavitation renders the paper useful only in a qualitative sense.

Sánchez-Caja et al. (1995) suggested the effects of cavitation during propeller-ice interaction could perhaps be used to explain high, forward directed blade bending loads seen in some full scale records. Using estimates of cavitation bubble collapse pressures and experimental results presented later in this thesis and previously published (Walker and Bose, 1994), the authors suggested that cloud cavitation shed from the back of one blade and collapsing on the face of the subsequent blade could result in a forward directed hydrodynamic load. While this thesis will present results to show that cavitation shed from a blade can indeed impinge on the pressure side of the subsequent blade, Sánchez-Caja's work provides no additional experimental results on which to base a load estimate.

Coincident with the work presented in this thesis on the effects of blockage and cavitation on the mean and instantaneous performance of ice class propellers, Mr. Michael Doucet investigated the risks of cavitation erosion during propeller-ice interaction. Mr.

Doucet's work forms another part of the research funded by the NSERC Strategic Grant (Doucet et al., 1995; Doucet et al., 1996).

Early performance tests of open propellers (Walker, Bose and Yamaguchi, 1994) and ducted propellers (Walker, Bose and Casey, 1995) within JRPA-6 research concluded that the extensive amounts of cloud cavitation present during propeller-ice interaction would likely pose a risk of cavitation erosion when propellers were blocked with ice. To further investigate that risk, Doucet et al. (1995) conducted a series of paint film tests with the R-Class open propeller over a range of cavitation numbers and advance coefficients. Subsequently, an analogous set of tests were conducted for ducted propellers (Doucet et al., 1996).

The authors concluded from the results of the erosion studies that full scale cavitation erosion was a possibility, but far more likely for ducted propellers than for open propellers. In each set of tests at model scale, both cavitation and erosion occurred even at atmospheric pressure. In all cases, extreme cavitation was coincident with high levels of vibration, further indicating a risk of fatigue on the propulsion system. In fact, recent examinations of full scale ducted propellers have shown similar locations of damage as was indicated in the experimental work.

In addition to the work outlined above, the work included in this thesis has been presented in a number of forums including: six refereed conference papers and four papers published or accepted for publication in three journals. The topic of those papers is the substance of this thesis. They are listed in the reference section at the back of this thesis.

2.2 Hydrodynamic Loads during Propeller Ice Interaction

While there have been few studies concentrating on the hydrodynamic effects of cavitation during propeller ice interaction, several studies have dealt with the hydrodynamic loads associated with propeller-ice interaction, either exclusively, or as part of a more general research project.

During the summers of 1983 and 1984, full scale measurements were recorded onboard the *M/V Robert LeMeur* by Laskow et al., (1986). Instrumentation was installed on the shaft line to record shaft torque, shaft thrust, blade bending moment and various other signals during open water, milling, single impact and blockage events. More than three hundred interaction events, each of seven seconds duration, were recorded. While there was no clear baseline by which to assess the interaction type, the authors defined a blockage event by an elevated level of shaft thrust for a period of more than three seconds.

The authors found blockage to cause high increases in mean values of shaft thrust and blade bending and lower increases in mean levels of shaft torque. The increased mean loads were of about the same levels as for milling and impact loads. However, the highest peak blade bending loads resulted from impacts whereas loads resulting from milling and blockage were lower in magnitude but of longer duration. The most characteristic feature of blockage was large and prolonged oscillation of the loads about the mean values. The prolonged nature of the blockage events resulted in high levels of vibration for the propeller, the shafting and the stern of the vessel, posing a risk of fatigue for the propulsion system.

The work offers estimates of the effects of blockage on a number of propulsion parameters. Most importantly, a comparison of blockage loads with contact loads was made. The lack of visual records during the full scale trials precludes any estimate of the occurrence, severity or effects of cavitation and somewhat restricts the reliability of the classification of impact, milling and blockage events based on the data record.

Further full scale work was carried out onboard the icebreaker *CCGS Sir John Franklin* during 1990 and 1991 by Williams et al. (1992). A series of tests were conducted in both open water and in ice. Bollard pull, ship speed, power and turning circle radii were measured in open water. Similar measurements were made in a variety of level ice conditions. Records were made of propeller thrust, torque and rotational speed as well as the power consumption of the electric drive motors. Measurements were made of the mechanical properties of the ice in which the tests were conducted.

The paper provides information on the operational conditions of the vessel, both in open water and during icebreaking. Measurements of thrust, torque, propeller rotational speed and ship speed showed the level of thrust and torque developed by the *Sir John Franklin* over a range of advance coefficients. Plots of the thrust and torque coefficients, K_T and K_Q, against the advance coefficient, J, indicated that the vessel travelled at an advance coefficient of about $J = 0.4$ when operating in ice of 0.5 metres thickness and at about $J = 0.8$ in open water. Additionally, a simple expression was given for ice thrust, or the increased thrust required to make way in a particular set of ice conditions, given the required ship speed and the ice and snow parameters.

The work is helpful in establishing full scale conditions in both open water and icebreaking operations for a known vessel for which there is a great deal of data available, both at model and full scale. The available data can be used to provide baseline comparisons with data recorded in the course of experiments in the towing tank and cavitation tunnel. Since the *Sir John Franklin* has open propellers, it is unlikely that any sustained non-contact blockage occurred throughout the course of the trials and the absence of a video record precludes clear determination of the types of interactions between the propellers and nearby ice pieces or the occurrence of cavitation. In addition, the ice thickness during the trials was very low and unlikely to have caused any propeller-ice interaction events.

The flow of ice blocks into a ducted propeller and the hydrodynamic effects of blockage was studied by Laskow (1988) by using wax blocks in the clear water towing tank at IMD. The paper describes a series of tests using a 1:15 scale model of the ice breaker *CCGS Louis St. Laurent*, equipped with a centreline duct and two open wing propellers. The project was initiated to establish the blockage phenomena as a function of vessel design parameters. Of relevance to this research was an attempt to isolate the influence of blockage on the power, torque and thrust of ducted propeller systems. The author gives corroborative evidence to the findings of Lindroos and Björkestam (1986) suggesting that blockage leads to increases in shaft thrust, shaft torque, vibration and absorbed power. In addition it was shown that blockage resulted in decreased duct thrust. The drop in duct thrust was greater than the increase in shaft thrust, resulting in a decrease

in total system thrust. Since the work was done at atmospheric pressure, no estimate of the effects of cavitation were made.

Keinonen and Browne (1990) systematically evaluated many parameters of ice loading on propulsion systems using model tests in the ice basin of IMD. The influence of ice thickness, ice strength, ice block size, feed rate, propeller revolutions, speed of advance and propeller speed were established. The effects were separated into contact and non-contact loads. Comparisons were made with data available from full-scale studies of the ice breakers *Jarvasaar* and *Robert LeMeur*.

Relevant to this research, the authors found non-contact hydrodynamic loads were a significant component of the loading regime for both open and ducted propellers when blocked with ice. For both torque and thrust, the induced hydrodynamic loads from nearby ice bodies resulted in elevated values of about twice the open water values. In addition, video photography of the experiments suggested that the flat plate model used by Lindroos and Björkestam is not representative of blockages likely to occur from icebreaking operations. In most cases, plate shaped blockages were oriented with one of the longer axes parallel to the direction of flow.

Newbury et al. (1993) carried out an experimental examination of hydrodynamic non-contact loads during propeller-ice interaction. The paper suggests propeller loads during milling can be summarised as the combination of hydrodynamic non-contact loads, crushed ice extrusion loads, direct ice contact loads and open water hydrodynamic loads. Each may occur simultaneously during milling and may occur at different areas of the blade. The paper presents an evaluation of the hydrodynamic non-contact propeller forces

that occur during propeller/ice interaction by measuring milling loads in air and water and compares the results to experiments measuring only the hydrodynamic loads during operation of a propeller behind a proximate blockage.

Two types of tests were performed. The first, done in air, measured thrust, torque, blade bending and blade spindle torque during ice milling. It was designed to measure the loads imposed on the propulsion system by only ice milling and ice piece extrusion for a range of parameters: propeller pitch; relative axial velocity between the propeller and ice piece; propeller rotational speed; size of the ice block; and ice strength. The second, done in water, repeated the test conditions of the first series, measuring the contact loads and the additional hydrodynamic loads resulting from operation in water. The latter being a combination of open water forces and loads resulting from operation of the propeller in the extreme wake of the proximate ice block. In addition, measurements were taken with the propeller operating in close proximity to the ice piece, with measurements of test parameters made over a range of distances between the propeller and the adjacent block. The authors suggest that by subtracting the results of the first series from those of the second series, the non-contact hydrodynamic loads can be isolated from the contact loads. They found that there was a large hydrodynamic component in the torque measured during the milling process, similar in magnitude to values of torque measured in the same conditions during tests in which the propeller was run adjacent to, but not in contact with, the ice block.

Difficulties recognised by the authors include: a great deal of scatter in the data due to the variation in ice mechanical properties and in the ice crushing mechanism and; a

limited data set from the underwater experiments resulting because the ice pieces used in the experiments often broke while being milled to match the propeller blade swept profile.

Shih and Zheng (1992) developed a two dimensional boundary element method to estimate the effects of proximity of an ice block to a propeller blade. The method assumed a block moved toward a blade section at the same speed as the surrounding fluid. As a result, there was no wake effect from the flow about the blockage. While this assumption imposes a limitation on the accuracy of the results, since the effect of operation in the wake is neglected, the paper does illuminate the increased hydrodynamic loading on a foil that is in close proximity to an adjacent surface. The authors found that proximity resulted in an increase in the peak load on the blade of about six times the open water values.

Shih and Zheng (1993) extended their numerical model to a three dimensional case using a similar boundary element method. Results from the three dimensional model suggested that maximum values of thrust and torque in blocked flow can be fifty percent higher than in open water conditions. Loads on individual blade sections can be as high as four times the associated open water results. The values are considerably lower than those presented in the authors' two dimensional model and it is suggested that this is as a result of radial flow over the blade in the three dimensional case.

The model had limitations imposed by computing capacity, including limited wake length and a coarse mesh. In addition, the flow about the block was considered to be ideal. No consideration was given to separation of the flow along the trailing edge of the block or to the boundary layers close to the block and blade. As a result, the model has

only limited application as the blade gets very close to the block and fails to model the case of a stationary block in front of the operating propeller. In addition, no attempt was made to consider the effects of a milled surface adjacent to the rotating propeller. As a result, proximity is only instantaneously modelled for one particular blade section whereas at the full scale, one could expect a considerable portion of the blade to be in close proximity to the ice block. While the method predicted lower loads associated with blockage than did the two dimensional case, the restrictions of the model limit the usefulness of the results.

Combining the results of model experiments, outlined in Newbury et al. (1993) with the two dimensional panel method discussed by Shih and Zheng (1992), Browne (1993) and Newbury et al. (1994) presented a semi-empirical model for hydrodynamic loads during non-contact propeller ice interaction with an ice block in close proximity to the propeller. Theoretical predictions were made by applying the numerical model (Shih and Zheng, 1992) to the geometry of the propeller model at a number of blade sections. Examples of numerical results were presented, with a sample of the pressure distribution over the back and face of the blade at the instant of peak loading and a trace of blade pressure at the leading edge as the blade section passes behind the blockage at various distances from the block. Predictions of pressure for trailing edge and leading edge locations were made for various blade positions with respect to the blockage.

A tabular comparison of the measured and predicted values was presented. It was shown that the predicted values of thrust and torque during blockage were an order of magnitude higher than the measured values. Predicted open water values were also high,

but to a lesser degree. The authors suggest that the differences were due to viscosity, radial flow over the propeller blade not modelled by the 2-D panel method, cavitation and overprediction of leading edge pressure drops.

Yamaguchi (1993) investigated the performance of the JRPA open propellers used in the ice tank and cavitation tunnel experiments for both uniform and blocked flow using a lifting surface code. For the blocked flow case, the author modelled the wake of the block as a step function such that the water flow speed was equal to the free stream velocity outside the blocked region and zero in the blocked region. Yamaguchi suggests that the effect of blockage can be broken into two components: the separation effect results in stalled flow behind the blockage due to the separation of flow about the ice piece; the displacement effect results in increased flow speed over the propeller blade back due to the wall effect of an ice piece in close proximity to the operating propeller. This is also called the proximity effect. While the lifting surface code was not capable of predicting the displacement/proximity effect, it was useful in predicting what portion of increased loads could be attributed to the separation effect. Comparing such a prediction to experimental results, which include both the displacement/proximity and separation effects, will permit an estimation of the magnitude of the displacement effect.

The author further investigated the effects of proximity by making a two dimensional steady flow calculation of a hydrofoil operating near a solid boundary using a numerical code developed by the author (Yamaguchi, 1988). Two cases were examined: a fully potential flow case and; an iterative solution taking the effects of the boundary layer into account. The calculations showed that while fully potential flow calculations suggest

the lift coefficient can increase to infinity as the distance between the wall and the foil is reduced to zero, the boundary layer calculations show that the practical limit of this increase is between five and ten times the uniform flow lift coefficient.

The work plainly describes the physics associated with non-contact propeller ice interaction and clearly illustrates many of the issues which must be addressed in developing an understanding of the loading regime to which a propeller is exposed during such interactions. Additionally, the work outlines the complexity of the problem and proposes a number of strategies for dealing with specific constituent problems as a piece-wise approach.

Based on a study of many hours of videotape records from full scale tests, Veitch and Laukia (1993) have discussed the mechanics of propeller ice interaction in terms of the approach of the block towards the propeller and the effects of blockage and contact. They suggest that interaction can be divided into three components: approach, blockage and contact. In the approach, the block can either be considered to be moving at the speed of the fluid, or slightly slower. As a result, the wake behind the block has very little effect on the hydrodynamic performance of the propeller. In the second phase, just prior to contact, the block is very close to the propeller and it is suggested that the wake effects may not be negligible. The authors describes the wake behind the block as turbulent, with very low axial velocity with respect to the propeller. The final phase is the contact of the ice block with the propeller. This latter phase was not the primary subject of this research and will not be discussed in detail here, however it has been extensively discussed by the author in his doctoral thesis (Veitch, 1995).

During the blockage phase, the authors suggest that the hydrodynamic load associated with the extreme wake behind the ice block can be estimated by the use of lift and drag coefficients. The coefficients can be estimated for the blade both in the obstructed area of the propeller disk where the flow would be stalled and in the unobstructed area of flow where the flow would not be stalled. The total load from the operation of the propeller in such conditions would be the sum of the loads resulting from the two flow regions.

The validity of Veitch's approach is dependent on whether it is an appropriate use of the lift and drag coefficients which were developed in the absence of an obstruction. More importantly, the method neglects the effects of proximity, as discussed above (Shih and Zheng, 1992 and 1993). Veitch (1995) followed up his 1993 paper with a simulation of the propeller-ice interaction in a numerical model developed as part of his doctoral thesis. In this work he continued to use a simple model of hydrodynamic loads associated with the interaction event; this is less of a concern for the case of the open propeller, used as a case study by the author, however it represents a considerable error in the case of the ducted propeller. In addition, the simple model fails to account for any variation of hydrodynamic loads due to the relative position of a blade with respect to the ice blockage. While his results may represent realistic solutions for the mean performance of the propeller, the approach does not adequately predict the instantaneous loads associated with blockage and cavitation during an interaction event; neglecting the effects of cavitation merely offset the error associated with neglecting the effects of proximity.

Similar to Veitch (1995), Koskinen et al. (1996) have presented the results of a simulation model, developed as part of the JRPA-6 between Canada and Finland. The work presents a comprehensive description of the propeller-ice interaction process and develops a simulation model with which interaction loads can be predicted. The authors compare their results to some available full scale data, specifically using the case of the *M/S Gudingen*, for which propeller blade bending loads and shaft thrust and torque loads exist.

The authors have developed a contact load model for both open and ducted propellers, and describe in some detail the types of interactions to which each propeller type might be exposed. Unlike other authors who place contact loads into two categories, milling and impacts (Laskow et al., 1986; Keinonen and Browne, 1990), Koskinen et al. propose a third category: tip loads caused by the tip of the propeller slicing through an ice piece traveling in a tangential direction to the motion of the propeller. In addition, they have described the blockage of a ducted propeller as two distinct processes: ordinary blockage, the case of a single large ice piece blocking the entrance of the duct and; dynamic blockage, caused by a rubble build up of smaller ice pieces in front of the duct.

Similar to Veitch's simulation (Veitch, 1995), the authors present a very simple model for hydrodynamic loads during propeller-ice interaction. The authors estimate the pressure on the back of the propeller blade to be a uniform distribution of pressure, equivalent to the leading edge pressure as calculated by Brown (1993), acting on that region of a propeller blade that is blocked by the ice piece. The authors attempt to account for the effects of cavitation by limiting the minimum level of pressure in that

blocked region to the vapour pressure of water. The authors suggest that such a simple model is justified due to the lack of understanding of the true hydrodynamic phenomena during the interaction.

Tamura and Yamaguchi (1995) have commenced a research project to examine the hydrodynamic loads during propeller ice interaction as part of an extensive research project examining the navigation of ships through the Northern Sea Route. In the paper, the authors proposed a loading scenario for propeller ice interaction which is comprised of three load components: ice contact loads; non-contact hydrodynamic loads and; loads due to the inertia of the ice and the added mass of the ice. The work proposes a research project in which an attempt is to be made to estimate separately the magnitudes of the three components from an experimental test program using a ducted propeller model. In a manner similar to the work presented in this thesis, the hydrodynamic loads are to be measured as an ice piece is brought in close proximity to the operating propeller, allowing the authors to ascertain the coincident effects of proximity and blockage. At this stage, the authors have merely presented their test program, along with some very preliminary data records. No significant analysis has been done and the program, to be conducted in an ice towing tank, will not account for the effects of cavitation.

Bose (1996) produced a potential flow panel method computer program to predict the hydrodynamic effects of propeller operation in the wake of a nearby ice piece. The software forms a part of the NSERC funded research project under which this current thesis falls. The time domain method can be used for the prediction of unsteady propeller performance and incorporates the effect of a proximate milled surface. Bose used a rigid

wake model and constant potential distributions on hyperboloidal shaped panels. The panels had a cosine distribution over the blade chord with the spanwise distribution being determined by the input. The predictions shown were obtained with 20 panels over the chord and 7 panels over the span. Panels were located on the hub and on a hub cone downstream of the hub but no blade/hub fillet was modeled. An estimate of the effects of flat plate frictional forces was made by summing the tangential forces on each panel resulting from a constant drag coefficient of 0.005. The work presents a numerical baseline against which measurements of the dynamic nature of propeller loads can be compared.

Recent work conducted by a number of the participants of the JRPA-6 endeavoured to provide additional insight into the full scale phenomena during propeller-ice interaction. A blade of the controllable pitch propeller (CPP) of the *USCGS Polar Star* was instrumented with a series of optical strain gauges designed to measure instantaneous values of blade bending. Additional instrumentation was installed on the propulsion machinery to measure propeller thrust and torque, among other propulsion parameters. While no written documentation was available from the research in time for inclusion in this thesis, images from videotape taken by underwater cameras during a number of interaction events was insightful since high levels of cavitation were apparent during contact between the propeller and incident ice pieces.

A comprehensive literature review of propeller-ice interaction has been done by Jussila and Soininen (1991). The authors have reviewed nine papers on propeller-ice interaction models, seven papers on full scale data and four papers on laboratory

experiments. Only two papers present any discussion of hydrodynamic loads during propeller-ice interaction. The first, on the full scale measurements of the *Robert LeMeur* by Laskow et al. (1986) is reviewed above. The second paper, by Kannari (1988), describes a full scale study of the effects of a duct on the propellers of the ice breaker *Karhu*, but discusses the hydrodynamic effects of the blockage on the shaft loads in a cursory manner.

3. METHODS, MODELS AND EQUIPMENT

3.1 Method

3.1.1 Propellers

1 General Information

The research has modeled, at reduced scale, the hydrodynamic effects of cavitation during propeller-ice interaction. The first phase of the research, conducted as part of the JRPA-6, used propeller models selected by the JRPA-6 project team for comparison with results acquired during experiments in the ice tank at IMD. The propellers, based loosely on a concept design for the Polar-8 icebreaker, represented no existing full scale vessel, but rather what was considered to be typical of open and ducted ice class propellers. Accordingly, no dimensions for a full scale vessel can be presented.

For the second phase of the research, conducted as part of the NSERC strategic grant, the propeller designs were selected based on the availability of full scale data (Michailidis and Murdey, 1981; Williams et al., 1992; Laskow, Spencer and Bayly, 1986). The design of the open propellers of the Canadian Coast Guard R-Class icebreaker was selected for the open propeller model. General particulars of the R-Class icebreaker *CCGS Sir John Franklin* are presented in Table 3-1. The Kaplan type ducted propeller of the Canmar *M/V Robert Lemeur* was selected for the ducted propeller model. Table 3-2 presents the particulars of the *Lemeur*. While this thesis presents no results of tests with the model of the *Lemeur's* propellers, the propeller configuration of the vessel is not unlike the ducted propeller configuration used in the earlier phase of the research and the

vessel description is included for completeness.

2 Typical configurations

To provide a frame of reference by which to assess the correctness of the models. photographs of full scale configurations are presented on page 31. Figure 3-1 presents a typical configuration of the open propellers of Canadian Coast Guard icebreakers. The photograph, taken by Mr. Michael Doucet, is of the Type 1100 propeller on the port side of the icebreaker *CCGS Ann Harvey* during a docking at the Newfoundland Dockyard Corporation. Figure 3-2 shows the analogous portion of the *M/V Robert Lemeur*. provided by Canadian Marine Drilling Limited. While neither vessel can be considered representative of all open or ducted propellers, the photographs show typical geometrical arrangements imposed on the propeller-ice interaction phenomena.

The photograph of the *Ann Harvey* suggests that the occurrence of non-contact blockage of the propeller is unlikely, since there is no structure near the propeller against which a stationary ice block might be supported without contacting the propeller. While there may be some possibility of an ice piece being lodged between the shaft and the hull. the situation is sufficiently unlikely to be irrelevant. For the open propeller, hydrodynamic loads should be considered to be constituent components of a contact loading regime imparted by moving ice pieces as discussed by Veitch (1995).

The configuration presented in the photograph of the *Lemeur*, however, presents a case in which non-contact loads could be easily expected. Large ice pieces lodging on the leading edge of the robust duct structure could significantly restrict the flow of water to the propeller. Ice pieces protruding into the duct can be milled by the propeller until the

rotating blades closely pass the milled surface of the lodged ice piece without making contact. In such a situation, the propulsion system is exposed to relatively prolonged hydrodynamic loads resulting from the extreme wake and the proximity of the ice piece.

3.1.2 Similitude

1 Necessity of cavitation tunnel tests

As was discussed in the review of relevant literature, predictions of the loading regimes to which the two propeller configurations are typically exposed have been based on results from full scale trials and model scale and laboratory experiments in towing tanks. Full scale efforts have attempted to measure the actual loading phenomena associated with the interaction between propellers and ice (Laskow et al., 1986; Williams et al., 1992), however, such measurements are difficult and expensive. As a result, considerable effort has been put toward measuring analogous loads in model scale experiments (Keinonen et al., 1990; Newbury et al., 1993; Veitch, 1995). The use of model scale experiments raises the question of similitude between full and model scale.

Model scale propeller-ice interaction experiments have been typically conducted in facilities such as IMD's towing/ice tank (Keinonen and Browne, 1992, Newbury et al., 1993, Newbury et al., 1994). Similitude between full and model scale conditions has been attempted by the use of EG/AD/S ice to model the mechanical properties of ice (Timco, 1986) and the execution of towing tank tests at full scale Froude numbers. In such towing tank tests, the inability to vary the ambient pressure precludes ensuring similitude between model and full scale pressure and therefore the effects of cavitation have been incorrectly modelled.

2 Definition of cavitation number

To investigate the effects of cavitation on the hydrodynamic loads associated with an interaction event, most of the experiments forming the current research were conducted in cavitation tunnels. Throughout the course of the test program, effort has been directed at ensuring similar cavitation numbers at model and full scale. This was done by running cavitation tunnel test programs near full scale cavitation numbers. The cavitation number used for comparison was defined in two ways. The first, used in the earlier part of the research, was based on water flow speed past the nearby ice piece:

$$\sigma_V = (P_O - P_V)/(\tfrac{1}{2}\rho V_A^2)$$

The second, used in the more recent experiments, was based on the rotational speed of the propeller;

$$\sigma_N = (P_O - P_V)/(\tfrac{1}{2}\rho(nD)^2).$$

While the two definitions are closely related, the effect of the difference in cavitation numbers on the model tests was to change the manner in which a constant cavitation number was maintained throughout a test series. For the former definition, the advance coefficient, J, was varied during a test series by changing the rotational speed of the propeller. In the latter case, the advance coefficient was changed by changing the flow speed in the tunnel test section. The selection of the former definition in the earlier phase of the research was made because it was felt that cavitation on the propeller would be influenced by the shear flow past the bluff body. However, it was subsequently found that the effect of cavitation during an interaction event was far less sensitive to flow speed than

to rotational speed and unacceptably low Reynold's numbers occurred when low propeller rotational speeds were used.

3 Cavitation number at full and model scale

Table 3-3 presents parameters from which cavitation numbers were calculated for a typical operating condition for an R-Class icebreaker. The full scale values are based on measurements presented in Williams et al. (1992) and the model scale values are presented for cavitation tunnel experiments (at full scale cavitation numbers) and for towing tank experiments (in which full scale Froude numbers were maintained). The table illustrates that minimum cavitation numbers achievable in a towing tank are far higher than full scale values: such numbers result in little or no cavitation during an interaction event. As will be seen. the absence of cavitation as a result of such high cavitation numbers substantially changes the level of measured hydrodynamic loads.

4 Discussion of gas content, nuclei

Other factors affecting the correlation between full scale and model scale cavitation behavior include gas content and distributions of microbubbles and nuclei in the water (Gorshkoff, 1975; Peterson et al, 1975, Kuiper, 1981; Gindroz, 1995) and the roughness of the propeller blade leading edge (Billet and Holl, 1980). Cavitation at full scale occurs in water at or near to the gas saturation point. To ensure similar conditions at model scale, low pressure experiments were run at gas content ratios, α/α_S equal to the ratio of the ambient test pressure to atmospheric pressure, P_A/P_{ATM} (Kato et al., 1981), where the gas content was measured by hand held oxygen content meters (such as a WTW Oxi 92 Oxygen Meter). Neither of the facilities at which cavitation tests were conducted

had the capability to measure cavitation nuclei distributions. However, Gindroz (1995) suggests that blade surface cavitation, as is typical during propeller-ice interaction, is less susceptible to nuclei distributions than tip vortex or bubble cavitation. Additionally, since preliminary experiments indicated that some cavitation inception occurred in the wake of the ice blockage at pressure ratios as high as $P_A/P_{ATM} = 1.09$, leading edge roughness was not required to initiate cavitation in a blocked flow. In fact, cavitation inception at such high pressures indicates that reasonable modeling of cavitation during propeller-ice interaction can be achieved just by ensuring tests are conducted at correct cavitation numbers. Parameters such as nuclei distributions and leading edge roughness are critically important in establishing the inception point: a point which is irrelevant in the current work.

5 Comparison with towing tank and full scale data

Finally, an assessment of similitude was made by comparison of results of tests conducted in the cavitation tunnel at the University of Tokyo with tests conducted in the towing tank at Memorial University (Luznik et al., 1995), results of towing tank tests on a scale model of an R-Class icebreaker (Murdey, 1980) and results of two series of full scale trials on the R-Class icebreaker CCGS Sir John Franklin (Michailidis and Murdey, 1981; and Williams et al., 1992).

Length Waterline (m)	92.12
Beam Maximum Waterline (m)	19.1
Draft Maximum (m)	7.21
Gross Tonnage (tonnes)	7718
Propellers	2 Open
Power (kW)	10,200

Table 3-1 Principal Dimensions of the R-Class Icebreakers

Length Overall (m)	82.80
Beam Moulded (m)	18.0
Draft Summer (m)	5.7
Gross Tonnage (tonnes)	3186
Propellers	2 Ducted
Power (kW)	7,162

Table 3-2 Principal Dimensions of the *M/V Robert Lemeur*

	Full Scale	*Tunnel*	*Tank*
N (rpm)	160	1200	726.2
D (m)	4.12	0.2	0.2
V_A (m/s)	4.4	1.6	1.0
P_A	101.3	17.24	101.3
J	0.4	0.4	0.4
Fn	2.093	0.766	2.093
σ_V	14.72	14.72	219.11
σ_{nD}	2.35	2.35	35

Table 3-3 Comparison of full scale and model scale cavitation numbers

Figure 3-1 Full Scale Configuration of a Type 1100 Icebreaker

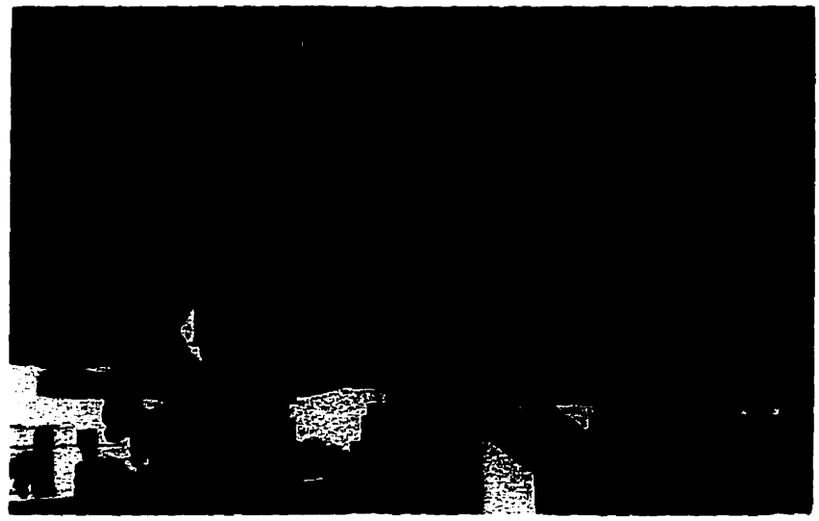

Figure 3-2 Full Scale Configuration of the *M/V Robert Lemeur*

3.2 Propeller Models

3.2.1 JRPA Open Propeller

1 General dimensions

The JRPA open propeller model was manufactured from manganese bronze by Offshore Research Limited of Vancouver. The propeller was loosely based on a B-Series design (Oosterveld and van Oossanen, 1975) modified for operation in ice. The propeller had a relatively large hub/diameter ratio representing typical dimensions of a controllable pitch propeller (although the model was fixed pitch) and excessively thick blade sections. Nominal chord lengths and thicknesses for the propeller are presented in Table 3-5. Principal dimensions for all propeller models are given in Table 3-4. The JRPA open propeller is shown in Figure 3-4. The manufacturer supplied no drawings for the propeller, nor was there any information available in previously published literature.

2 Blockage

This open propeller was first tested with a 0.28 m x 0.28 m x 0.089 m simulated ice blockage fabricated from high density polystyrene foam, based on the dimensions of an ice block used in similar tests conducted in the ice tank at IMD. A recess was cut in the blockage with a 48 mm cut depth to simulate a milled channel. A second, more robust blockage was constructed from epoxy coated wood, subsequent to the erosion of the polystyrene block by cavitation. The test apparatus for typical open propeller experiments is illustrated in Figure 3-3. The JRPA-6 blockage is shown in Figure 3-5.

3.2.2 R-Class Open Propeller

1 General dimensions

In the second series of open propeller tests, the propeller used was a 200 mm model of the four bladed 1200 series propellers used on the Canadian Coast Guard R-Class icebreakers. The propeller was manufactured by Dominis Engineering on a CNC milling machine to a tolerance of ±0.05 mm based on design drawings supplied by the Canadian Coast Guard. Principal dimensions of the propeller are presented in Table 3-4. A drawing of the propeller and experimental apparatus is presented in Figure 3-3. A drawing of the propeller is presented in Figure 3-6 and the section dimensions are presented in Figure 3-7.

2 Blockage

The simulated ice blockage used with the R-Class propeller measured 0.210 m by 0.210 m by 0.75 m and was fabricated from high density polyethylene (HDPE). The installation is shown in Figure 3-3. Again, a milled recess was cut into the downstream face of the blockage, matching the profile contour of the propeller. The blockage was fabricated from three laminates of HDPE to allow a range of blockage configurations to be tested. Tests in the University of Tokyo's tunnel were conducted for the full blockage case at a 2 mm gap. Tests in the towing tank at MUN were conducted for a number of blockage cases and a range of proximities. The blockage dimensions are presented in Figure 3-8.

3.2.3 JRPA Ducted Propeller

1 General dimensions

In the ducted propeller experiments, two propeller models were used. Again manufactured from manganese bronze by Offshore Research Limited. the designs were selected based on the requirements of the JRPA-6 team. The propellers had Kaplan type blades (van Gent and Oosterveld, 1983) of similar design to each other but with different pitches. One had a pitch/diameter ratio, P/D, of 1.17 and the other with P/D = 0.8. Similarly to the JRPA open propeller, they had relatively large hub/diameter ratios, representing typical dimensions of controllable pitch propellers (although the models were of fixed pitch design) and thick, ice class blade sections. Nominal chord lengths and thicknesses are presented in Table 3-6. The propellers are shown in Figure 3-9. Again, the manufacturer supplied no drawings for the propeller, nor was there information available in previously published literature.

2 The duct

The ducted propellers were fitted with a MARIN Type-37 accelerating nozzle (van Gent and Oosterveld, 1983) manufactured from transparent polycarbonate by Technical Services at Memorial University. The duct was attached to the tunnel ceiling by means of an aluminum bracket instrumented with strain gauges to allow the measurement of the axial thrust developed by the duct. Electronic signals produced by the strain gauges were amplified using a Measurements Group model 2100A Strain Gauge Conditioner System. Output from the amplifier was fed to an 80386 microcomputer through a 12 bit Keithley S570 data acquisition board. The duct configuration is presented in Figure 3-10.

3 Blockages

The ducted propellers were both tested with 0.140 m x 0.140 m x 0.063 m wooden blockages. The faces adjacent to the propellers were cut to match the leading edge profiles of the respective propellers, simulating a milled surface. In addition, the high pitch ducted propeller was tested with a 0.114 m x 0.114 m x 0.056 m wooden blockage with three pressure sensors installed in the face of the blockage adjacent to the propeller. The sensors were located adjacent to the 80 mm radius of the propeller, one at the centerline of the tunnel and one at 37° either side of the centerline. Electronic signals from the pressure sensors were processed in the same way as those for duct load measurement. Dimensions of the blockages are shown in Figure 3-11. The positions of the pressure sensors are shown in Figure 3-12.

	R-Class	*JRPA Open*	*JRPA Ducted*
D	0.2	0.2	0.2
P/D	.779	0.8	0.8; 1.17
$A_D A_O$	0.67	0.63	0.63
Blades	4	4	4
Hub/Diameter	0.27	0.38	0.38

Table 3-4 Propeller model general dimensions

Radius *mm*	*C* *mm*	*t* *mm*
50	84.2	9.53
60	101.2	7.95
70	107.2	6.73
80	104.4	5.77
90	88.1	4.45
100	0.0	

Table 3-5 JRPA open propeller dimensions

Radius *mm*	*C* *mm*	*t* *mm*
50	68.07	7.75
60	76.20	6.35
70	81.28	5.33
80	85.34	4.32
90	87.63	3.58
100	87.38	2.79

Table 3-6 JRPA Ducted Propeller Dimensions

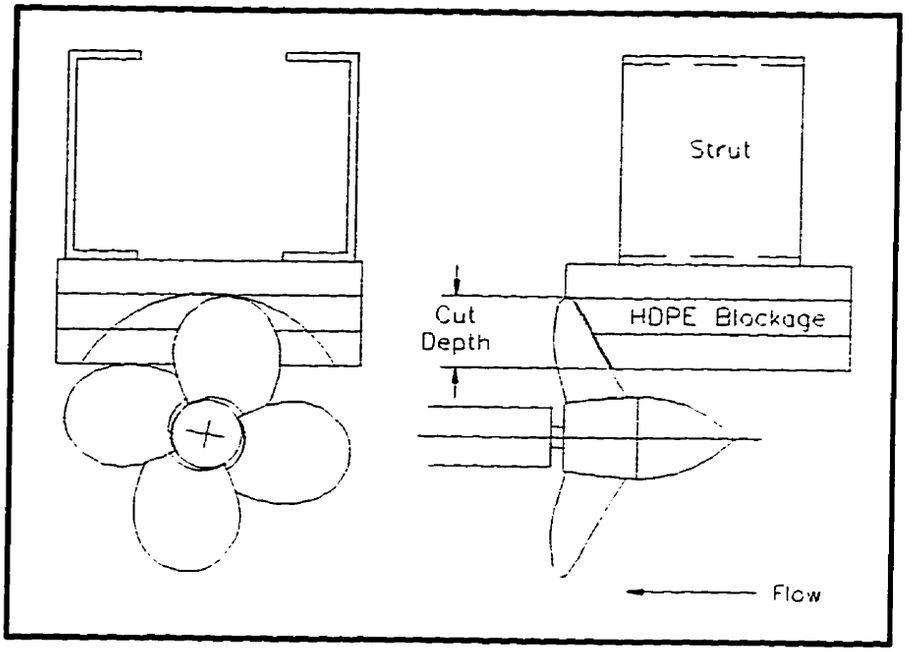

Figure 3-3 Open Propeller Test Configuration

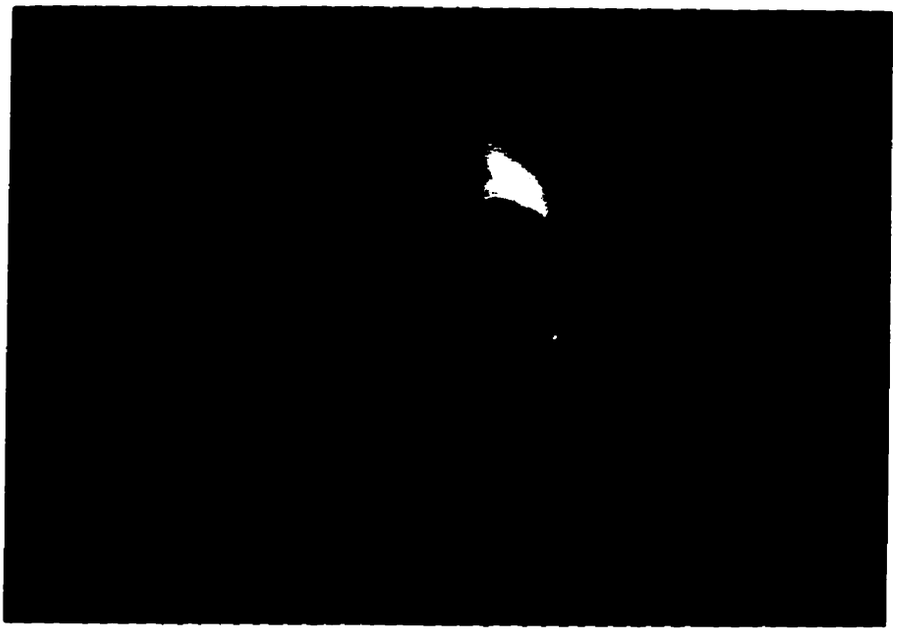

Figure 3-4 JRPA Open Propeller

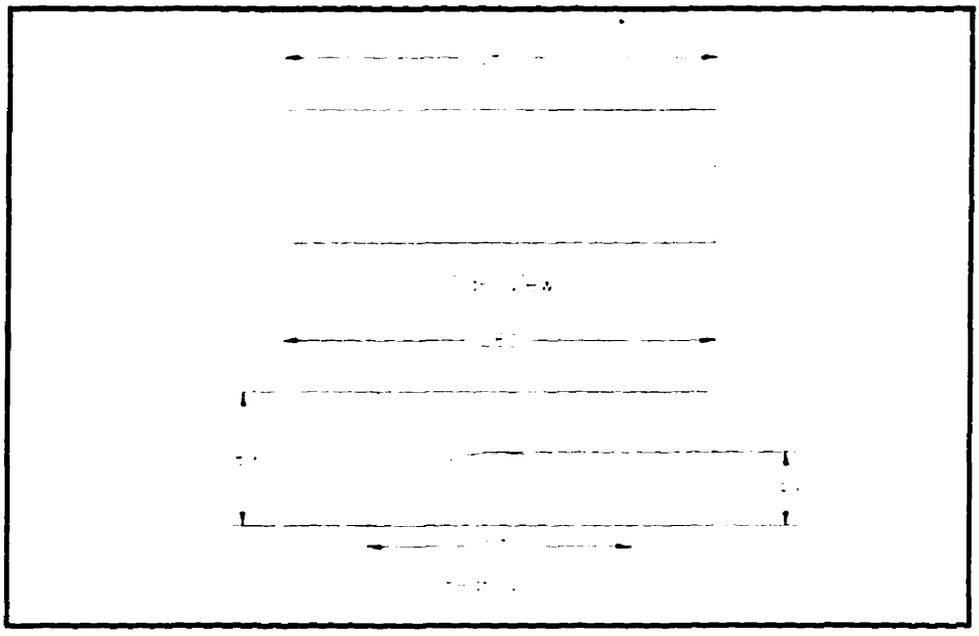

Figure 3-5 JRPA Open Propeller Blockage

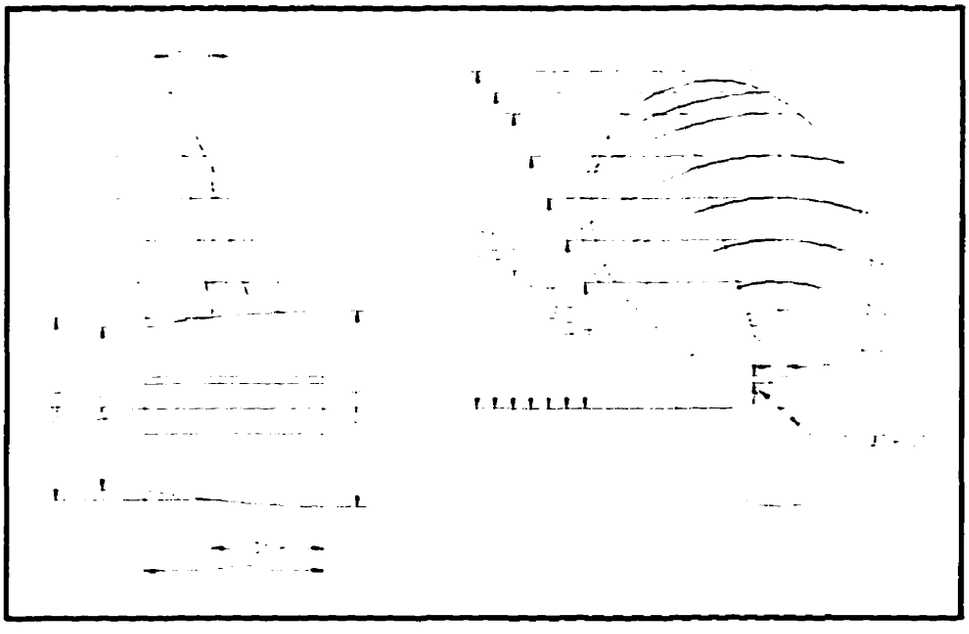

Figure 3-6 Profiles of an R-Class Propeller

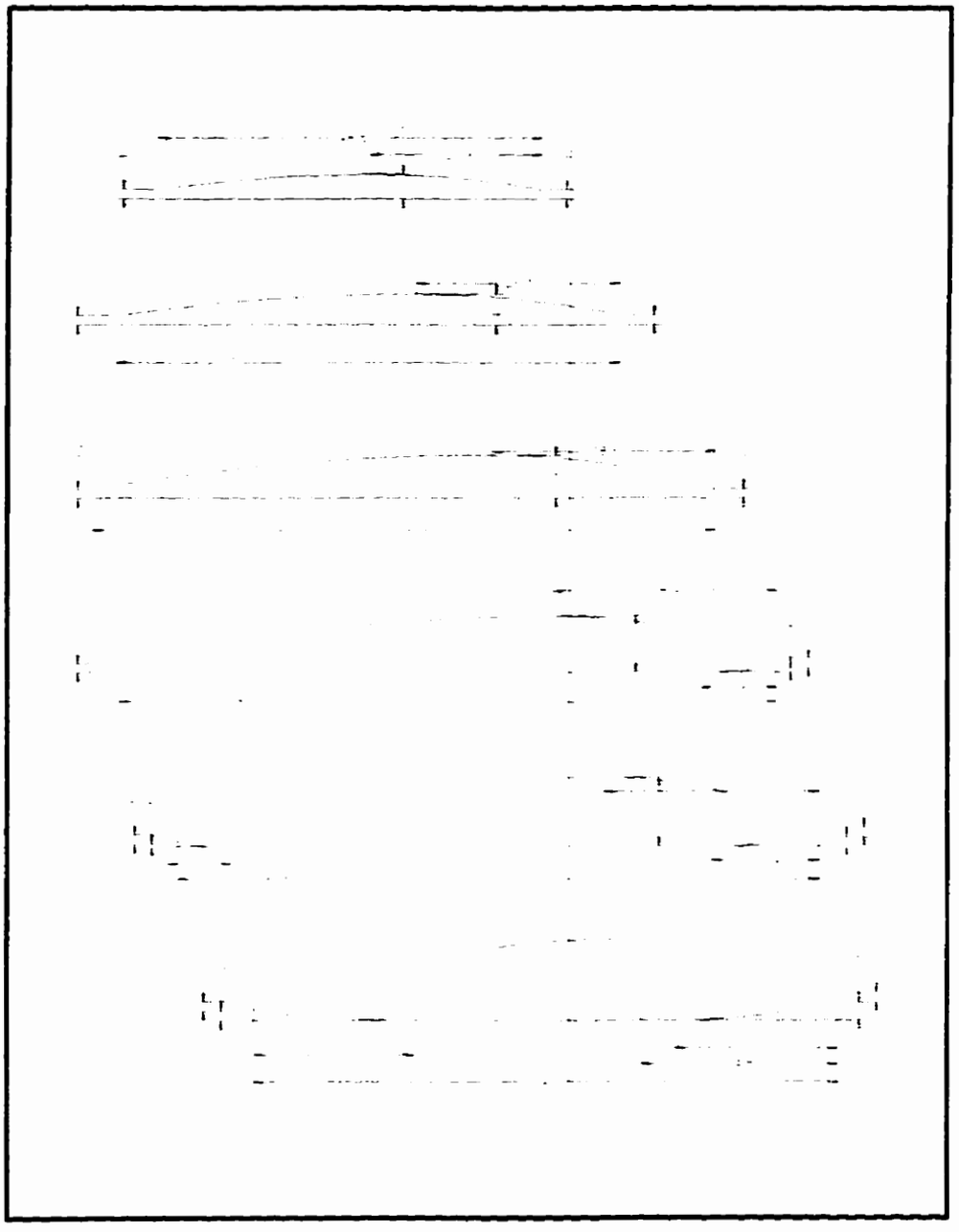

Figure 3-7 Blade Sections of an R-Class Propeller

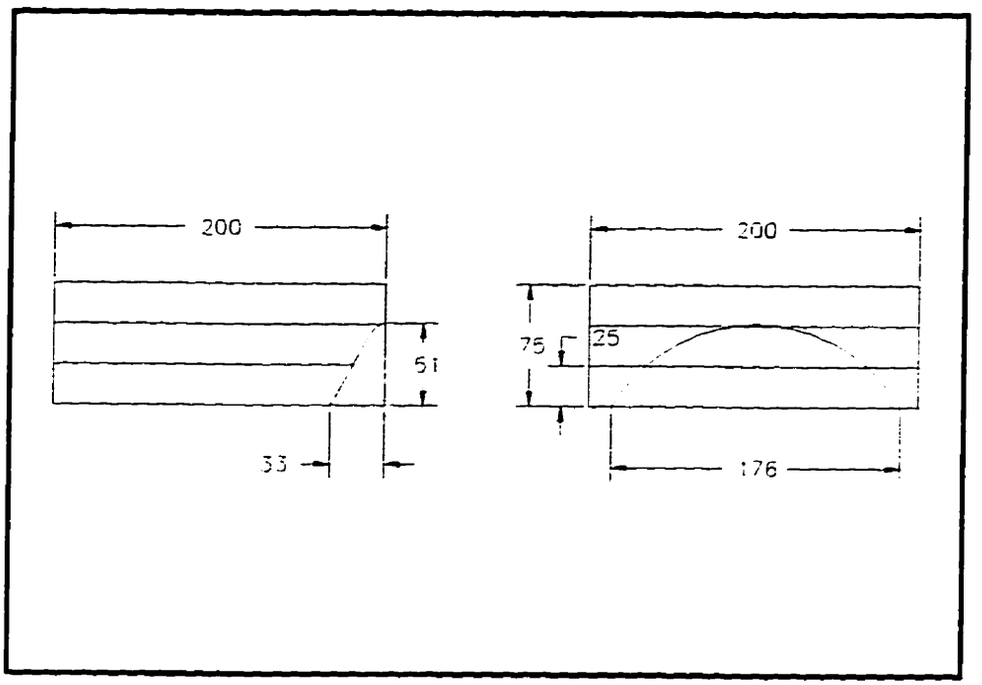

Figure 3-8 R-Class Blockage

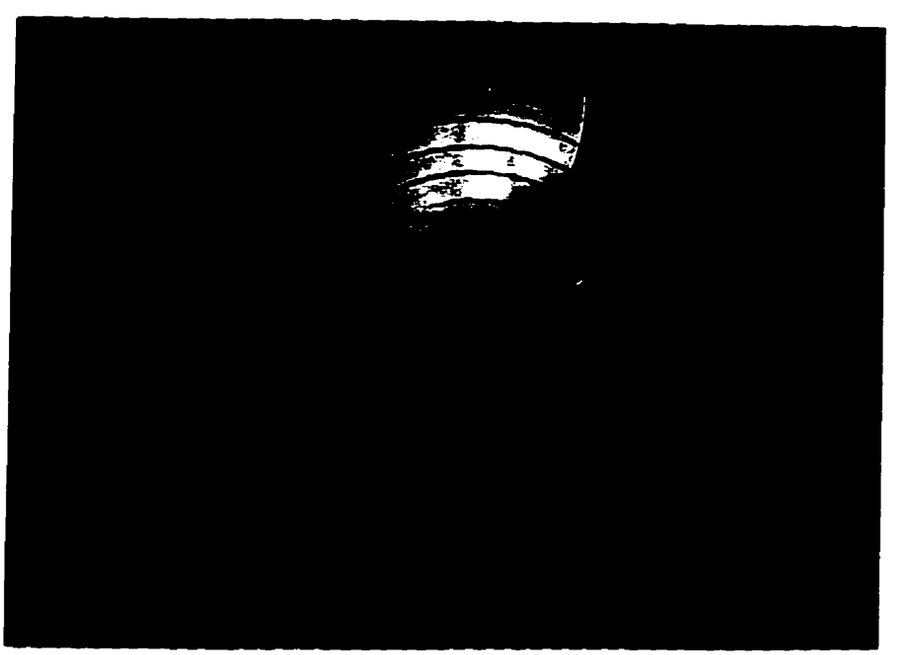

Figure 3-9 JRPA Ducted Propellers

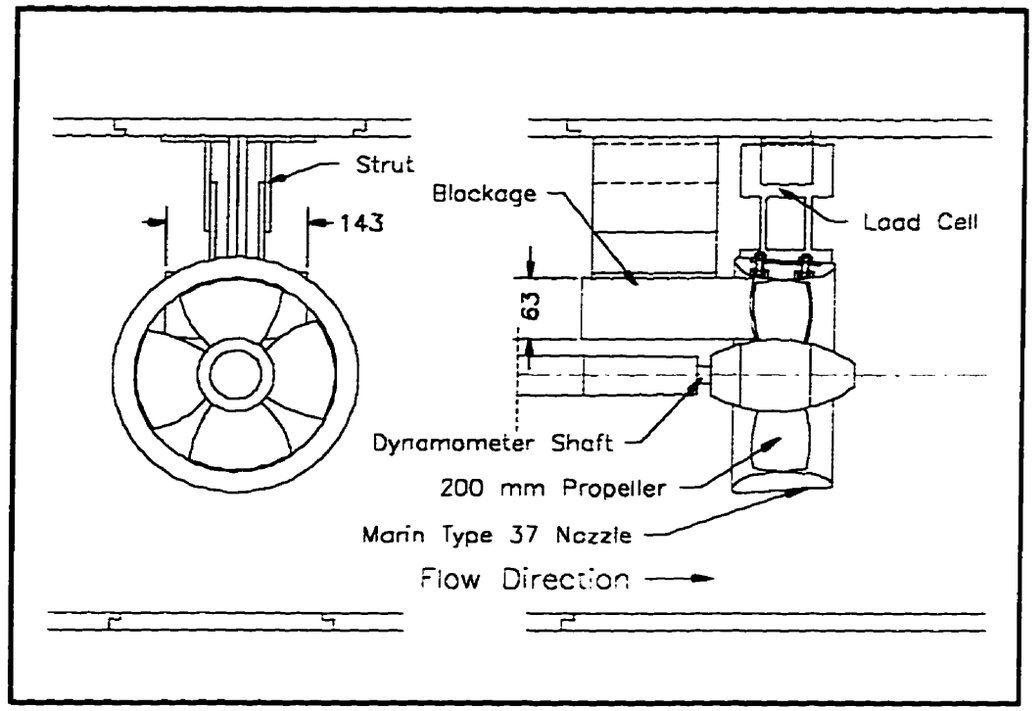

Figure 3-10 JRPA Duct Configuration

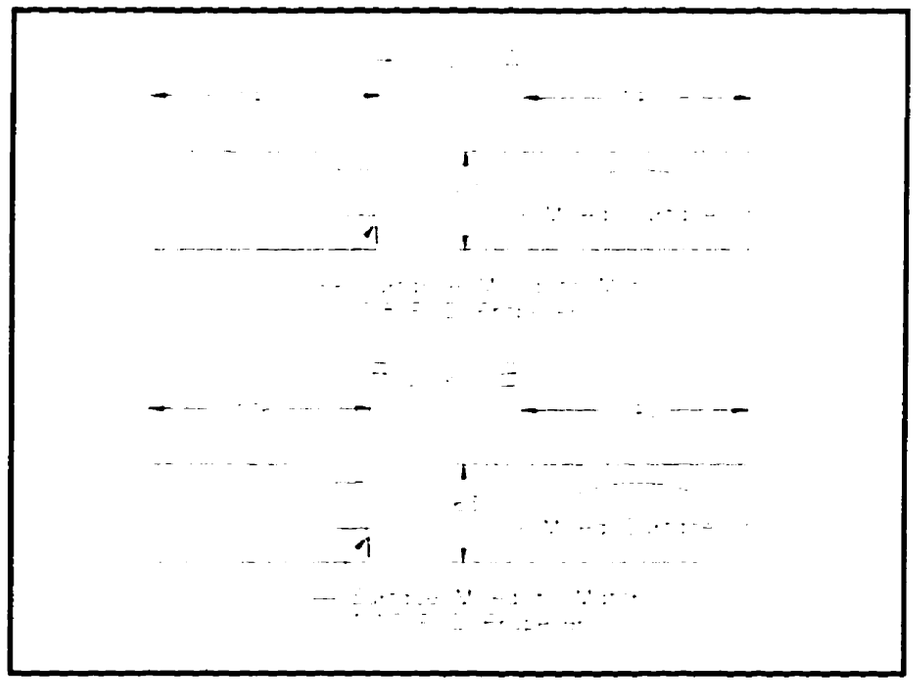

Figure 3-11 JRPA Ducted Blockages

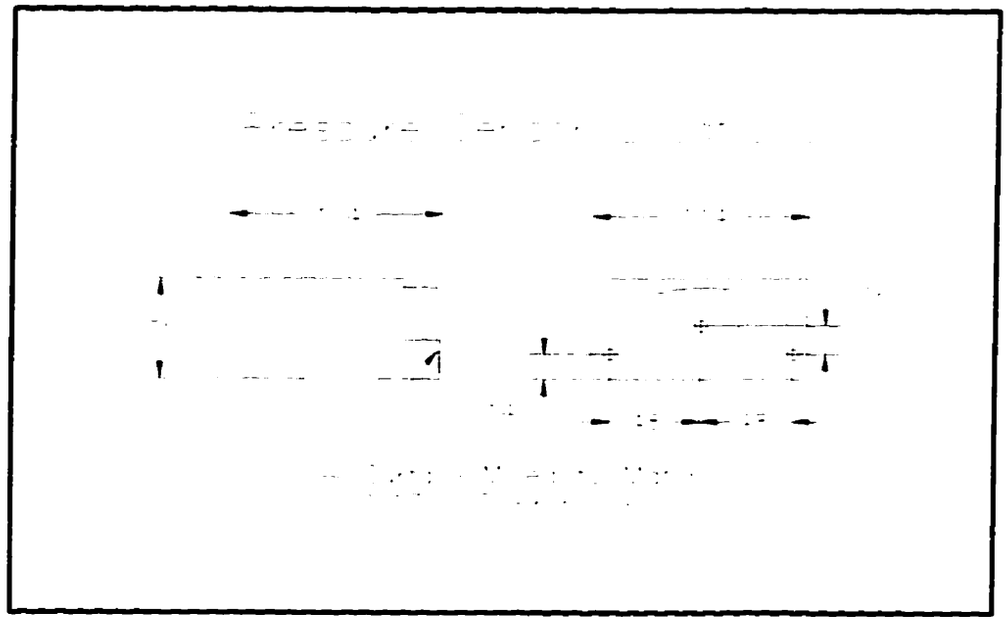

Figure 3-12 JRPA Block Instrumented with Pressure Gauges

3.3 Equipment

3.3.1 IMD Cavitation Tunnel

The cavitation tunnel at the Institute for Marine Dynamics was used for experiments with the open and ducted propellers tested in the earlier part of the research program as part of the JRPA-6. The facility has been described in detail in previous documentation (Doucet, 1992). Aspects of the facility of relevance to this work are summarized below. The general characteristics of the tunnel are outlined in Table 3-7. A photograph of the IMD cavitation tunnel is presented in Figure 3-13.

1 Thrust and torque measurement

Propeller thrust and torque were recorded by using two different dynamometers. For all tests, a Kempf and Remmers mechanical dynamometer was used. The apparatus measured the average thrust and torque developed by the propeller by means of mechanical balance scales connected directly to the upstream protruding end of the propeller shaft. The principal advantage of an upstream dynamometer is that it allows the development of an unobstructed hub vortex. The main disadvantage is the inability of the facility to test a propeller in fully uniform flow: this was not relevant for the current research.

Tests to measure the dynamic effects of cavitation on thrust and torque during blockage of the open propeller model were conducted using a strain gauged dynamometer in parallel with the mechanical apparatus. A description of the equipment and its performance is described in previous documentation (Bose, 1993). The instrument provided a basis on which to compare the dynamic nature of torque in uniform flow with

torque resulting from propeller operations in blocked flow with and without cavitation. Dynamic measurements of thrust were not possible due to: the stiffness of the load cell: cross talk between bending and thrust; a bent propeller shaft and; water damage of the thrust strain gauges.

2 Flow speed measurement

The tunnel at IMD has two types of manometers: mercury and water (Doucet, 1992). Flow speed during the tests in the IMD tunnel was measured using water manometers only. The maximum accuracy of flow measurement using manometers is limited to estimating the height of the water column to within a half a division, or 0.5 mm. The flow speed, governed by the selection of the cavitation number, σ_v, was at a level such that ±0.5 mm resulted in an error of ±0.5% using the water manometers and ±6.3% using the mercury manometers. As the mercury manometer lines introduced locations for the development of vapor bubbles and were not required for flow speed measurement, the mercury manometer/barometer system was disconnected

The operation of a propeller or the installation of a bluff body in the flow of a cavitation tunnel introduces changes to the pressure distributions within the test section. In facilities where the test section flow speed is calculated from the pressure differences between two locations in the flow, corrections must be made for changes in pressure at one or both locations caused by changes other than variations in flow speed.

Water velocity in the cavitation tunnel at IMD is calculated from the pressure difference between a location upstream of the diffuser and a location in the test section

downstream of the diffuser. The ratio between velocities upstream and downstream of the diffuser is known since it is a function of the cross-sectional area ratio of the two locations. This relationship permits the measurement of flow speed based on the principle of a venturimeter (Mironer, 1979). The measurements are influenced by both the operation of the propeller in the restricted test section and by the installation of the blockage in the flow.

Velocities have been corrected for the effect of propeller operation in the restricted test section according to the method outlined by Lindgren (1963). To correct for errors as a result of the installation of the blockage, a series of two dimensional panel method calculations were done by Yamaguchi (1993). The result of his work showed that the effect of blockage was a uniform increase in the advance coefficient of 1.5%. Velocity measurements were corrected accordingly.

3 Pressure measurement

Ambient pressure at the shaft line was measured indirectly by recording the gauge pressure at the free surface in the vacuum chamber of the tunnel and the depth of water from the shaft line to the free surface. The ambient pressure was calculated as the sum of the gauge pressure and the hydrostatic pressure associated with the head of water above the shaft line.

Since the mercury manometer/barometer system was not in use for the series of tests on the JRPA propellers, the pressure at the shaft line was not directly measured. The lack of direct measurement at the shaft line precluded the compensation of the tunnel pressure for pressure reductions due to flow through the tunnel test section. However,

since the flow speeds used in the tests were low. the errors associated with the pressure changes were not significant.

4 Cavitation patterns

Cavitation patterns were filmed using an S-VHS video camera with motion slowed or frozen by a variable frequency strobe light. Some still photography was taken of initial tests. however it was found that video proved to be a better medium for subsequent analysis and assessment and the photography was discontinued.

3.3.2 University of Tokyo Cavitation Tunnel

The University of Tokyo's cavitation tunnel has been described by Kato et al.. (1981) and was used to measure the performance of the R-Class propeller model over a range of cavitation numbers. The facility is well instrumented and controlled. Experiments conducted at the facility provided insight into the dynamic nature of the loads associated with cavitation and baseline results against which to compare additional work conducted at the Institute for Marine Dynamics. Principal dimensions of the cavitation tunnel relevant to this research are given in Table 3-8.

1 Thrust and torque measurement

Propeller thrust and torque were recorded using an electronic dynamometer downstream of the propeller. The apparatus measured the average thrust and torque developed by the propeller by means of an instrumented load cell. The propeller shaft was powered through a bevel gear gearbox driven by an electric motor installed on the top of the tunnel. The low natural frequency of the load cell and mechanical noise introduced by backlash in the gearbox precluded dynamic measurement of thrust and torque. Unlike the

mechanical dynamometer in the IMD tunnel, the facility in Tokyo can measure propeller performance in true uniform flow since it is located downstream of the propeller. However the effects of a hub vortex on propeller performance cannot be modelled.

2 Block load measurement

Tests in blocked flow at the Tokyo facility were conducted with the blockage mounted on a three component load cell capable of measuring forces with and across the flow direction and moments about the load cell axis. During each test, records were made of each component. All time domain signals were recorded by a series of memory banks at a sampling rate of 5000 Hz for a period of 1.6 seconds and subsequently downloaded to diskette using a microcomputer. Measurement of the mean load on the blockage permitted the calculation of the total system thrust inclusive of the drag load associated with the blockage. This permitted the estimation of the propulsion system efficiency. The time domain record of block load gave an indication of the instantaneous blockage loads, with and without cavitation. The load cell had a natural frequency, ω_n, of around 140 Hz, higher than both that of the propeller dynamometer ($\omega_n \approx 60$ Hz) and the blade pass exciting frequency ($\omega = 80$ Hz). As a result, it was felt that the ratio of the excitation frequency to the natural frequency of the dynamometer ($\omega/\omega_n = 0.57$) was sufficiently low enough to give an indication of the dynamic nature of the loading regime.

3 Flow speed measurement

Flow speed was manually monitored and controlled. Variations from required values during testing required manual intervention, however very little variation from initial settings occurred during this test program. Flow speed was measured both by using

pressure sensors upstream and downstream of the test section contraction, as in the IMD tunnel, and by a laser Doppler velocimeter (LDV) focused on a point in the flow outside the region affected by the propeller and blockage.

Results from tests at the University of Tokyo presented in this thesis use only the flow speed measured by the LDV. By focusing the crossed laser beams emitted by the LDV at a point at which there was minimal influence by either the action of the propeller, or by the installation of a bluff body forward of the propeller, no velocity correction was required. The measurement point was selected based on the past experience of personnel at the University of Tokyo and by a series of velocity profiles conducted with the blockage installed in the tunnel.

4 Pressure measurement

Pressure was automatically monitored and adjusted by the control system of the Tokyo tunnel. The system automatically compensated the test section pressure for head loss associated with flow speed through the test section, based on the original setting entered by the system operator. Once a target pressure was set, no further operator intervention of pressure control was required throughout a test series at a given pressure.

The automated control system proved to be beneficial, since pressure measurement and control was more critical in the series of tests conducted in the Tokyo series, due to the different definition of cavitation number. Since the cavitation number, σ_{nD}, is maintained at a constant value throughout a test by maintaining a constant rotational speed, n, the advance coefficient was changed by varying the flow speed, V_A. As a result, flow speeds in the test section ranged as high as $V_A = 2.8$ m/s. The dynamic head loss

associated with this flow speed is around 4000 Pa, nearly four times the head loss associated with the maximum flow speed used during tests in the IMD tunnel.

3.3.3 Memorial University Towing Tank

The towing/wave tank at the Ocean Engineering Research Center was used to measure the performance of the R-Class propeller at atmospheric pressure for a range of blockage conditions. The tank is 58 meters long, 4.6 meters wide and has a maximum water depth of 3.0 meters. Experiments were conducted in the tank in both uniform and blocked flow. The blocked flow tests were done for two levels of blockage and for a range of propeller-block gaps. The test plan and apparatus was developed as part of the research for this thesis. as was the interpretation of the results. The tests were conducted and data reduction done by a cooperative work-term student in 1994 (Luznik et al., 1995).

1 Propeller Test Boat Configuration

The towing carriage is electrically driven with a maximum velocity of 5.0 m/s. A propeller performance test boat was mounted on the carriage as shown in Figure 3-14. The propeller was driven by a 220 VAC, three phase, single speed motor with a rotational speed of 1750 RPM. The propeller rotational speed, N, was controlled by the selection of the drive pulleys. With a pulley ratio of approximately 1:1.3, the minimum rotational speed with this equipment configuration was 1320 revolutions per minute.

2 Data Acquisition

During performance tests in the towing tank, records were taken of propeller thrust and torque using a Kempf and Remmers Model R-33 electronic dynamometer.

Propeller shaft rotational speed was measured using both an analog tachometer and a pulse generator positioned to produce one pulse per revolution. Carriage speed was measured with an optical sensor which measured the rotational speed of an accurately machined idler wheel in contact with the carriage rails. With the exception of the analog tachometer which measured propeller rotational speed, all signals were logged using a 16 bit Keithley S575 data acquisition system and recorded using an 80286 microcomputer. The analog measurement of propeller speed was shown on a separate electronic display and manually recorded.

Test Section Dimension	0.5 m x 0.5 m x 2.2 m
Maximum Water Speed	10.0 m/s
Maximum Propeller Speed	60 rps
Test Section Pressures	0.1 - 1.0 atm

Table 3-7 IMD Tunnel Dimensions

Test Section Dimension	0.45 m x 0.45 m x 2.1 m
Maximum Water Speed	11.2 m/s
Maximum Propeller Speed	50 rps
Test Section Pressures	0.1 - 3.0 atm

Table 3-8 University of Tokyo Cavitation Tunnel Dimensions

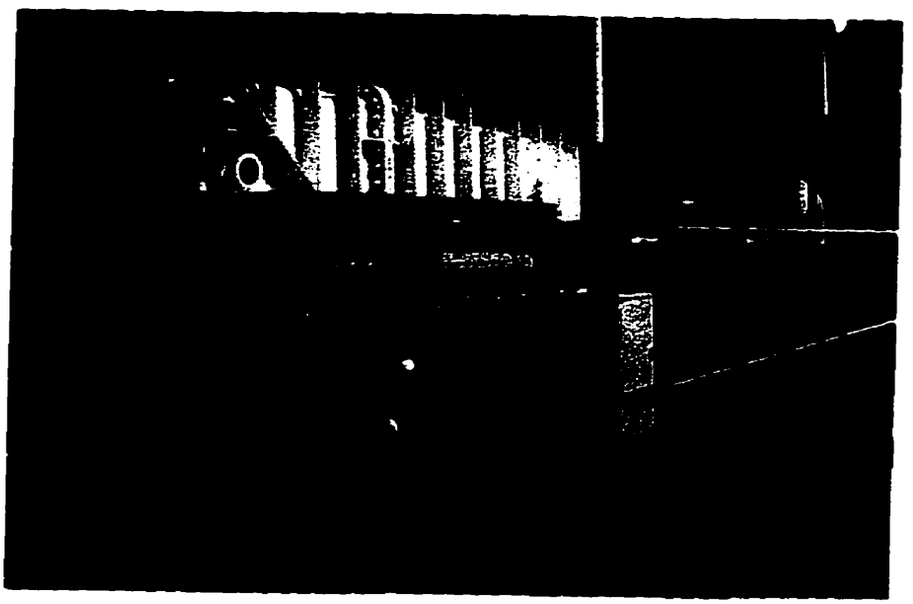

Figure 3-13 Typical Cavitation Tunnel

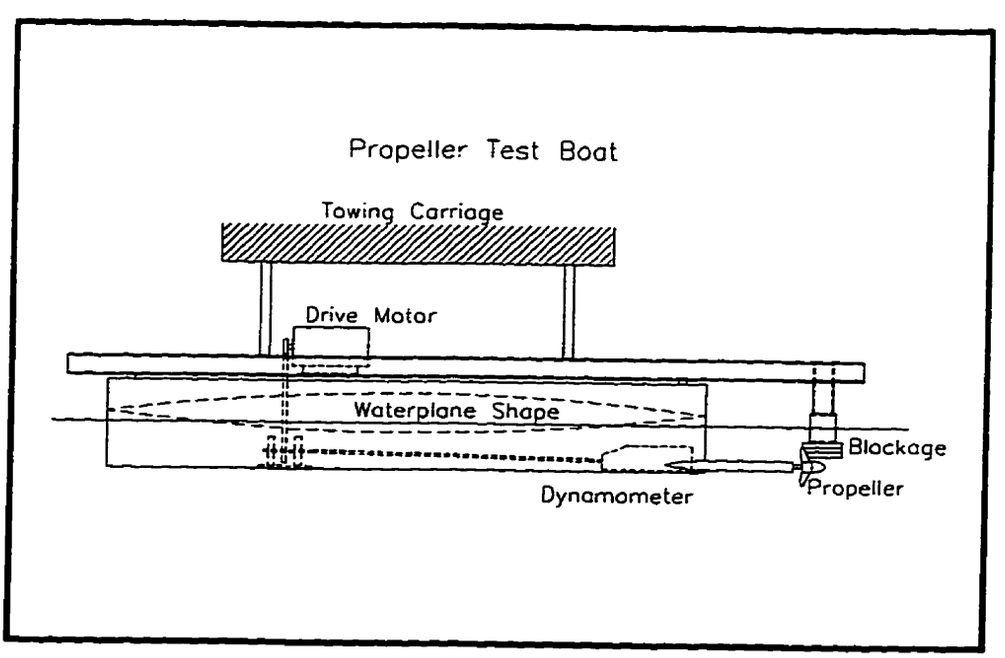

Figure 3-14 Towing Tank Test Apparatus

4. RESULTS

4.1 JRPA Open Propeller

Tests with the JRPA open propeller in the cavitation tunnel at IMD, both in uniform and blocked flow, were initially done using a mechanical dynamometer for average load measurement. Subsequently, an electronic dynamometer was installed and time domain measurements of thrust and torque were recorded. Tests in uniform flow were compared to predictions from polynomial equations fitted to the experimental results of the B-Series propellers (Oosterveld and Oossanen, 1975). Propeller performance in uniform flow provides a benchmark against which to compare mean and dynamic measurements of thrust and torque in blocked flow.

4.1.1 Performance in Uniform Flow

4.1.1.1 Mean Loads

4.1.1.1.1 Test Conditions

Tests in uniform flow were conducted at a flow speed of V_A = 1.0 m/s. The rotational speed of the propeller was varied from n = 5.4 rps to n = 30 rps, corresponding to a range of advance coefficients from J = 0.16 to J = 0.92. All tests in uniform flow were conducted at a pressure ratio, P_A/P_{ATM}, of 1.09, the sum of atmospheric pressure and the static head of water above the propeller shaft line.

4.1.1.1.2 Results

i) Experimental results

Figure 4-1 presents the results of tests in unblocked uniform flow. Thrust and torque were measured with the mechanical dynamometer. Individual points are plotted for the thrust coefficient, K_T, and torque coefficient, K_Q. A quadratic polynomial was fitted to the thrust data using a least squares curve fit. A similar cubic polynomial was fitted to the torque data. Provided for comparison are performance curves for a B-4.100 propeller, which most closely matches the model blade geometry; the actual blade area ratio of the ice class propeller was reduced by the large hub diameter.

ii) Polynomial comparison

The experimental values of thrust were similar to those of the B-series propeller, however the model propeller results displayed a lower slope than the B-4.100 in both the thrust and torque curves. The correlation is reasonable since the B-4.100 data represents experimental results for a propeller which is only approximately similar to the ice-class model. The experimental values of thrust coefficients were slightly lower for the model at low advance coefficients and slightly above the predictions at higher advance coefficients. The values of the torque coefficient for the model displayed a similar trend but are higher than for the B-series predictions for almost the entire range of advance coefficients. However, the standard B-series data is for a Reynolds number of $Rn_{C=0.7} = 2x10^6$ whereas in these tests the Reynolds number varied from $Rn_{C=0.7} = 1.5x10^6$ to $Rn_{C=0.7} = 3.1x10^5$ for advance coefficients of J = 0.2 to 0.9, respectively. The low Reynolds numbers were especially problematical at high advance ratios: low rotational speeds resulted in Reynolds

numbers at which laminar flow was likely, resulting in increased section drag and higher values of the torque coefficient in comparison to the B-series results. Also contributing to increased values of torque are the large hub size of the model and the increased thickness of the ice class blades causing an increased form drag of the blade sections.

iii) Dynamic character of torque

Figure 4-2 presents a record of torque at an advance coefficient of $J = 0.21$. The measurement was taken over a period of one second at a rotational speed of $n = 11.9$ rps and a pressure ratio, P_A/P_{ATM}, of 1.09. The figure shows a slight oscillation of $\Delta K_Q = \pm 0.010$ about the mean value of $K_Q = 0.037$. Most of the variation was due to random electrical noise, present at similar levels with no propeller rotation.

4.1.2 Performance in Blocked Flow

4.1.2.1 Mean Loads

4.1.2.1.1 Test Conditions

i) Velocity, Pressure and Shaft Speed

Three series of tests were done in blocked flow, during which the propeller load was measured with the mechanical dynamometer. The first was conducted at a pressure ratio of $P_A/P_{ATM} = 1.09$. The latter two were conducted at reduced pressure, $P_A/P_{ATM} = 0.43$. The test done at atmospheric pressure was run with a water speed of 1.0 m/s. Low pressure tests were run at water speeds of $V_A = 1.0$ m/s and $V_A = 1.5$ m/s with corresponding cavitation numbers of $\sigma_V = 85$ and $\sigma_V = 37$, respectively. Again the

rotational speed was varied throughout the test program to produce a range of advance coefficients.

ii) Gap

In all blocked flow tests with the JRPA open propeller, the ratio of the gap between the propeller and the adjacent face of ice blockage, G, and the propeller diameter, D, was approximately G/D = 0.01. Due to compliance of the shaft system, the gap required continuous adjustment throughout the course of the experiments to compensate for variations in the gap between the block and the propeller which was caused by changes in the thrust developed by the propeller. Since adjustment was based on a visual estimate of the gap size through the tunnel window, there was considerable variation in gap from one test to another. The scatter apparent in the test data shown in Figure 4-3 and Figure 4-4 reflects this variation.

4.1.2.1.2 Mean Results

i) Effects of Blockage

Results from tests in blocked flow at atmospheric pressure are shown in Figure 4-3. As with the uniform flow results, polynomial least squares lines have been fitted to the data. The lines fitted through the uniform flow data in Figure 4-1 are repeated for comparison. The figure shows that the maximum level of thrust and torque in blocked flow occurred at an advance coefficient of J = 0.2, which was the minimum achievable advance coefficient in the tunnel. The thrust coefficient increased from $K_T = 0.27$ in uniform flow to $K_T = 0.40$ in blocked flow. The torque coefficient went from $K_Q = 0.039$ for the unblocked case to $K_Q = 0.051$ in blocked flow.

ii) Effects of Proximity

The increase in thrust and torque can be explained in part as the effect of a segment of the propeller operating in the stalled flow of the simulated ice piece. That portion of the propeller behind the ice piece was effectively at bollard pull, or an advance coefficient of $J = 0.0$, and generated higher thrust and torque than the segment of the propeller operating outside the wake of the block, which was at an advance coefficient of $J = 0.2$. This is only a partial explanation, however, since the figure indicates that for a propeller operating in such blocked conditions, the values of thrust and torque coefficients at an advance coefficient of $J = 0.0$ would be around $K_T = 0.43$ and $K_Q = 0.058$. In uniform flow on the other hand, the values of thrust and torque coefficients at bollard pull conditions would be around $K_T = 0.34$ and $K_Q = 0.046$. If the increases of thrust and torque coefficients were only due to the effect of a part of the propeller operating at bollard pull, the results of experiments in uniform and blocked flow should be approximately equal at the bollard pull condition.

Shih and Zheng (1992) showed that the operation of a two dimensional foil section adjacent to a nearby solid surface resulted in increased lift on the foil section due to accelerated flow over the foil back. Bose (1996) showed that for the case of a propeller in blocked flow, this proximity effect resulted in an increase in the thrust coefficient in excess of that attributable to the operation of a segment of the propeller disk at the bollard condition. This was substantiated by tests subsequently conducted in the towing tank at Memorial with the R-Class propeller. Those tests are described in section 4.2.2.1.2.

iii) Effects of Cavitation

The curve fitted results of performance tests at atmospheric pressure in blocked flow are repeated in Figure 4-4, along with the results of tests at cavitation numbers σ_V = 84 and σ_V = 37. Since the advance coefficient was changed by varying the rotational speed throughout the test. no single value of a cavitation number, σ_{nD}, based on rotational speed can be presented. Offset errors between the curves resulted from the difficulty in maintaining a constant gap between the block and propeller for each test and preclude a precise quantification of changes in K_T and K_Q due to cavitation. However, the reduced levels of thrust and torque coefficients at low advance coefficients as the cavitation number was decreased indicates a reduction in the mean level of hydrodynamic load on the propeller as a result of cavitation.

4.1.2.1.3 Dynamic Results

i) Effects of Blockage

A comparison of the time domain signals in unblocked and blocked flow for experiments with similar flow conditions qualitatively shows the effect of blockage on the oscillation of instantaneous values of the thrust and torque coefficients. Figure 4-5 displays results typical of tests in blocked flow. The test conditions for the experiment were similar to those illustrated in Figure 4-2, with a propeller rotational speed of n = 11.9 rps. and an advance coefficient of J = 0.21. There was little or no cavitation present during the test.

The torque signal in Figure 4-5 exhibits a regular periodic oscillation at the blade pass frequency of 48Hz which was not measured in the torque signal in uniform flow as

presented in Figure 4-2. The standard deviation of $\underline{\sigma}$ = 0.395 represents an increase in oscillation about the mean value of over three times that shown in Figure 4-2, where the standard deviation about the mean was $\underline{\sigma}$ = 0.116. The mean value of torque, Q = 2.4 Nm, corresponding to K_Q = 0.053 is an increase of 46% over the mean value in uniform flow of Q = 1.7 Nm (K_Q = 0.037) and agrees with the results presented in Figure 4-3, where blockage resulted in an increase in the torque coefficient from K_Q = 0.039 in the unblocked case to a value of K_Q = 0.051 in blocked flow at an advance coefficient of J = 0.2.

ii) Effects of Cavitation

Figure 4-6 and Figure 4-7 present the time domain torque measurements recorded during tests in blocked flow for two cavitation numbers. Results presented in Figure 4-6 were taken during a test conducted at a propeller speed of n = 20.0 rps and an advance ratio of J = 0.13. The pressure ratio was P_A/P_{ATM} = 1.08. Associated cavitation numbers were σ_V = 818 and σ_{nD} = 13.4. Figure 4-7 illustrates the torque record for a similar experiment run at a reduced pressure of P_A/P_{ATM} = 0.33. In that test, the induced water speed of V_A = 0.38 m/s corresponded to an advance coefficient of J = 0.09 and cavitation numbers of σ_V = 434 and σ_{nD} = 3.89. While no full scale data was available for the JRPA class propeller, typical cavitation numbers for a full scale R-Class propeller at a similar advance coefficient would be around σ_V = 155 and σ_{nD} = 2.0.

During the test at the lower cavitation number (σ_{nD} = 3.89) substantial cavitation was developed and the time record shows an increase in the oscillatory nature of torque about the mean value. At a pressure ratio of P_A/P_{ATM} = 1.08 (Figure 4-6) the standard

deviation of the oscillation about the mean was $\underline{\sigma} = 0.47$. At a pressure ratio of $P_A/P_{ATM} = 0.33$ (Figure 4-7), the standard deviation of the oscillation increased to $\underline{\sigma} = 1.06$. This increase in oscillation was accompanied by an increase in noise and vibration discernible from the outside of the tunnel.

4.1.2.2 Patterns of cavitation

Violent cloud cavitation, with many small entrained vortex cavities, resulted from the propeller working in the extreme wake of the blockage. Figure 4-8 illustrates the pattern of cavitation as a propeller blade enters and exits the milled recess in the simulated ice block. While the severity was dramatically increased at lower cavitation numbers, the pattern was often exhibited even at atmospheric pressure.

When the angle, ϕ, was 0°, the blade had not yet entered the recess and was working in the unrestricted flow beneath the block. Cavitation which was visible was a result of normal operation in uniform flow. At atmospheric pressure, an intermittent tip vortex cavity was seen but there was no evidence of any other cavitation on the blade. At the lowest cavitation number, $\sigma_V = 37$, and at an advance coefficient of around $J = 0.2$, the blade exhibited a fully developed tip vortex cavity and a leading edge sheet cavity over approximately 10% of the back of the blade. The sheet cavity and tip vortex cavity combined towards the tip of the blade, forming a single twisted core downstream from the blades.

As the blade entered the recess, the leading edge vortex interacted with a horizontal shear flow vortex formed at the lower edge of the blockage recess. In this region the two vortices were approximately parallel and were rotating in the same

direction. As a result, they merged forming a large vortex cavity covering that area of the blade which was inside the recess. This was most apparent at a blade angle of $\phi = 45°$.

As the blade moved across the recess the shear flow behind the block and leading edge vortices became progressively misaligned. When the blade angle, ϕ, was 90°, the diameter of the merged vortex cavity could be seen to be rapidly increasing and decreasing in an oscillatory manner, and the length of the cavity had become shorter. Occasionally two or more separate unstable vortex cores could be seen. As the pressure dropped in front of the leading edge the shear flow vortex formed a separated vortex cavity along the lower left edge of the recess.

As the blade angle rotated to $\phi = 135°$, the leading edge vortex and the shear flow vortex approached a perpendicular orientation with respect to each other. This resulted in violent cloud cavitation which included many small, unstable vortex cavities as well as a large number of bubbles. At atmospheric pressure, the cloud ranged from the edge of the blockage to cover the extent of the blade remaining in the recess. At the cavitation number $\sigma_v = 37$, it extended as far as the face of the following blade, posing a possible erosion risk to both blades. As the blade subsequently moved out of the recess, the cloud progressively disappeared and was nearly dissipated by the time the blade angle had changed to $\phi = 180°$.

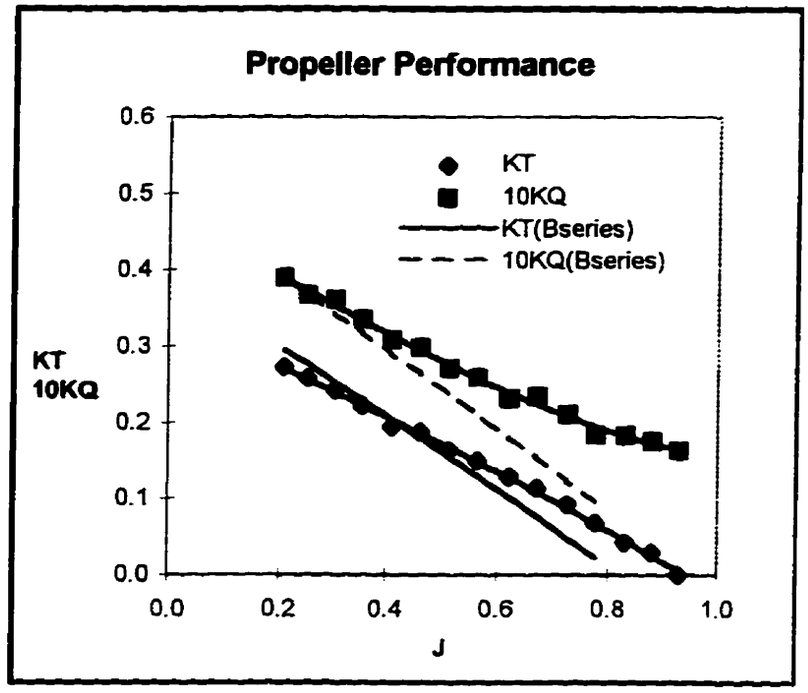

Figure 4-1 JRPA Open Propeller Performance, Uniform Flow

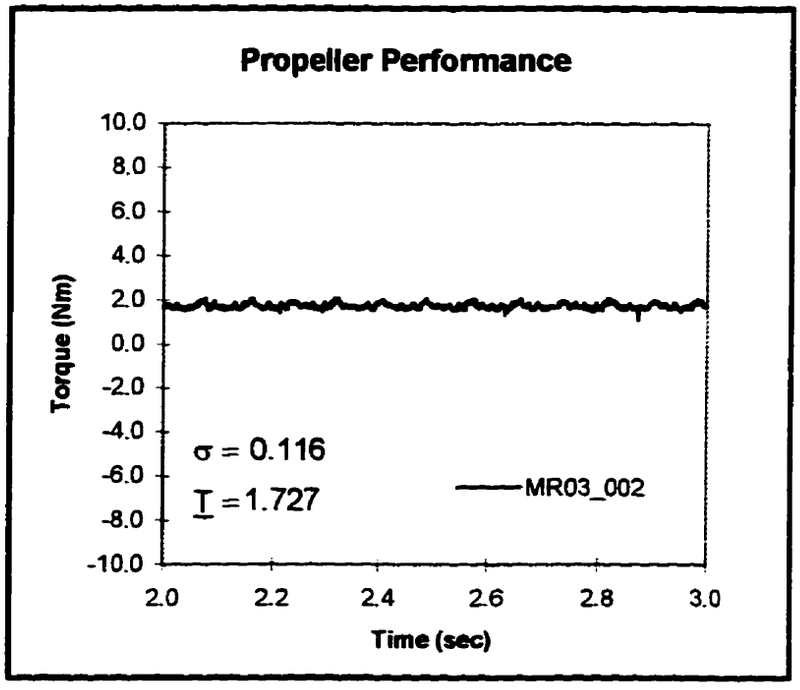

Figure 4-2 Torque in Uniform Flow
n = 12 rps, P_A/P_{ATM} = 1.09, J = 0.21

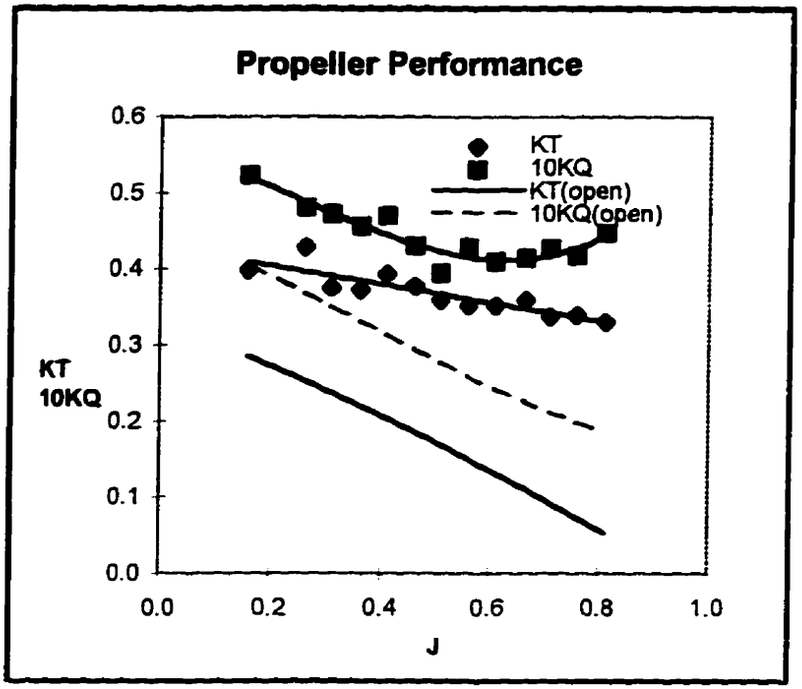

Figure 4-3 JRPA Open Propeller Performance, Blocked Flow

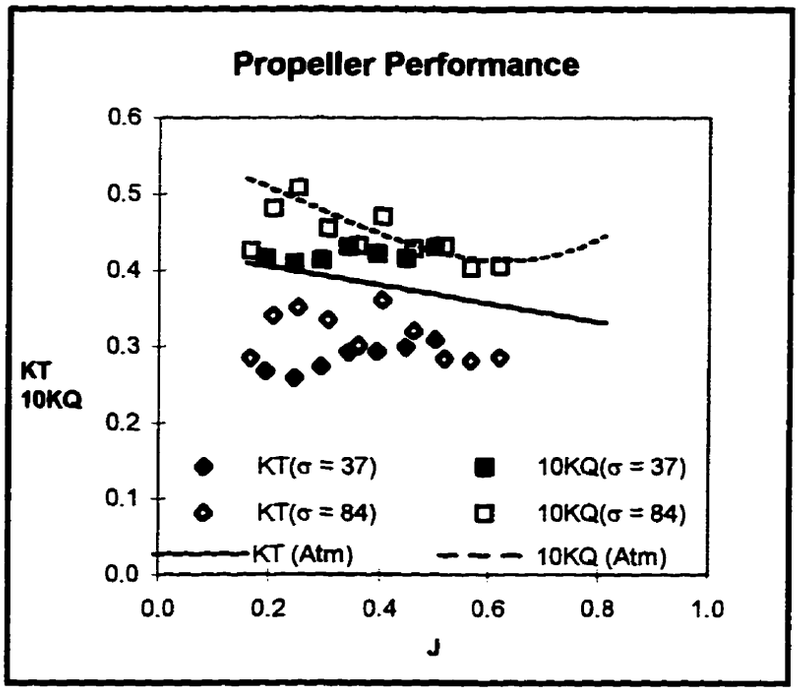

Figure 4-4 JRPA Open Propeller Performance, Blocked Flow

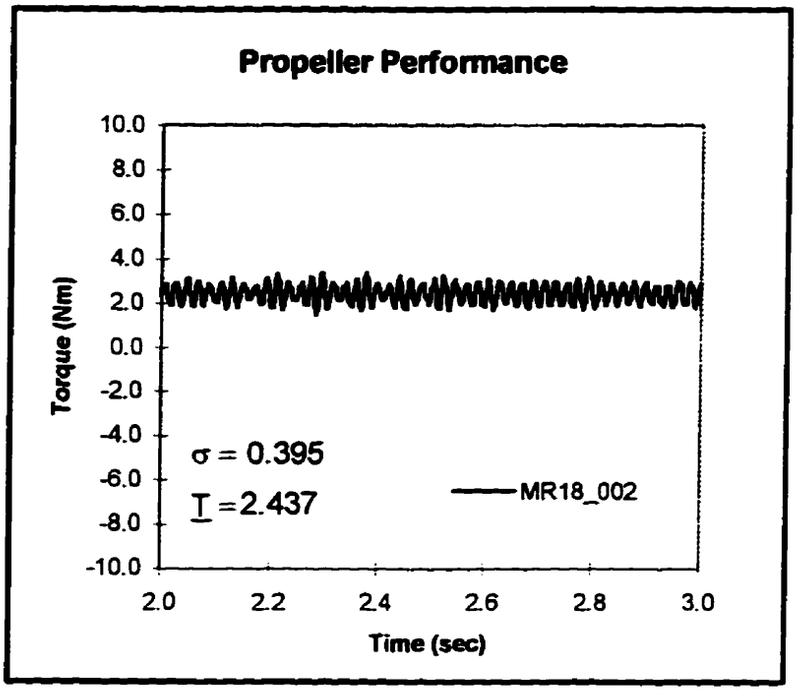

Figure 4-5 Torque in Blocked Flow
n = 12 rps, P_A/P_{ATM} = 1.09, J = 0.21

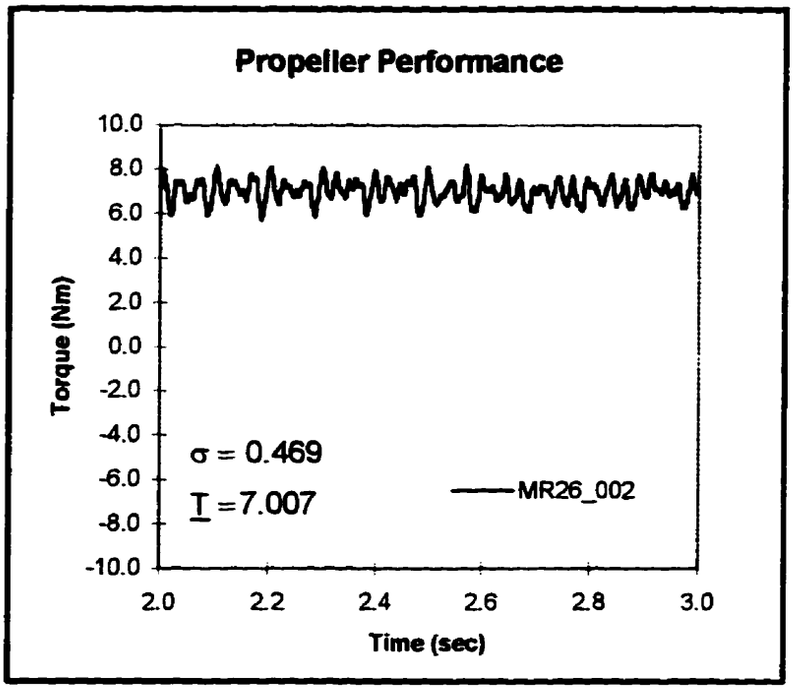

Figure 4-6 Torque in Blocked Flow
n = 20 rps, P_A/P_{ATM} = 1.08, J = 0.13

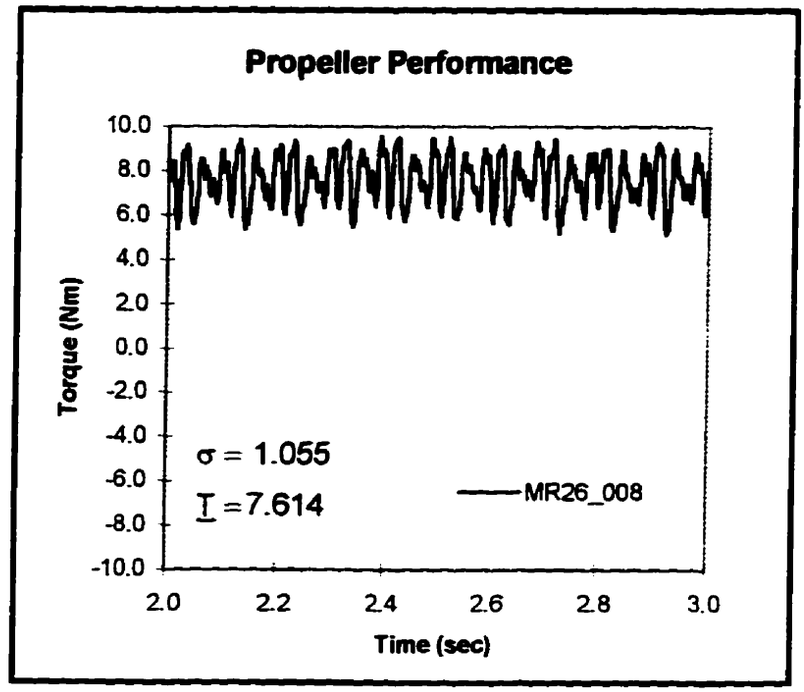

Figure 4-7 Torque in Blocked Flow
n = 20 rps, P_A/P_{ATM} = 0.33, J = 0.09

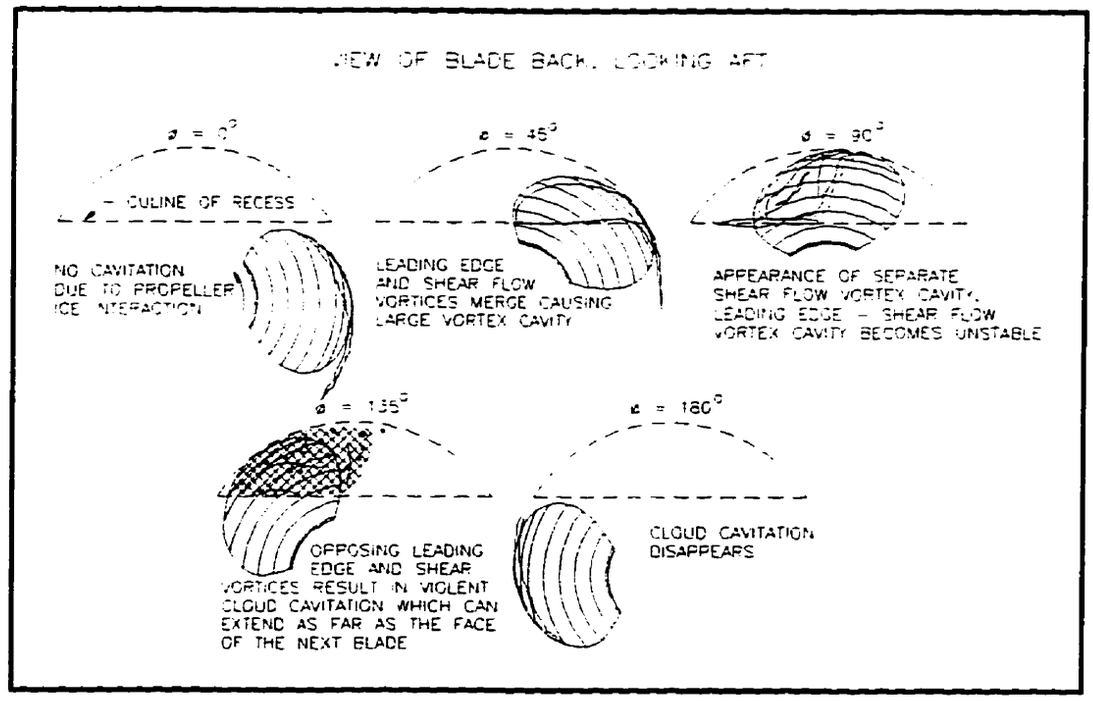

Figure 4-8 JRPA Open Propeller Cavitation

4.2 R-Class Open Propeller

Results of tests with the JRPA open and ducted propellers served to provide substantial insight into the effects of cavitation during propeller-ice interaction. However, the experimental nature of the electronic dynamometer, the geometrical accuracy of the propeller models and the choice of cavitation numbers all contributed to uncertainty levels which preclude definitive conclusions. Subsequent tests with the model scale R-class propeller provided much more detailed results on the operation of an open propeller in blocked flow.

The R-Class propeller model was tested in both the cavitation tunnel of the University of Tokyo and the towing tank of Memorial University. The experimental results provided data from which to assess: the average and unsteady effects of cavitation during propeller ice interaction; the effects of proximity between the ice and the operating propeller; and the effects of variations in blockage level. Full scale and previous model scale performance results are used to provide a baseline against which to compare uniform flow test results from both the tunnel and the towing tank. The effects of blockage, proximity and cavitation are then compared with those uniform flow results.

4.2.1 Performance In Uniform Flow

4.2.1.1 Mean Loads

4.2.1.1.1 Test Conditions

i) Cavitation Tunnel

As the cavitation number was based on the rotational speed of the propeller, tests run in the cavitation tunnel of the University of Tokyo were conducted at a constant rotational speed. The advance coefficient was varied by changing the water flow speed. Tests in uniform flow were conducted at a rotational speed of n = 30 rps. All tests in blocked flow were conducted at a rotational speed of n = 20 rps. This resulted in a blade pass frequency (the rate at which propeller blades pass into the recess of the simulated ice blockage) of 80Hz.

ii) Towing Tank

Tests in the open water of the towing tank at Memorial were conducted by Mr. Luksa Luznik, a co-operative engineering student hired for two work terms to assist in the research project. Test plans and the interpretation of results were done by the author as part of this research. Mr. Luznik carried out the test plan as outlined and was responsible for data reduction.

Due to inflexibility of the drive configuration of the propeller test boat, all tests throughout the experimental program in the towing tank were conducted at a rotational speed of n = 22 rps. The propeller advance coefficient, J, was controlled by the propeller advance speed, V_A, by changing carriage speed. The apparatus was installed at an

elevation such that the shaftline submergence was 200 mm, equal to the diameter of the propeller.

4.2.1.1.2 Results

Results from both the tunnel tests and the tank tests in uniform flow are presented in Figure 4-9. Measurements of thrust and torque were taken over the range of advance coefficients from J = 0.2 to J = 0.7 at increments of $\Delta J = 0.05$ in the tunnel and $\Delta J = 0.1$ in the tank. The figure presents the advance coefficient along the horizontal axis and the coefficients of thrust, K_T, and torque, $10K_Q$, along the vertical axis. It shows very good correlation between tests run in the two facilities, with a maximum difference in the thrust coefficients of 0.006 and a maximum difference in the torque coefficients of 0.001 (2.5% and 0.9% of the values measured in the towing tank, respectively). The excellent correlation between data recorded in the tunnel and the measurements made in the unrestricted flow of the towing tank, coupled with velocity profile measurements made with the laser doppler velocimeter (LDV) in Tokyo, indicates no correction is required for blockage effects of the tunnel walls (Lindgren, 1963).

For comparison, a line fitted to full scale results presented by Michailidis and Murdey (1981) is shown for both the thrust coefficient and the torque coefficient in Figure 4-9. The full scale results were corrected for wake using the Taylor wake fraction (Harvald, 1983) calculated from self-propulsion data using stock propeller models (Murdey, 1980). Model and full scale torque coefficient measurements are very close, with a difference ranging from 0.002 to 0.017, with the better correlation between the two sets of data at low advance coefficients. Model scale thrust coefficients, on the other

hand, are somewhat higher than the full scale results over the full range of advance coefficients, with a difference ranging from 0.017 to 0.038. Notwithstanding the differences, the full scale results show the model's performance is a reasonable estimate of the performance of the propulsion system of the R-Class icebreakers.

Differences can be attributed to scale effects, difficulties in making accurate full scale measurements and uncertainties associated with the calculation of wake fractions. which had maximum values of $w_T = 0.15$ and $w_Q = 0.14$. In addition, the measurement of thrust at the full scale is often inaccurate due to the very low strain levels which occur in the shaft system. This is likely a contributing factor to the discrepancy between full and model scale. The full scale results presented in the referenced paper give performance estimates for four different conditions: open water; operation in a broken channel: icebreaking operations in 0.65 m thick ice; and icebreaking in 0.80 m thick ice. Typical advance coefficients for each operation were near values of $J_S = 0.72$, $J_S = 0.65$, $J_S = 0.3$ and $J_S = 0.15$, respectively; the model tests covered a similar range.

4.2.2 Performance In Blocked Flow

4.2.2.1 Mean Loads

4.2.2.1.1 Test Conditions

i) Cavitation Tunnel

All tests in blocked flow in the cavitation tunnel at the University of Tokyo were conducted at a rotational speed, n, of 20 rps. Tests were conducted at a number of advance coefficients for pressures ranging from $P_A/P_{ATM} = 1.09$ to $P_A/P_{ATM} = .161$, associated with

cavitation numbers from $\sigma_{nD} = 13.5$ to $\sigma_{nD} = 1.8$, respectively. The tests were conducted at a gap ratio of G/D = 0.01 and a cut depth ratio of H/D = 0.25.

ii) Towing Tank

Tests in blocked flow conducted in the towing tank at Memorial University were run at the same conditions as those tests conducted in uniform flow: the rotational speed was n = 22 rps and the advance coefficient, J, was varied by changing the carriage speed. The tests in the towing tank were were run over a range of values of both the gap ratio, G/D, and the cut depth ratio, H/D.

4.2.2.1.2 Results

i) Effects of Blockage

Figure 4-10 presents the mean values of thrust and torque coefficients versus the advance coefficient for tests conducted in blocked flow. The tests were conducted at an ambient tunnel pressure of $P_A/P_{ATM} = 1.09$, the non-cavitating condition. The associated cavitation number was $\sigma_{nD} = 13.5$. Polynomial curves are plotted through the data using least squares curve fits. The lines fitted to the uniform flow data presented in Figure 4-9 are repeated for comparison.

The operation of the propeller in blocked flow resulted in an increase in the coefficients of both thrust and torque over the full range of advance coefficients examined. At an advance coefficient of J = 0.2, the lowest advance coefficient tested in blocked flow, thrust was increased from $K_T = 0.28$ to $K_T = 0.41$; torque was increased from $K_Q = 0.034$ to $K_Q = 0.046$. At the highest advance coefficient, J = 0.7, thrust was increased from $K_T = 0.09$ to $K_T = 0.27$ and torque was increased from $K_Q = 0.016$ to $K_Q = 0.033$. The

difference between uniform flow and blocked flow results became larger as the advance coefficient increased, indicating hydrodynamic loads due to blockage are insensitive to the velocity of the water flowing past the block.

ii) Effects of Blockage Ratio

Figure 4-11 and Figure 4-12 present results of experiments conducted in the towing tank with two different blockage cut depths, 25 mm and 50 mm (H/D = 0.125 and H/D = 0.25, respectively). Again, polynomial curves were fitted to the data. In each case the polynomial curves fitted to uniform flow data measured in the towing tank as shown in Figure 4-9 are presented for comparison.

Blockage caused an increase in propeller loading for both cut depth ratios across the full range of advance coefficients, except for the test at an advance coefficient of J = 0.7 and H/D = 0.125. At the lowest tested advance coefficient, J = 0.2, the thrust coefficient increased from $K_T = 0.28$ in uniform flow to $K_T = 0.31$ and $K_T = 0.41$ for the 25 mm and 50 mm blockage depths, respectively. At this advance coefficient, the torque coefficient increased from $K_Q = 0.034$ in uniform flow to $K_Q = 0.038$ in the case of a 25 mm blockage and $K_Q = 0.047$ with the blockage depth of 50 mm. At the highest advance coefficient, J = 0.7, the thrust coefficient in uniform flow was $K_T = 0.09$ and the torque coefficient was $K_Q = 0.016$. Similar to lower speeds of advance, the 50 mm blockage resulted in an increase in both the thrust and torque coefficients, to $K_T = 0.25$ and $K_Q = 0.032$. However, the 25 mm cut depth case resulted in a reduction of the mean load on the propeller. The thrust coefficient dropped to $K_T = 0.05$ and the torque coefficient dropped to $K_Q = 0.011$. Since there is no data available for the wake behind the blockage

during these experiments. it is difficult to explain fully the reason for the large drop in the smaller blockage case, however it is thought to be as a result of ventilation behind the block at high speed, since in the case of the reduced blockage, the bottom surface of the block was closer to the free surface of the water. A similar reduction was seen in the results from tests with a two millimeter gap, and consistent results are apparent in the records of both the thrust and torque coefficients for the two series of tests. In any case. the drop occurs at high speed, outside the range of icebreaking operations.

iii) Effects of blockage on tunnel results

Figure 4-13 presents the results of tests in both the cavitation tunnel and the towing tank for similar conditions. The towing tank results are from test series with gaps of both G/D = 0.005 and G/D = 0.01. For that series. the figure presents the average of four data points conducted in the same nominal condition; difficulties in exactly establishing the gap resulted in a substantial difference between the high and low values. since the gap ranged from around one to about two millimeters.

The figure shows a reasonable correlation between the minimum test results from the towing tank and the cavitation tunnel. While there is scatter associated with difficulties in establishing the gap ratio in towing tank tests, the tank results closely follow the trend of the tunnel results. The minimum value results (for a gap ratio of G/D = 0.01) are almost identical to the cavitation tunnel results, with the exception of the values measured at the highest advance coefficient. Other than at that point. the maximum difference of K_Q was 0.0008; the analogous differences in K_T was 0.004. Similarly to the case in uniform flow, the figure indicates that there is no need to correct the cavitation

tunnel results for effects associated with the installation of the bluff body blockage since the LDV velocity measurement were independent of blockage effects.

iv) Effects of Proximity

Figure 4-14 presents the relationship between the proximity of the ice block to the propeller and the mean performance of the propeller. In this figure the horizontal axis gives the gap ratio, G/D. Again, the vertical axis gives the values of the thrust coefficient, K_T, and the torque coefficient, $10K_Q$. All tests presented in the figure were done at an advance coefficient of $J = 0.4$ with a blockage cut depth ratio of $H/D = 0.25$. For comparison, the values of the thrust and torque coefficients in uniform flow at the same advance coefficient are plotted as horizontal lines.

The figure again shows blockage resulted in elevated mean values of the thrust and torque coefficients over uniform flow values. However, it further indicates the increased loading can be considered to have two main components. The first was a fixed increase due to the operation of the propeller in the wake of the blockage. The second component was a wall effect which is a non-linear function of the gap between the blade and the block surface; the so-called proximity effect.

In blocked flow, the upper part of the propeller operated in the slow fluid of the separated wake of the blockage. This resulted in an effective decrease of the local advance coefficient of the blade sections and an associated increase in thrust and torque coefficients. Although the wake structure does vary with distance from the block, the increase in load associated with this reduced mean axial wake flow can be considered to be the difference between the horizontal lines representing the thrust and torque

coefficients in uniform flow, with $K_T = 0.21$ and $K_Q = 0.028$, and the values measured in blocked flow at gaps equal to or greater than 10 mm, $K_T = 0.25$ and $K_Q = 0.033$: increases of about 19% and 18% over uniform flow values, respectively.

As the distance between the propeller and block was reduced, the flow velocity over the back of a given blade increased due to the operation of the blades in close proximity to the solid boundary of the block. The increased flow speed resulted in decreased fluid pressure and, as a result, increased thrust and torque. This is seen in Figure 4-14 where the gap ratio was less than about 0.05. While experimental scatter, as discussed above in Section 4.2.2.1.2.iii, precludes stating an exact value, the increases were up to a level between 65% and 75% higher than the uniform flow values for both the thrust and torque coefficients.

The mounting apparatus resulted in an accuracy in the distance between the propeller and the block of about ±0.5 mm. This was not a concern in tests where the gap was not varied or when the gap was greater than five millimetres, in which cases the uncertainty was small in comparison to the total distance. It did have an effect when the gap ratio was less than or equal to G/D = 0.01. As is seen in the Figure 4-14, two tests with a nominal gap of one millimetre (G/D = 0.005) resulted in differences in thrust and torque coefficients of $\Delta K_T = 0.024$ and $\Delta K_Q = 0.046$.

v) Effects of Cavitation on K_T and K_Q

Figure 4-15 and Figure 4-16 show the thrust and torque coefficients against advance coefficient over the range of cavitation numbers examined. Figure 4-15 shows the change in the thrust coefficient as tunnel pressure was reduced from $\sigma_{nD} = 13.5$ to $\sigma_{nD} = 1.8$. Figure 4-16

gives the analogous information for the torque coefficient. The results for thrust and torque coefficients for the noncavitating condition presented in Figure 4-10 are included. Axes in the two figures again show the load coefficients on the vertical axis and the advance coefficient on the horizontal axis.

With the exception of torque coefficient measurements at $\sigma = 8.2$, the effect of decreased cavitation number, and subsequently increased cavitation, on mean propeller performance was a reduction in both the thrust and torque coefficients over the full range of advance coefficients. At $J = 0.2$, average thrust dropped from $K_T = 0.41$ at $\sigma_{nD} = 13.5$ to $K_T = 0.26$ at $\sigma_{nD} = 1.8$. At the same time, torque decreased from $K_Q = 0.046$ to $K_Q = 0.035$. Similarly, at an advance coefficient of $J = 0.7$, thrust dropped from $K_T = 0.27$ to $K_T = 0.14$ and torque decreased from $K_Q = 0.033$ to $K_Q = 0.022$. At a slightly reduced cavitation number, $\sigma_{nD} = 8.2$, minimal cavitation resulted in a slight increase in the torque coefficient and no noticeable change in the measured values of thrust. This is similar to the effects of cavitation in uniform flow where the initial development of a cavity increases the form drag of the foil section by effectively increasing its thickness but with no analogous effect on section lift.

To illustrate more clearly the effect of reduced pressure on mean performance, Figure 4-17 through Figure 4-22 present the same data, but with the thrust and torque coefficients, plotted against cavitation number. In each of the figures the thrust and torque coefficients, K_T and $10K_Q$, are presented on the vertical axis and the cavitation number, σ, is plotted on the horizontal axis. All data points presented on a given figure were recorded at the same advance coefficient.

At high cavitation numbers, say for $\sigma_{nD} > 5.0$, the propeller performance showed only a limited sensitivity to changes in cavitation number. In the range of $3.0 < \sigma_{nD} < 5.0$, coefficients of thrust and torque showed the greatest rate of change with respect to changes in pressure. At values less than $\sigma_{nD} = 3.0$, the sensitivity to cavitation number was again reduced.

For example, at an advance coefficient of $J = 0.4$, shown in Figure 4-19, the rate of change of the thrust coefficient with respect to cavitation number was lowest between $\sigma_{nD} = 13.5$ and $\sigma_{nD} = 8.2$, with $\Delta K_T/\Delta\sigma_{nD} = 0.000$. Between $\sigma_{nD} = 3.3$ and $\sigma_{nD} = 4.2$, $\Delta K_T/\Delta\sigma_{nD} = 0.033$, which was the maximum value achieved. Within the range from $\sigma_{nD} = 2.6$ to $\sigma_{nD} = 1.8$, the rate of change of the thrust coefficient had dropped to $\Delta K_T/\Delta\sigma_{nD} = 0.019$. The torque coefficient showed a similar trend, going from $\Delta K_Q/\Delta\sigma_{nD} = -0.0003$ in the first interval to $\Delta K_Q/\Delta\sigma_{nD} = 0.0038$ in the second and reducing again to $\Delta K_Q/\Delta\sigma_{nD} = 0.0011$ in the third.

At the full scale, the shaft rotational speeds of R-Class icebreakers during icebreaking operations range from N = 120 to N = 170 rpm (Williams et al., 1992; Michailidis and Murdey, 1981). Such rates result in cavitation numbers from about $\sigma_{nD} = 4.0$ to around $\sigma_{nD} = 2.0$, respectively; these numbers are within the region of reduced performance due to cavitation. Full scale blockage of an open propeller is often associated with milling contact between the propeller and the obstructing blockage. Since reductions in thrust and torque due to cavitation occur as a result of such blockages, milling loads are coincident with reduced hydrodynamic loads. The effect is an increase in the overall aftwards directed load on the propeller; the sum of the aftwards directed contact force and the reduction in the forward directed hydrodynamic load. For example, at a full scale rotational speed of N = 160 and an advance coefficient of J = 0.2, a reduction in the thrust coefficient of 0.15 as a result of cavitation corresponds to a drop

in full scale hydrodynamic thrust of around 300 kN. In unblocked flow, at similar operating conditions, the propeller would develop around 600 kN of thrust. In this case, the increase in aftwards directed load due to cavitation is about one half the magnitude of the thrust that would be developed by the propeller in unblocked flow.

vi) Patterns of Cavitation

Typical cavitation patterns visible on an open propeller in blocked flow have been described in detail above and the forms of cavitation incident on the R-Class propeller were consistent with those results. Figure 4-23 shows the nature of cavitation incident on the propeller blade as it passes into and out of the milled recess of the blockage at an advance coefficient of $J = 0.2$ and a cavitation number, σ_{nD}, of 1.8. A horizontal line has been drawn at the location of the lower edge of the blockage recess. While the most severe cavitation was visible at this advance coefficient and cavitation number, cavitation was visible in each test.

Prior to entering the separated flow behind the blockage, a leading edge sheet cavity was visible on the blade, beginning at $r/R = 0.9$. This merged with a tip vortex cavity, forming a twisted core downstream. As the blade entered the recess, a vortex cavity formed between the blade and the block within the area of overlap. Progress of the blade across the recess resulted in the vortex cavity becoming unstable. The cavity had begun to break down into cloud cavitation by the time the blade had reached an angle of $\phi = 45°$. At an angle of $\phi = 90°$, when 60% of the blade was in the recess, severe cloud cavitation fully covered the obstructed area of the blade and filled the region between the back of the reference blade and the face of the subsequent blade. As the blade returned to unobstructed flow outside the wake of the

block. the cloud cavitation dissipated and patterns seen prior to the blade entering the blockage recess were again visible on the propeller.

vii) Effect of Cavitation on K_B

Figure 4-24 gives the nondimensional block load, measured simultaneously with the results presented in Figure 4-15 and Figure 4-16 using a three axis load cell. The figure includes the effects of both the bluff body drag resulting from the flow of water past the block and the suction effects of the nearby propeller for the range of cavitation numbers tested. The horizontal axis again presents the advance coefficient, J. The vertical axis presents the nondimensional block load coefficient, K_B. where the block load coefficient is presented as positive in the downstream direction and is defined as:

$$K_B = F/(\rho n^2 D^4),$$

Total block load increased as the advance coefficient increased. but decreased as the cavitation number was reduced. The figure shows that at $\sigma = 13.5$. block load increased from $K_B = 0.25$ at $J = 0.2$ to $K_B = 0.37$ at $J = 0.7$. Similarly at $\sigma = 1.8$. block load increased from $K_B = 0.11$ to $K_B = 0.19$ for the same advance coefficients. The level of total block load was comparable in magnitude to the thrust developed by the propeller. At a cavitation number of $\sigma = 13.5$ and an advance coefficient of $J = 0.52$, the block load coefficient was equal to the propeller thrust coefficient of about $K_T = 0.31$: at this point, the total system thrust of the propeller combined with the block ($K_T + K_B$) was zero.

viii) Block loads and efficiency

Figure 4-25 again presents the performance of the propeller in blocked flow at the highest cavitation number. The vertical axis shows the coefficients of thrust, torque and

block load as well as the propeller efficiency, η_o. Efficiency was calculated using the combined load of the propeller thrust and block load coefficients. The addition of blockage loads to the overall thrust equation resulted in a dramatic reduction in the performance of the propulsion system. At this cavitation number, $\sigma = 13.5$, the maximum efficiency over the range of advance coefficients tested was $\eta_o = 0.128$. In comparison, the peak efficiency of the propeller in uniform flow was $\eta_o = 0.60$. Efficiency dropped to zero as the total mean system thrust decreased to zero at $J = 0.52$. This is consistent with discussions in earlier literature (Laskow, 1988; Walker et al., 1993) where it was suggested that while blockage resulted in higher propeller efficiency, total propulsion system efficiency would likely be decreased. Similarly, the performance at lower cavitation numbers in blocked flow was poor.

ix) Block Load vs. Thrust

Figure 4-26 presents the nondimensional block load with the mean fluid drag on the block subtracted from the total measured load. The axes present the same parameters as in Figure 4-24. It is assumed that the modified block load coefficient results only from the operation of the nearby propeller. This gives an indication of the loading on the propeller blades when they were adjacent to the block and provides additional insight to the results presented in Figure 4-15 and Figure 4-16, which showed the mean performance of the entire propeller.

Comparison of Figure 4-26 with Figure 4-15 shows that reductions in the block load coefficients due to cavitation are coincident with almost identical drops in the thrust coefficient. At an advance coefficient of $J = 0.2$, the block load coefficient dropped by

$\Delta K_B = 0.14$. from $K_B = 0.24$ at $\sigma = 13.5$ to $K_B = 0.10$ at $\sigma = 1.8$. This compares with a drop in the thrust coefficient by $\Delta KT = 0.14$. from $K_T = 0.41$ at $\sigma = 13.5$ to $K_T = 0.26$ at $\sigma = 1.8$. At an advance coefficient of $J = 0.7$, the block load coefficient dropped by $\Delta K_B = 0.18$. from $K_B = 0.27$ at $\sigma = 13.5$ to $K_B = 0.09$ at $\sigma = 1.8$. Analogously, the thrust coefficient dropped by $\Delta K_T = 0.13$, from $K_T = 0.27$ at $\sigma = 13.5$ to $K_T = 0.14$ at $\sigma = 1.8$. The majority of the reduction in thrust on the propeller, then, occurred within the region of the propeller disk subtended by the blockage and measurements of changes in block load are indicative of changes in the load on the propeller.

4.2.2.2 Dynamic Effects

i) Effects of cavitation in blocked flow

The mean results only present a partial description of the loading regime in which a propeller blade operates as it enters and exits the blocked region. To illustrate the unsteady loading associated with blockage, time domain records of the block load coefficient can be assessed. For each test condition examined, propeller thrust and torque and block load were measured during a 1.6 second period which was started when a reference blade was about to enter the milled recess of the block. Figure 4-27 shows a series of five angular positions of the propeller, where $\phi = 0°$ is the angular position at which a propeller blade is about to enter the milled recess and $\phi = 90°$ represents a quarter rotation of the propeller, when the subsequent blade is at the same position. Figure 4-28 presents the wake behind the blockage. It was measured 24.5 mm downstream of the block using the laser doppler velocimeter, and illustrates the flow regime in which the propeller was operating.

Time domain records of the block load coefficient at an advance coefficient of $J = 0.4$ and cavitation numbers of $\sigma = 13.5$ and $\sigma = 1.8$ are presented in Figure 4-29. At the higher cavitation number, the mean value was $K_B = 0.25$. The variation about the mean value was approximately ± 0.1. Consistent with results shown in Figure 4-26, reduced cavitation numbers resulted in reduced block load: the average block load coefficient at $\sigma = 1.8$ in Figure 4-29 was $K_B = 0.09$. However, at this lower cavitation number the variation about the mean increased dramatically to around ± 0.23. Results were analysed for each cavitation number and advance coefficient tested and it was seen that the oscillation about the mean value progressively increased as pressure was reduced from the highest cavitation number to the lowest and the same trend was apparent in the results at each advance coefficient.

Less clear in Figure 4-29 is an apparent phase shift between time domain records of the block load coefficients at $\sigma = 13.5$ and $\sigma = 1.8$. To illustrate this more clearly Figure 4-30 shows the block load coefficient versus the angular orientation of the propeller for the same advance coefficient and cavitation numbers as presented in Figure 4-29. The vertical axis again shows the coefficient, K_B. The horizontal axis presents the orientation of the propeller, from $\phi = 0°$ to $\phi = 90°$. For each cavitation number, three curves are shown on the figure. The middle curve represents the instantaneous average of the block load coefficient calculated from 127 load measurements recorded when the propeller was at that angular position. The upper and lower curves show the range within which fell 95% of the measurements used in the calculation of the mean.

During the first half of the quarter rotation at a cavitation number of $\sigma = 13.5$, the average block load coefficient was $K_B = 0.20$, slightly under the full record mean of $K_B = 0.25$. During the second half of the quarter rotation, the average block load coefficient was $K_B = 0.30$, slightly above the full record mean. Alternatively, at a cavitation number of $\sigma = 1.8$, the average block load coefficient during the first half of the quarter rotation, $K_B = 0.15$, was above the mean value of $K_B = 0.09$, while during the second half, the average value of $K_B = 0.04$ was below the record mean. At the lower cavitation number, the instantaneous values of the block load coefficient during the first half of the quarter rotation of the propeller were slightly less than those for the higher cavitation number. During the second half of the quarter rotation, the instantaneous values of the block load coefficient were dramatically less at $\sigma = 1.8$ than at $\sigma = 13.5$.

The difference in phase between the results at high and low cavitation numbers can be explained by a comparison of Figure 4-27, showing the angular orientation of the propeller, with Figure 4-28, which shows the flow regime in which the propeller operates. At an angle of $\phi = 22.5°$, the midpoint angle in the first half of the quarter rotation, the reference blade had not reached the region of minimum flow speed shown in Figure 4-28. The preceding blade had already passed beyond that region. However, when the reference blade was at $\phi = 67.5°$, the midpoint in the second half of the quarter rotation, the leading edge of the blade was halfway through the region of minimum flow.

In the absence of cavitation, at $\sigma = 13.5$, the operation of the propeller blade within the region of minimum flow resulted in the development of higher suction on the blade back and an increase in the coefficients of thrust, torque and block load compared

with the previous blade position. When cavitation was present, most severely at a cavitation number of $\sigma = 1.8$, the development of increased suction and increased coefficients of thrust, torque and block load, was prevented.

Additionally, this region was coincident with violent cloud cavitation, as described in section 4.2.1.1.2 (vi). The cumulative effect, possibly caused by cavitation impact pressure on the surface of the block from the collapsing cloud cavitation, was a reduction of the measured block load coefficient in the second half of the quarter rotation to a minimum instantaneous value of $K_B = -0.05$. While the low natural frequency of the propeller dynamometer precluded measuring this load variation on the propeller itself, it is likely that a similar load modification would have occurred on part or all of the associated propeller blade.

ii) Numerical Comparisons

Numerical predictions with which these experimental results can be compared were made by Neil Bose using a potential flow panel method written by him and described in previous documentation (Bose, 1996). The time domain method can be used for the prediction of unsteady propeller performance and incorporates the effect of a proximate milled surface.

The mean lines of block load at high and low cavitation numbers presented in Figure 4-30 are repeated in Figure 4-31. Also plotted in the figure are the time series panel method predictions of the total propeller thrust coefficient, the thrust coefficient of a single propeller blade, and the sum of the thrust developed by the key blade and the preceding blade while it remains in the blockage recess. The latter prediction would most

closely represent the loading regime imposed on the blockage by the propeller. The calculation uses the assumed wake flow behind the block, described previously, and a gap of 5 mm between the ice face and the propeller. The calculations were done using a time step such that the propeller rotated ten degrees during each step and the results shown are from the third cycle after the assumed start of the motion in the calculation. Despite these differences, there are similarities between the form of the records for the predicted propeller thrust coefficient and the block load drag coefficient at the high cavitation number, $\sigma_{nD} = 13.5$.

The variation in the total of propeller thrust coefficient developed by blades within the blockage recess has roughly the same amplitude as the variation in the drag coefficient of the block. However, the variation in the thrust coefficient of the whole propeller is much lower. The peaks in the amplitude of the key blade thrust coefficient and the block drag coefficient are roughly in phase with one another.

The comparable numerical and experimental results indicate that the time domain measurement of the block load gives an indication of the unsteady nature of the loads acting on the propeller blades. In addition, results shown in Section 4.2.2.1.2(ix) showed that mean changes in propeller thrust due to cavitation are directly comparable to changes in the mean block load. As the changes between results at high and low cavitation numbers, apparent in Figure 4-30, occur only as a result of a drop in ambient tunnel pressure, the differences in the unsteady nature of the block load record were due to changes in the imposed loading regime, not by differences in the mechanical response of the measurement system. The same changes in load are imposed on the propeller blade;

cavitation resulted a dramatic reduction of thrust in the second half of the blade pass. possibly resulting in an aftward directed total hydrodynamic load.

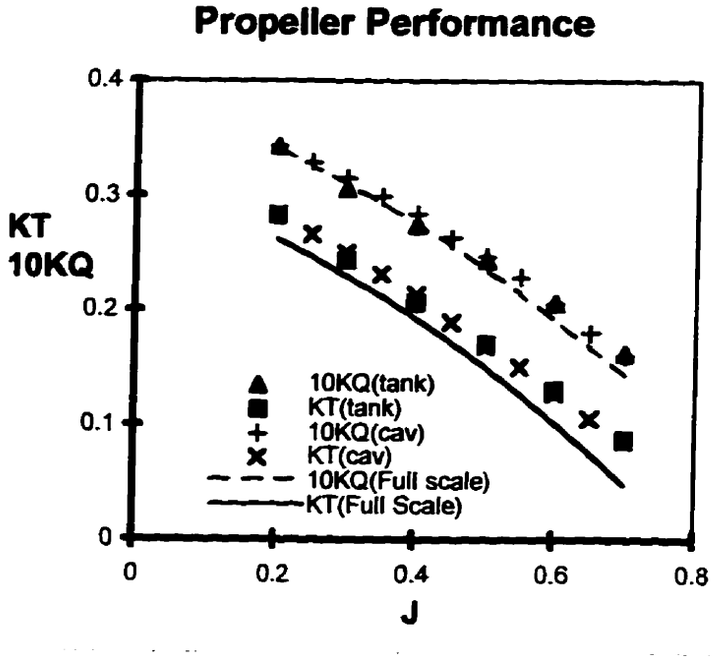

Figure 4-9 Uniform Flow Performance, R-Class Propeller

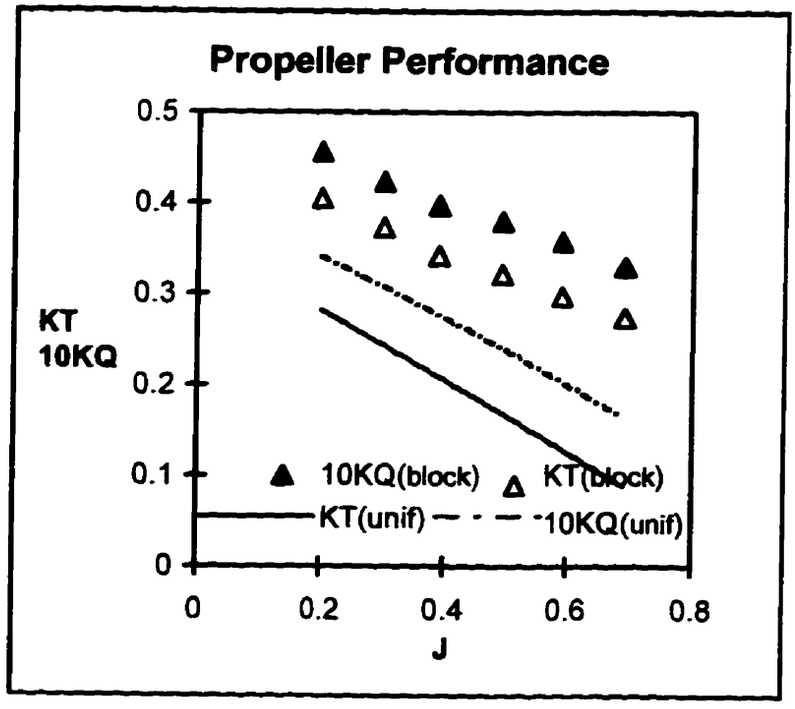

Figure 4-10 Blocked Flow Performance, R-Class Propeller

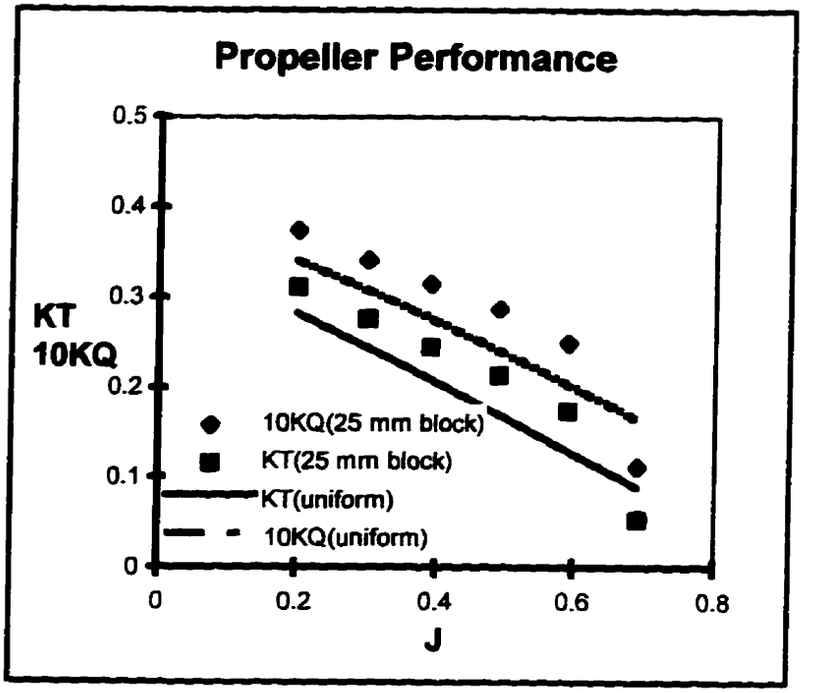

Figure 4-11 Performance in Blocked Flow, H/D = 0.125

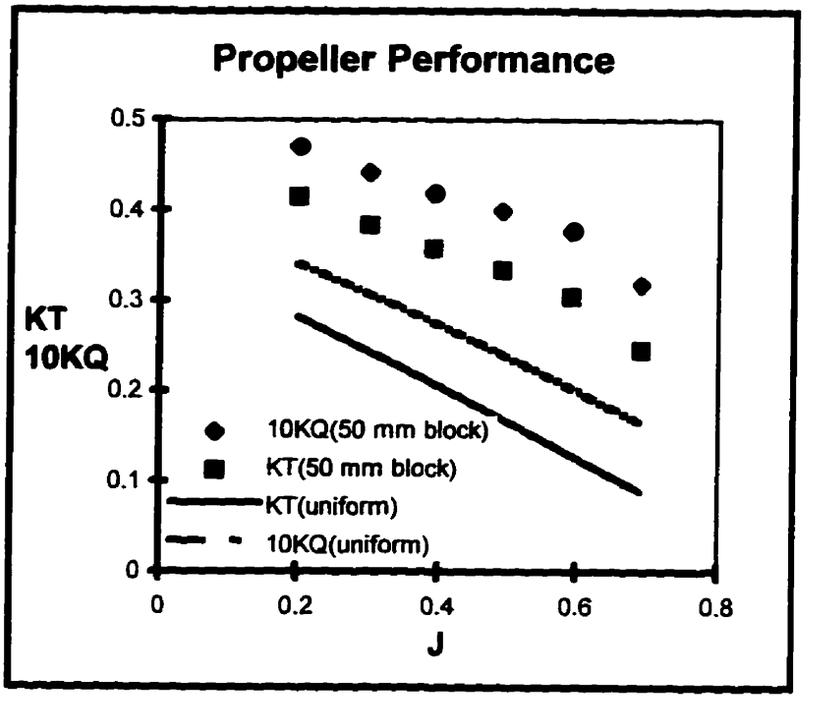

Figure 4-12 Performance in Blocked Flow, H/D = 0.25

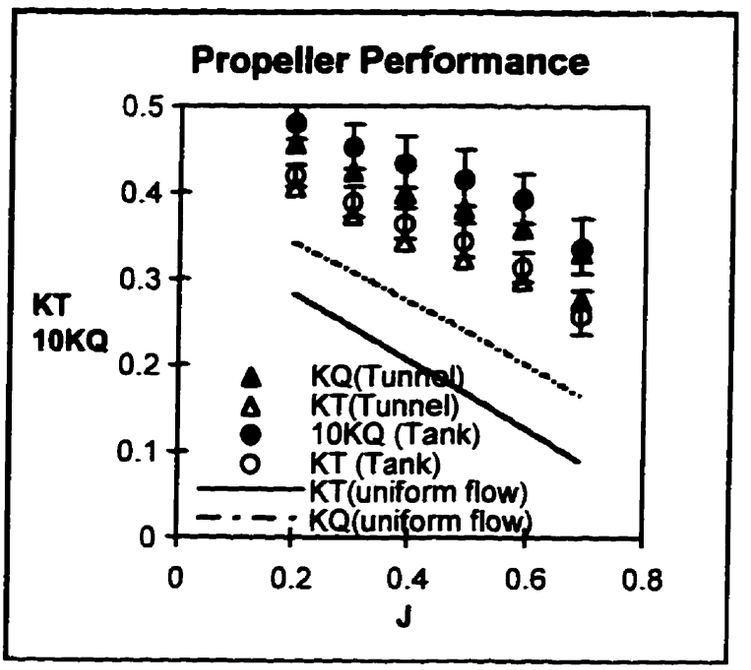

Figure 4-13 Comparison of Tank and Tunnel Results

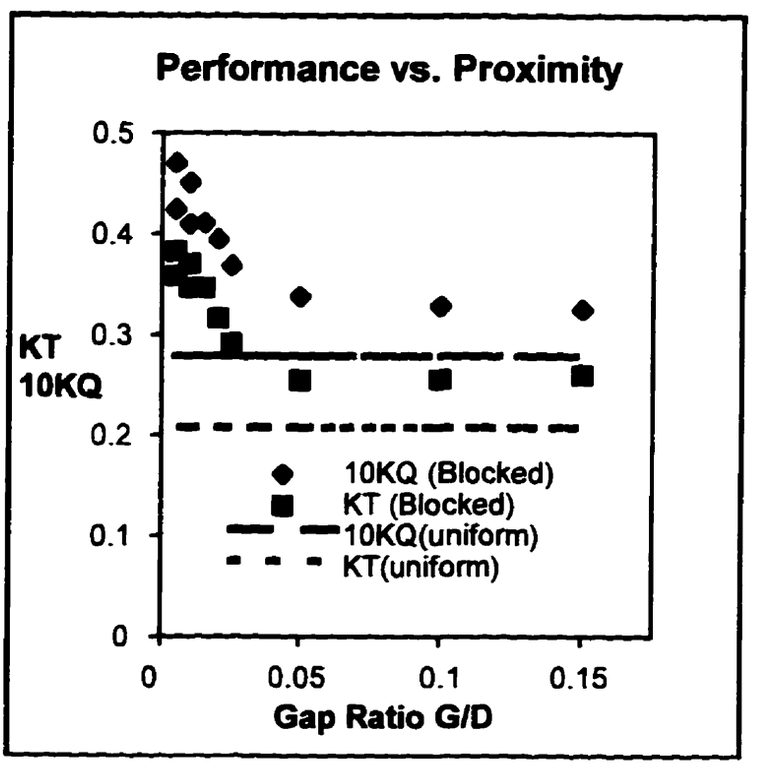

Figure 4-14 Effects of Wake and Proximity on Mean Performance

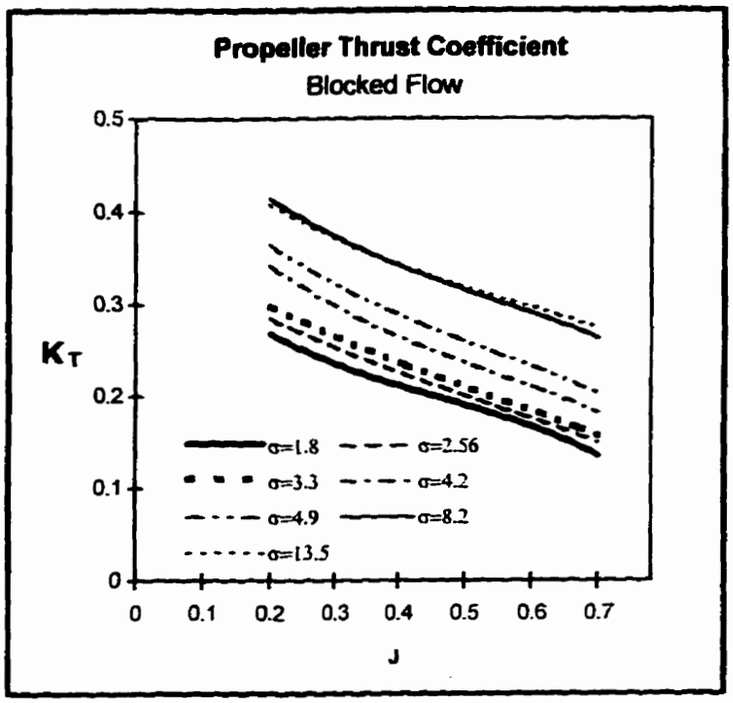

Figure 4-15 Effects of Cavitation on Thrust

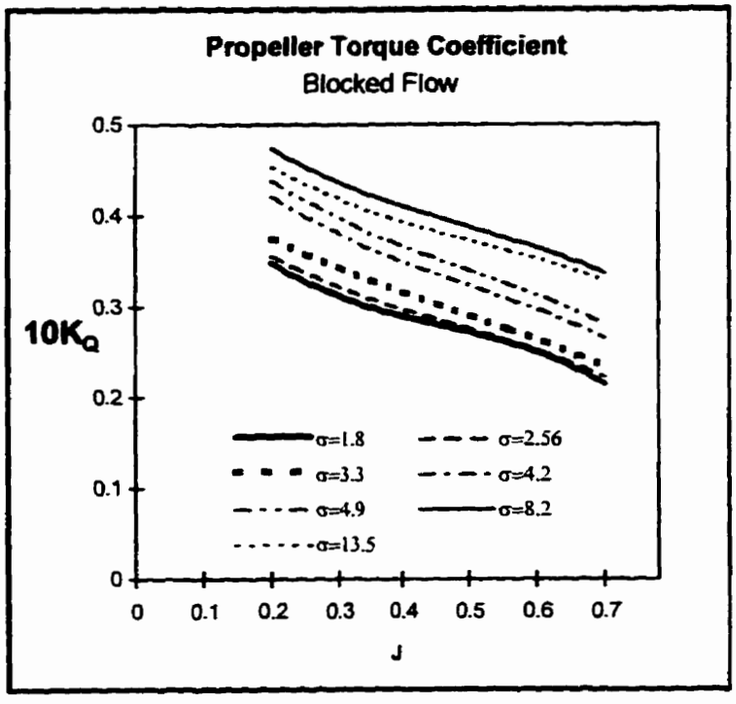

Figure 4-16 Effects of Cavitation on Torque

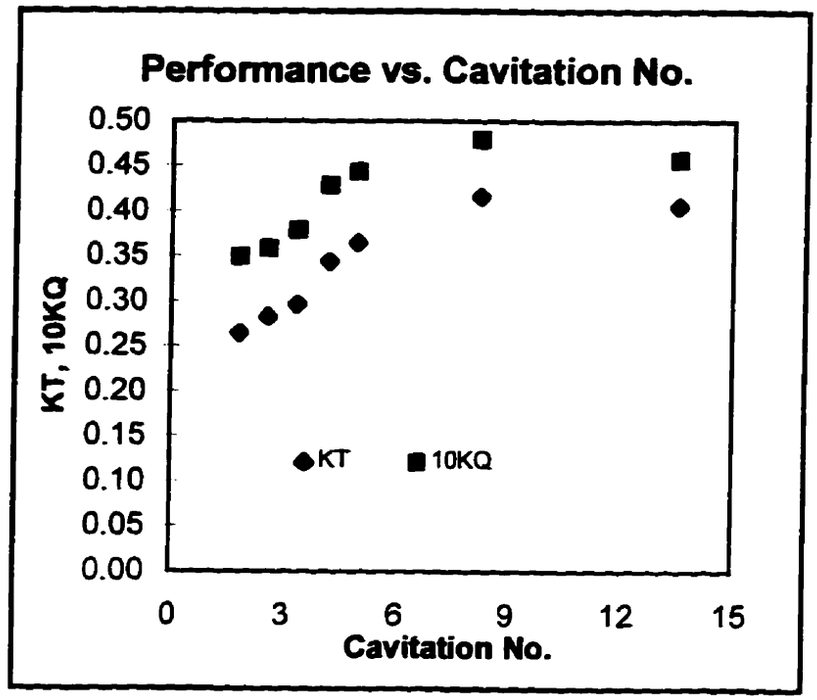

Figure 4-17 Performance vs. Cavitation Number, J = 0.2

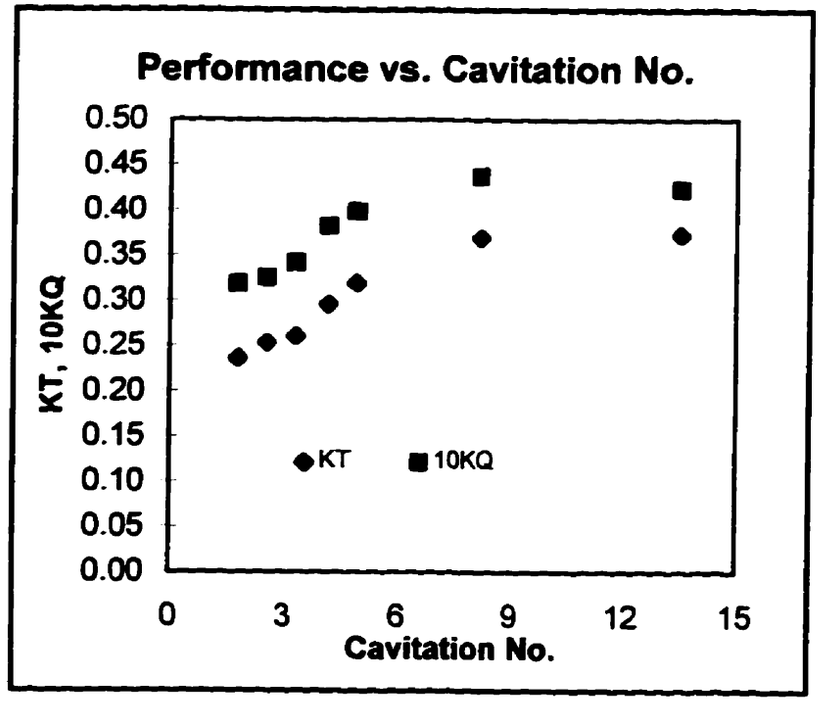

Figure 4-18 Performance vs. Cavitation Number, J = 0.3

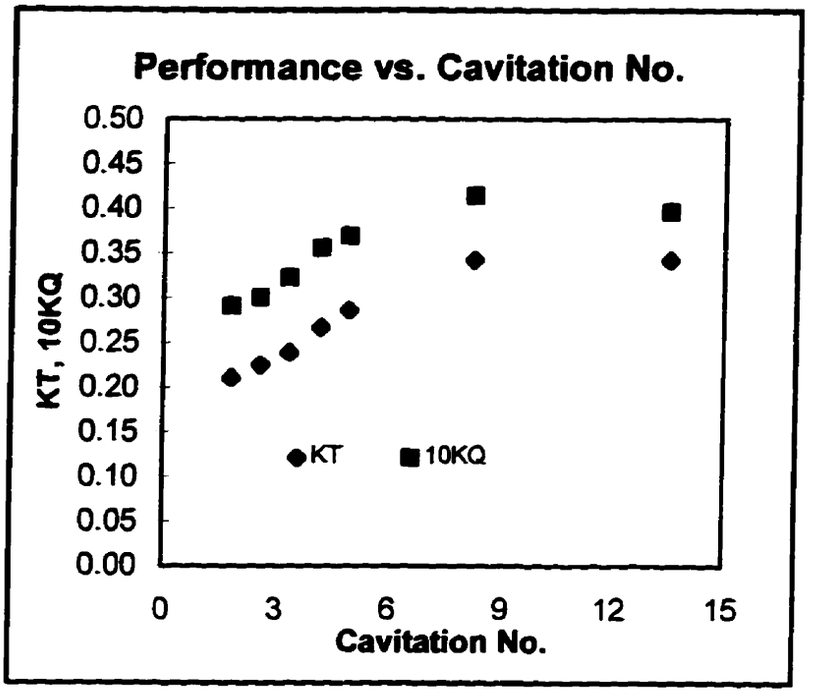

Figure 4-19 Performance vs. Cavitation Number, J = 0.4

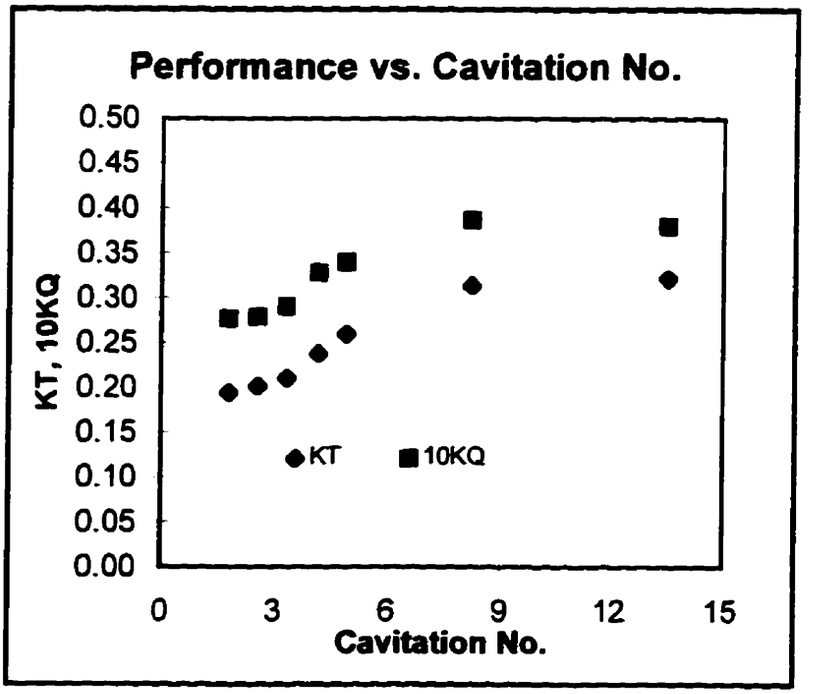

Figure 4-20 Performance vs. Cavitation Number, J = 0.5

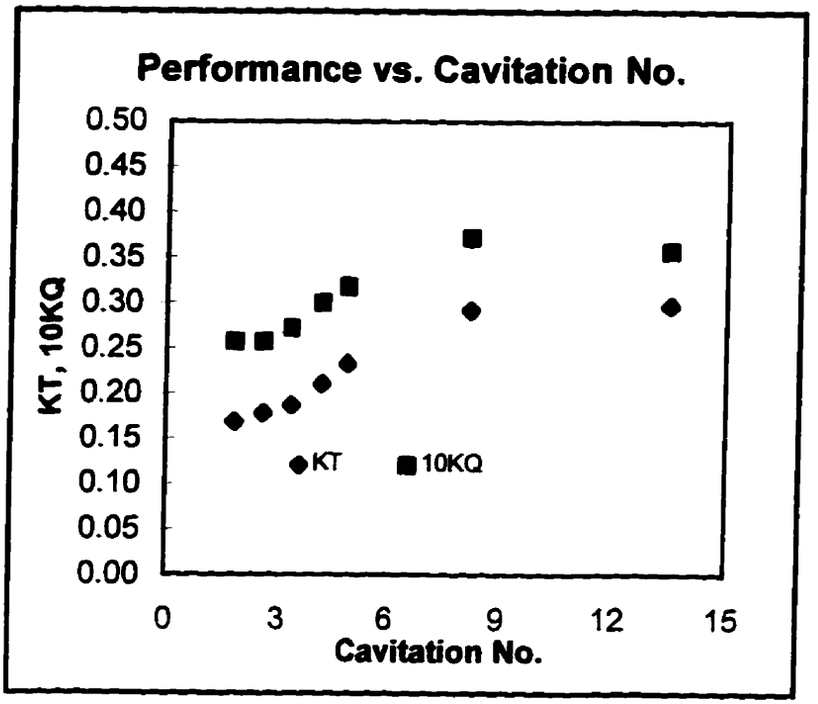

Figure 4-21 Performance vs. Cavitation Number, J = 0.6

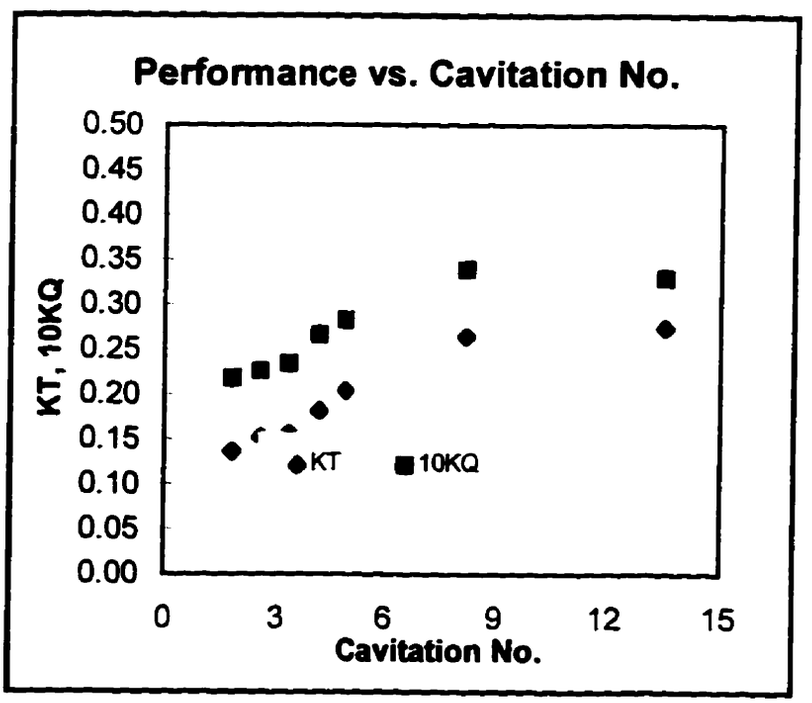

Figure 4-22 Performance vs. Cavitation Number, J = 0.7

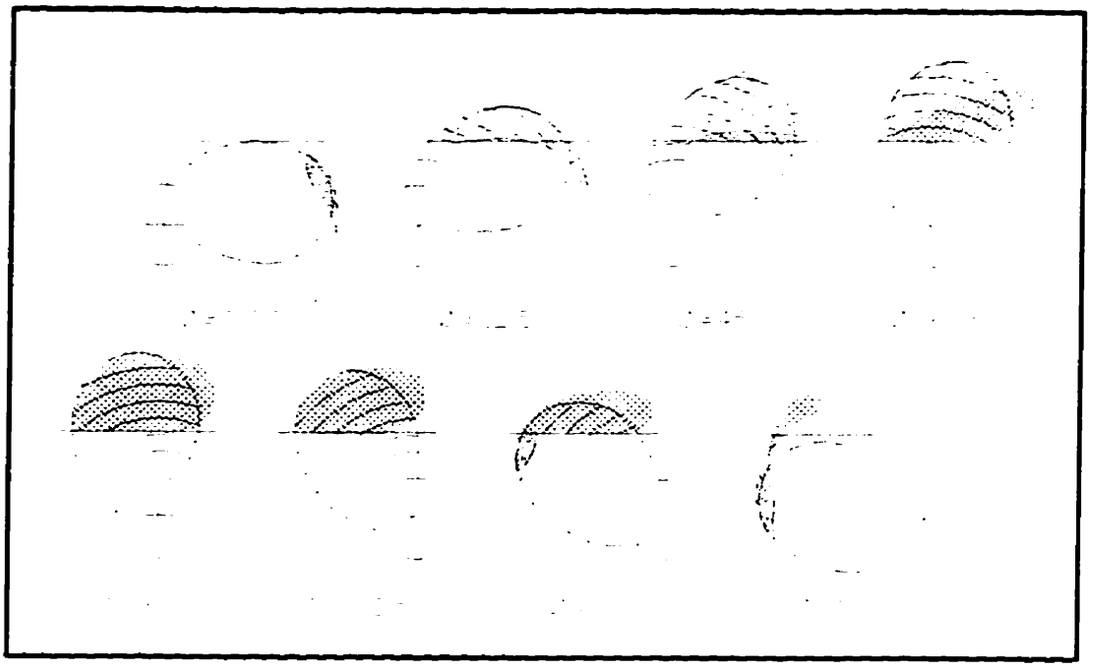

Figure 4-23 R-Class Propeller Cavitation

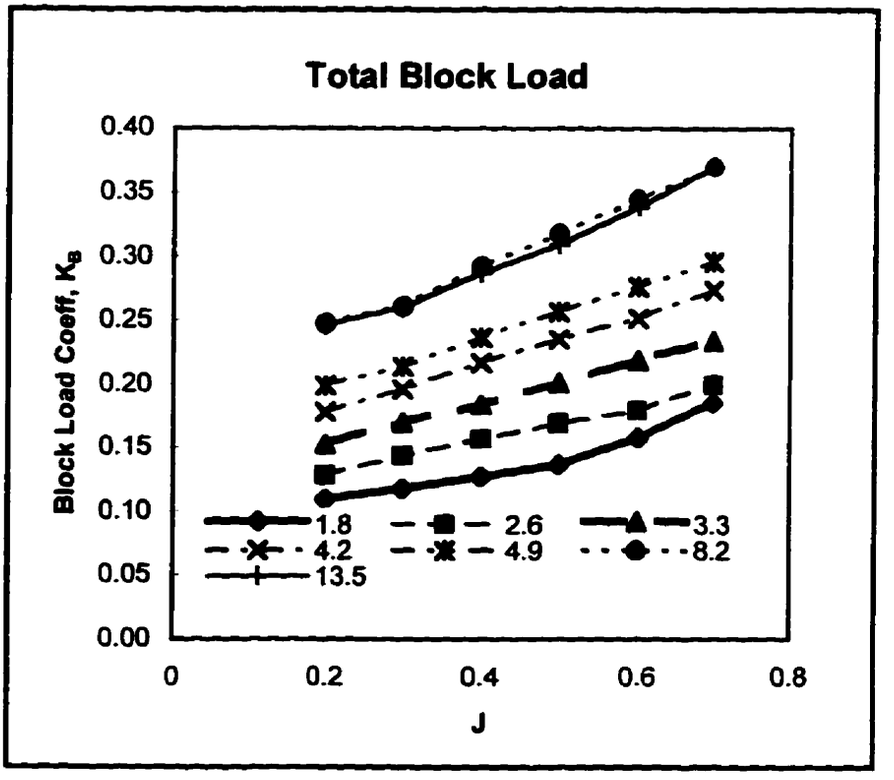

Figure 4-24 Effects of Cavitation on Block Load

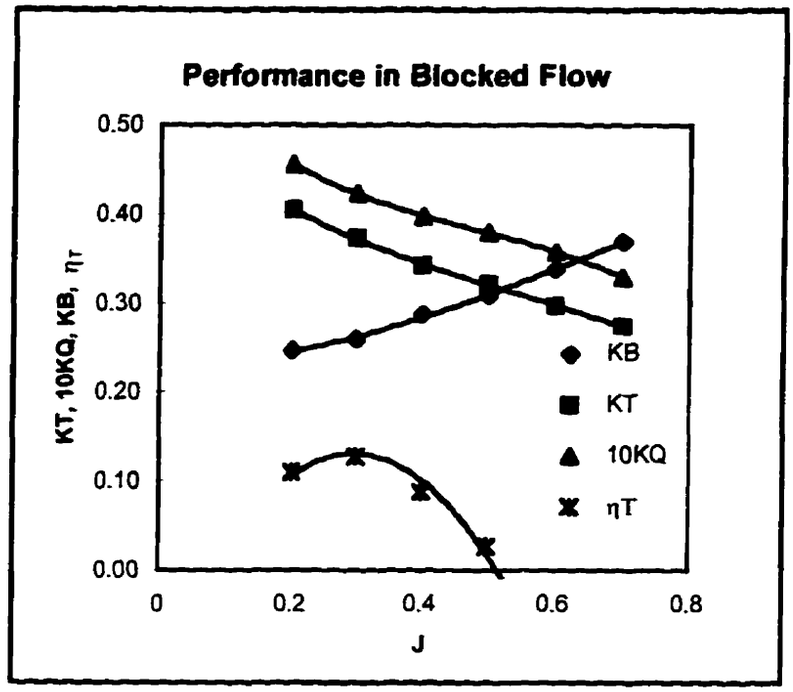

Figure 4-25 Propulsion Efficiency in Blocked Flow

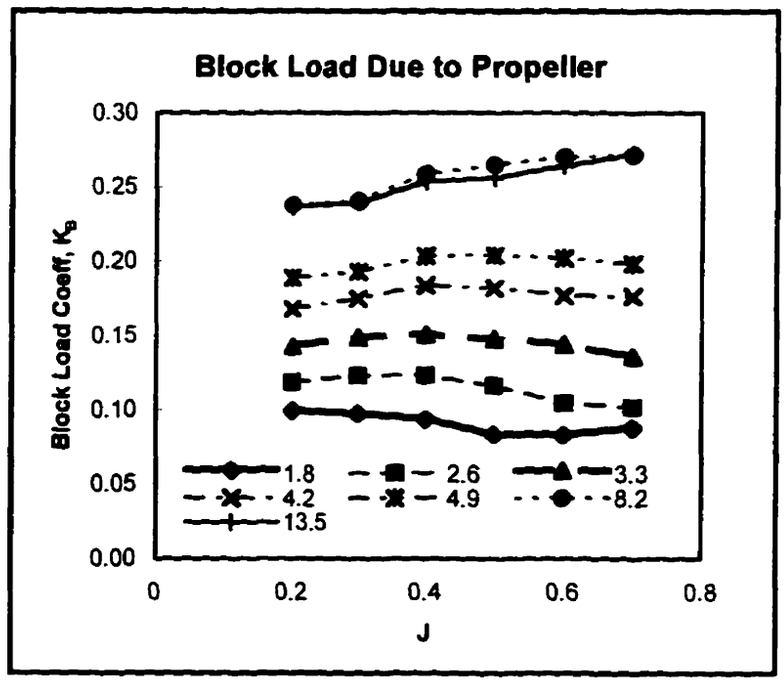

Figure 4-26 Block Load Coefficient due to Propeller Load

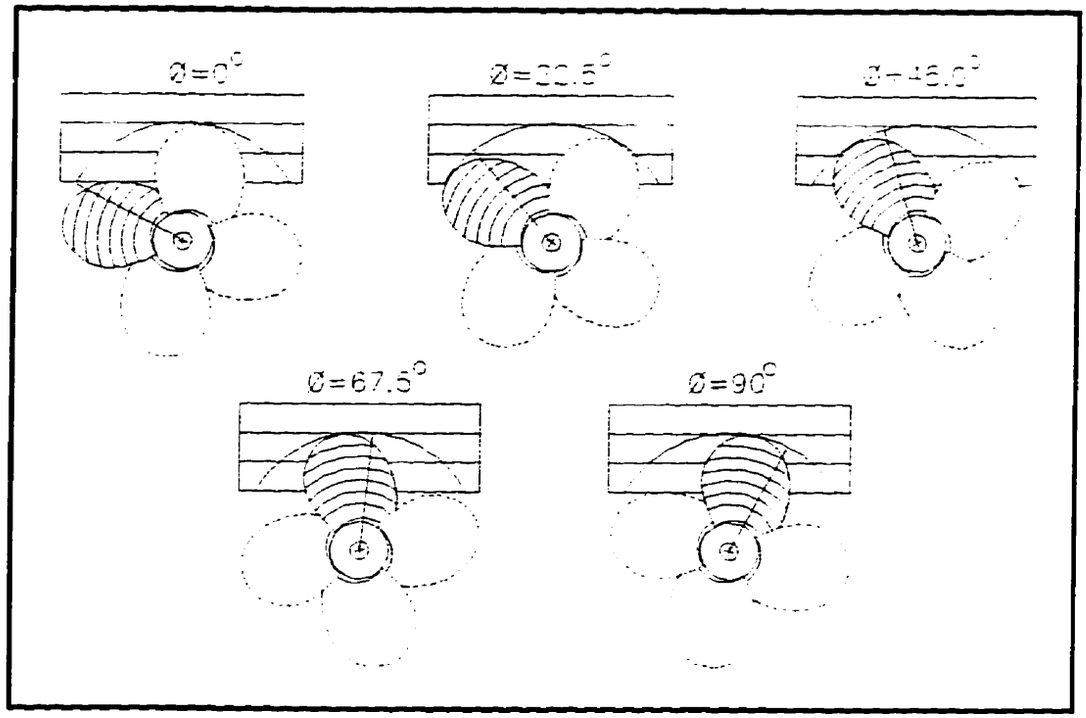

Figure 4-27 Blade Angle Orientation

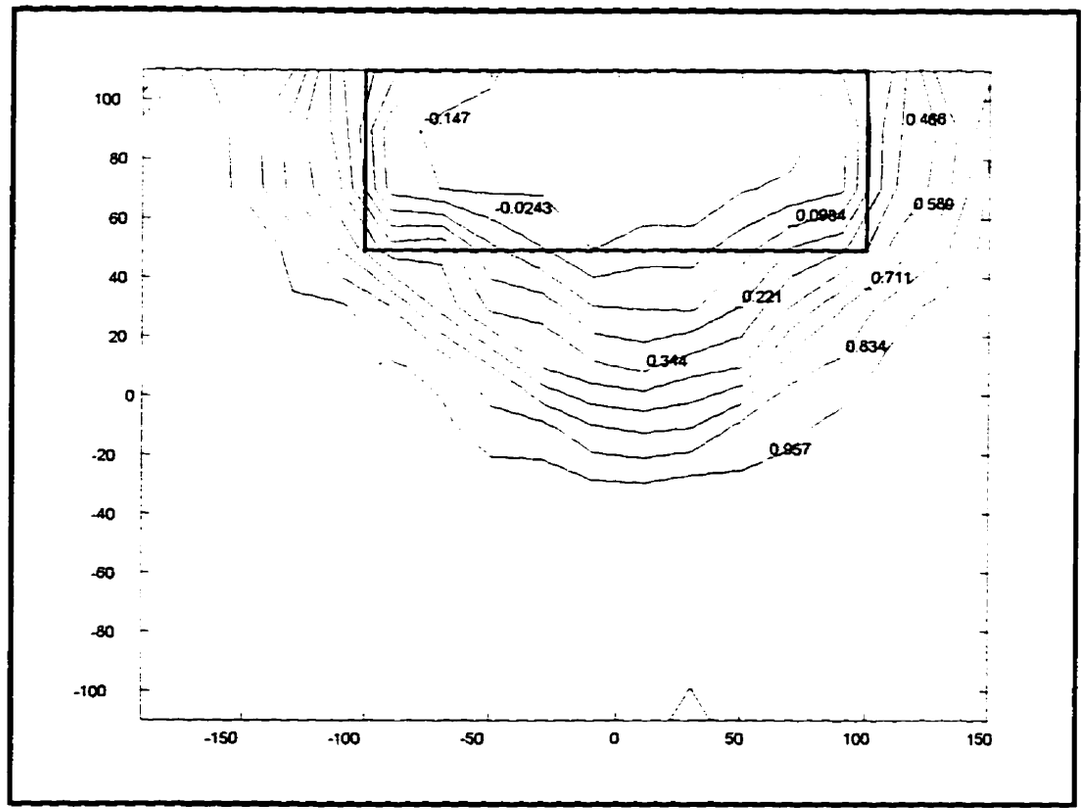

Figure 4-28 Measured Wake Behind Blockage, V_A = 1.6 m/s

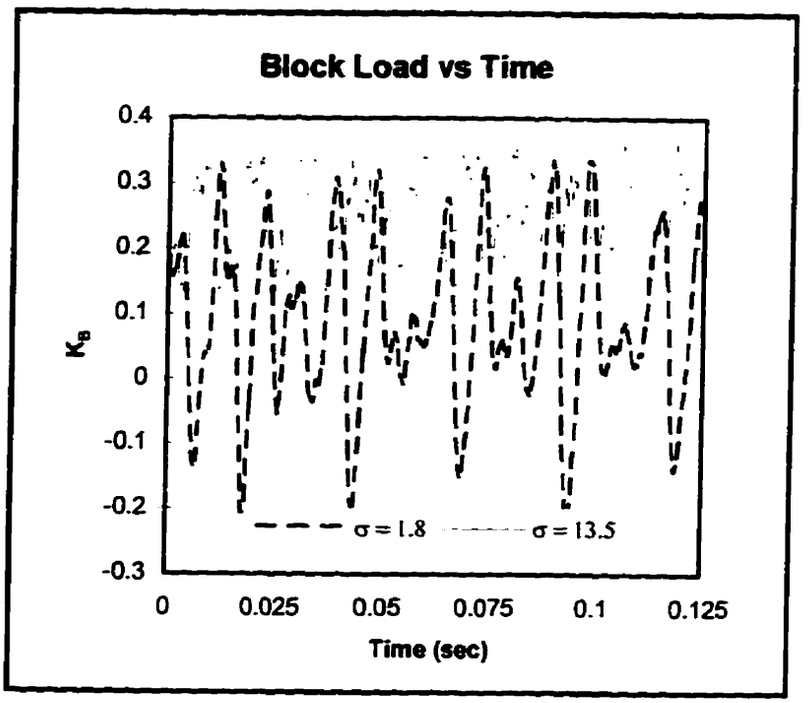

Figure 4-29 Block Load at High and Low Cavitation Numbers

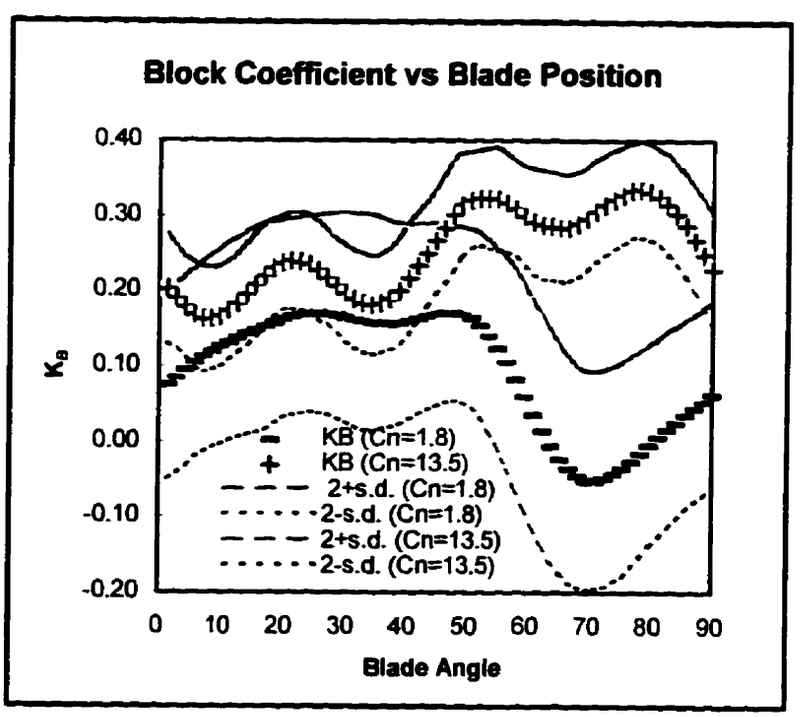

Figure 4-30 Block Load vs. Blade Position for

High and Low Cavitation Numbers

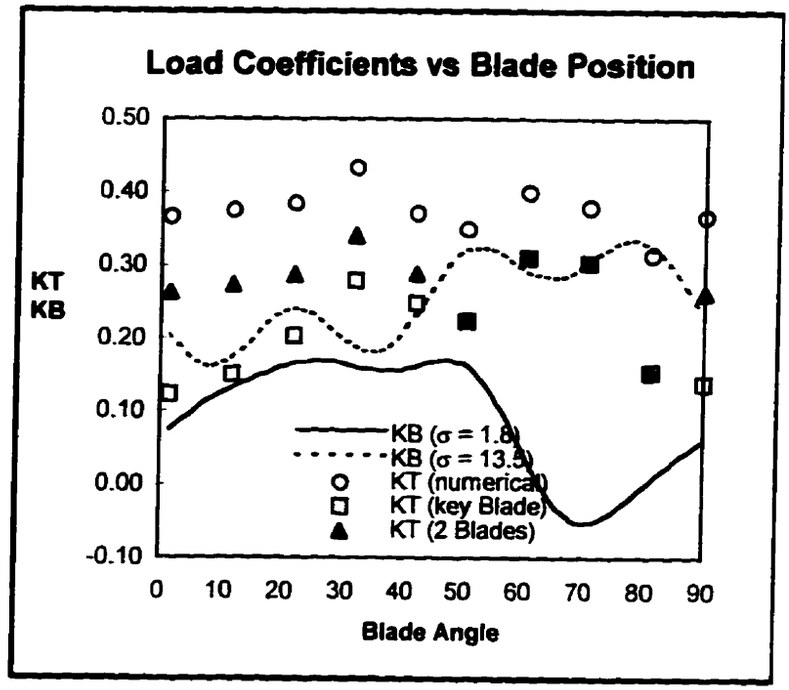

Figure 4-31 Comparison of Numerical and Experimental Results

4.3 JRPA Ducted Propellers

While the simplicity of testing an open propeller arrangment resulted in considerably more data for the open propeller case than for the ducted propeller. it is the ducted propeller configuration which is most susceptible to non-contact blockage by ice at full-scale operations. Results from the test program conducted with the ducted propellers as part the JRPA-6 did provide preliminary insight into the effects of blockage and cavitation on ducted propeller operations. In addition, comparisons with results taken from tests with open propellers indicate that conclusions drawn on the basis of results from tests with an open propeller are equally relevant for the operation of a ducted propeller in ice blocked flow.

Four series of tests were done on the ducted propellers. The higher pitch propeller. P/D = 1.17. was tested in uniform flow. In that series of experiments, measurements were taken of propeller thrust and torque and duct thrust. The results were subsequently compared to empirical estimates by van Gent and Oosterveld (1983) based on experimental results of the Ka-Series propellers. The propeller was then tested in blocked flow for three cavitation numbers, showing that the effects of cavitation were similar to those which occurred in the open propeller case. The blocked flow tests were subsequently repeated with the low pitch propeller (P/D = 0.8). Finally, the high pitch model was tested in the wake of a block in which pressure sensors were installed on the face adjacent to the propeller.

The tests with the ducted propellers and the non-instrumented blocks were done with the assistance of a work term student from Memorial, Ms. Suzanne Casey, who was responsible for recording and reducing the experimental data. The test program planning and management and the analysis of results were done by the author of this thesis.

4.3.1 Performance in Uniform Flow

4.3.1.1 Mean Loads

4.3.1.1.1 Test Conditions

Two series of tests were conducted in uniform flow at a high ambient pressure, $P_A/P_{ATM} = 1.08$, for the higher pitched propeller. The tests were done to obtain performance coefficients for comparison both with tests done in blocked flow and with standard polynomials for Kaplan series propellers (van Gent and Oosterveld, 1983). Initially, the propeller was run with a constant rotational speed, n = 10.0 rps, for a number of flow speeds to obtain results over a range of advance coefficients at a moderately high Reynolds numbers. The second series of tests were run with a constant water speed, V_A = 1.2 m/s, for a range of propeller speeds, giving data over a range of advance coefficients with operating conditions similar to those of subsequent tests in blocked flow. For each test, propeller thrust and torque were recorded using a mechanical dynamometer and duct thrust was recorded with a strain gauged mounting bracket.

The measurement of duct thrust was useful for comparison with numerical data to ensure the correct performance of the apparatus in uniform flow. However, at the full scale, an ice piece would be partially or fully supported by the duct. In the series of tests

conducted for this work. all blockages were rigidly attached to the tunnel ceiling. Duct thrust measurements in blocked flow therefore do not represent a realistic situation and are not presented.

4.3.1.1.2 Results

i) Experimental and empirical comparisons

Results from experiments with the high pitch ducted propeller in unblocked uniform flow are presented in Figure 4-32. Coefficients of propeller thrust and torque and duct thrust are plotted on the vertical axis. The advance coefficient, J, is shown along the horizontal axis. As in similar figures for open propellers presented above, polynomial curves were fitted to the experimental data. Finally, shown for comparison is the performance of a Kaplan 4-70 propeller with a MARIN Type 37 accelerating duct predicted from the Ka-series polynomials (van Gent and Oosterveld. 1983).

The experimental results for the duct thrust coefficient, K_{TD}, correspond closely with the polynomial predictions. Similarly, the maximum difference between the experimental and predicted propeller thrust coefficients, K_T, indicate a close correlation. The difference in the predicted and experimental propeller thrust coefficients increased from about $\Delta K_T = 0.01$ at the lowest advance coefficient, $J = 0.3$, to a maximum of $\Delta K_T = 0.06$ at $J = 1.0$. The measured values for the torque coefficient, however, were higher over the range of advance coefficients examined, varying from a difference of about $\Delta K_Q = 0.002$ at an advance coefficient of $J = 0.3$ to $\Delta K_Q = 0.010$ at $J = 0.8$.

Variation between experimental and numerical results can again be partially

explained by differences in the geometries of the ice class propeller models and the Ka-4.70 propeller, including hub sizes, blade thicknesses and blade area ratios: these certainly impact the experimentally measured torque coefficients. Additionally, the Ka-4.70 results were based on model tests conducted at different Reynolds numbers than those at which these experiments were conducted. Notwithstanding the differences, the experimental results compare sufficiently well with the empirical predictions to allow the use of the experimental results as a baseline against which to compare the results of tests in blocked flow.

4.3.2 Performance In Blocked Flow

4.3.2.1 Mean Loads

4.3.2.1.1 Test Conditions

Again, simulated ice blocks were installed upstream of the propeller and duct as described in Chapter 3. Improved control of the distance between the propeller and the block, as compared with analogous tests with the JPRA open propeller, was achieved by the installation of a thrust bearing between the propeller hub and the outer sleeve of the dynamometer shaft. This succeeded in reducing the level of scatter at atmospheric pressure, compared with open propeller results. For the ducted propeller tests, all experiments were carried out with a minimum gap ratio of G/D = 0.005 between the blockage surface and the forwardmost blade of a given propeller, . Variations between the

geometry of successive blades on the model propellers led to blade to block gap ratios ranging up to G/D = 0.01

Three series of tests were conducted with the high pitch propeller over a range of pressures. The high pressure series, $P_A/P_{ATM} = 1.09$, had an associated cavitation number of $\sigma_V = 860$. The first low pressure test, $P_A/P_{ATM} = 0.55$, was at a cavitation number of $\sigma_V = 496$. Finally, a third series, $P_A/P_{ATM} = 0.48$, was at a cavitation number of $\sigma_V = 415$.

The rotational speed of the propeller for the test series was restricted to a maximum value of n = 16.7 rps. Higher rotational speeds caused the duct to vibrate, coming into contact with the rotating propeller. The minimum advance coefficient was restricted to the value achieved by the water velocity induced by the maximum propeller rotational speed used during the test. In each series, the induced water speed was around $V_A = 0.5$ m/s with an associated minimum advance coefficient of around J = 0.15.

Two series of tests were run with the low pitch (P/D = 0.8) propeller in blocked flow. In the first, an ambient pressure ratio of $P_A/P_{ATM} = 1.08$ resulted in a cavitation number of $\sigma_V = 834$. The second series was run at a pressure ratio of $P_A/P_{ATM} = 0.46$, corresponding to $\sigma_V = 347$. The selection of rotational speed and speed of advance was done in the same manner as with the high pitch propeller, with a maximum rotational speed of n = 16.7 rps and a minimum advance coefficient of J = 0.15.

4.3.2.1.2 Results

i) Effects of Blockage

Coefficients of propeller thrust and torque from experiments conducted in blocked flow with the high pitch propeller at a pressure ratio of $P_A/P_{ATm} = 1.08$ are presented in Figure 4-33. Again, polynomial curves have been fitted to the experimental data and the fitted curves from the experimental results in uniform flow are repeated for comparison. The axes again represent the load coefficients on the vertical axis with the advance coefficient presented along the horizontal axis.

Similarly to the results for open propellers, blockage resulted in a substantial increase in both thrust and torque coefficients in blocked flow compared with the uniform flow values. At an advance coefficient of about $J = 0.3$, the propeller thrust coefficient increased from $K_T = 0.26$ in uniform flow to $K_T = 0.60$ when it operated in the wake of the nearby blockage. For the torque coefficient at the same advance coefficient, there was an increase from $K_Q = 0.057$ in uniform flow to $K_Q = 0.099$ in the blocked flow case.

ii) Effects of Cavitation

Figure 4-34 presents the results of tests conducted in blocked flow at cavitation numbers of $\sigma_V = 496$ and $\sigma_V = 415$, respectively. The curves fitted to results of the performance tests in blocked flow at $P_A/P_{ATm} = 1.08$ are redrawn for comparison. The horizontal and vertical axes represent the same parameters as in Figure 4-33.

Limited differences were noted between measurements of the thrust coefficient for all three tests over the range of advance coefficients. Only slight reductions in the mean values of thrust were seen as the advance coefficient approached $J = 0.15$ for the tests at reduced cavitation numbers. The minimum value of $K_T = 0.60$ for a cavitation number of

$\sigma_V = 415$ represented a reduction of only $\Delta K_T = 0.03$ from the tests at atmospheric pressure, $\sigma_V = 860$. The variation between the results measured at different cavitation numbers was within the scatter of the experimental data. Notwithstanding the magnitude of differences due to cavitation, the small reductions in the thrust coefficient were consistent with the much clearer results seen in tests with the open propellers.

Measured mean values of the torque coefficient for tests at reduced cavitation numbers, $\sigma_V = 496$ and $\sigma_V = 415$, were lower than results from the test conducted at higher pressure ($\sigma_V = 860$) over the entire range of advance coefficients. At $J = 0.16$ for the high pressure test, the torque coefficient, K_Q, was 1.09 while at $\sigma_V = 496$, the torque coefficient was reduced to $K_Q = 1.03$. At low values of the advance coefficient, the torque coefficient data for the lower cavitation numbers showed a slight reduction as a result of cavitation. However, there was considerable variation between the mean values of torque over the range of advance coefficients examined. Similarly to the thrust coefficient in blocked flow, the significance of differences between the torque coefficients measured at high and low cavitation numbers can best be assessed in light of the results of tests with the open propeller.

Tests at even lower cavitation numbers should have produced more pronounced reductions in both the thrust and the torque coefficients. However, constraints imposed by the test apparatus resulted in a minimum attainable advance coefficient of 0.15. Limitations dictated by the deaeration capabilities of the tunnel resulted in a minimum pressure of $P_A = 47$ kPa. Reducing the cavitation number below a value of $\sigma_V = 415$ would

have required an increased flow speed with an associated increase in the advance coefficient: the reduced loading resulting from the higher advance coefficient would have negated the effect of the reduced cavitation number.

iii) Effects of Pitch

Similar blocked flow experiments to those described above were repeated for the low pitched propeller (P/D = 0.8). Tests were run at ambient pressure ratios of P_A/P_{ATM} = 1.08 and P_A/P_{ATM} = 0.46 with associated cavitation numbers of σ_V = 834 and σ_V = 347, respectively. While the tests were useful in a qualitative sense, no additional quantitative information on the effects of cavitation during propeller ice interaction could be assessed.

The reduced pitch resulted in lower mean values of thrust and torque coefficients over the range of advance coefficients tested compared with the performance of the high pitch propeller. The limitations imposed by the apparatus resulted in similar difficulties in attaining test conditions of similtaneously low cavitation numbers and low advance coefficients, with measured differences well within the range of experimental scatter.

Finally, the reduced pitch resulted in less severe cavitation. While the patterns were similar to those seen on the high pitch propeller (described below) minimal cavitation was visible at high pressure, while at reduced cavitation numbers the forms were less severe and extensive than for the high pitched case.

4.3.2.2 Patterns of cavitation

Cavitation patterns observed on the back and face of the propeller blade as it entered and exited the wake of the ice blockage are illustrated in Figure 4-35 and Figure

4-36. respectively. Patterns of cavitation developed on the adjacent face of the simulated ice block are shown in Figure 4-37. Although all forms of cavitation were more severe at the lower cavitation numbers, $\sigma_V = 415$ and $\sigma_V = 496$, they were also visible at $P_A/P_{ATM} = 1.08$.

When the angle, ϕ, of the blade was 0° with respect to the horizontal, the blade had not yet entered the wake of the ice block. As a result, no visible cavitation formed on the propeller. However, along the horizontal trailing edge of the block, a combination of sheet cavitation and cloud cavitation was visible between the reference blade at $\phi = 0°$ and the preceding blade, already at $\phi = 90°$.

As the propeller blade entered the wake of the ice block, sheet cavitation began to form on the leading edge of the blade back. At an angle of $\phi = 30°$, the sheet extended from approximately sixty percent of the blade radius to the tip of the propeller. The effect of the propeller at this angle resulted in the formation of a sheet cavity along the vertical edge of the block. This combined into a stable vortex cavity with the leading edge sheet cavity on the blade back at one end and the block sheet cavity at the other.

At the same point, the propeller blade cut through the sheet cavity along the lower edge of the block. The sheet cavity reappeared between the blade and the block. The opposing orientation of flow over the leading edge of the blade face and the trailing edge of the block resulted in the formation of cloud cavitation. The cloud extended over that area of the blade face in the wake of the block, from the hub to eighty percent of the blade radius.

At an angle of $\phi = 60°$, the leading edge sheet cavity extended from the root to the tip on the blade back. Interaction between the blade sheet cavity and a sheet cavity formed along the bottom edge of the block resulted in severe cloud cavitation between the lower part of the blade back and the block. At the blade tip, the leading edge sheet developed into a detached tip vortex which extended approximately from the blade corner to the lower right corner of the block, as seen in Figure 4-35. The cloud cavitation on the face of the blade had separated from the cloud trailing the preceding blade and moved away from the leading edge. The area and severity of the face cavitation had reduced.

At the vertical blade position, $\phi = 90°$, the cloud cavitation on the blade back enlarged towards the tip, with an associated increase in area and severity. The leading edge sheet cavity extended along the tip of the blade as the detached tip vortex disappeared. The cloud cavitation on the blade face had almost completely dissipated.

After a further rotation of 30°, to an angle of $\phi = 120°$, the sheet cavity on the blade back had contracted along both the leading edge and the blade tip, covering only a small region on the corner of the blade. The cloud cavitation continued to increase between the block and the propeller blade, extending along the entire tip and covered most of the area of the blade obstructed by the block.

As the propeller blade began to leave the obstructed flow behind the blockage, the leading edge sheet cavity disappeared. The region of cloud cavitation extended to the trailing edge of the blade back, but decreased in size and severity as it dissipated near the

leading edge. Upon further rotation, to $\phi = 180°$, the blade was no longer in the wake of the blockage, causing the collapse of the cloud cavitation.

As in the case of the open propeller, cavitation initially began to form on the ducted propeller as sheet cavitation as the propeller blade entered the wake of the block. As the blade passed through the wake, the sheet cavitation progressively gave way to cloud cavitation and by the point at which the blade was exiting the wake of the blockage, the cavitation incident on the surface of the blade was entirely cloud cavitation. Since cavitation is a function of the pressure distribution and flow regime on the propeller blade surface, the similar forms of cavitation on ducted and open propellers are indicative of similar pressure distributions: as such, the nature of loading on the blades would equally be similar.

4.3.2.3 Block Face Pressure

4.3.2.3.1 Test Conditions

The final series of tests with ducted propellers was conducted with an instrumented blockage (described in Chapter 3) installed upstream of the propeller. A minimum gap ratio of G/D = 0.005 (1 mm) between the blockage and the leading edge of the forwardmost blade on the high pitch propeller (P/D = 1.17) was established. A slight variation in the surface of the blockage resulted in a 1.5 mm gap at the port sensor for that blade and variations between individual blade geometries resulted in a maximum gap of about 2.5 mm at that sensor for the blade with the aftermost leading edge.

Test conditions were based on similar tests previously run in the ice tank at IMD. The tests were run at rotational speeds of n = 8.9 rps, n = 11.8 rps and n = 17.7 rps and advance speeds of V_A = 0.42 m/s and V_A = 0.84 m/s. Tests at the highest rotational speed, n = 17.7 rps, were run with induced flow speeds of between V_A = 0.83 and V_A = 0.86.

All tests were run at two different pressures. At the highest pressure, P_A/P_{ATM} = 1.08, the range of advance speeds corresponded to cavitation numbers from σ_v = 1219 for V_A = 0.42 m/s to σ_v = 308 for V_A = 0.84 m/s. At the lower pressure, P_A/P_{ATM} = 0.46, the same advance speeds resulted in cavitation numbers σ_V = 507 and σ_V = 127, respectively.

For each test, records were taken of the fluid pressure at each pressure sensor. In addition, a record was made of an electrical pulse generated when the leading edge of the reference blade was at the upper centreline position, adjacent to the middle sensor. The data acquisition hardware capacity limited the simultaneous sampling rate for four channels to 2800 Hertz. This corresponds to a range from one sample per 2.28° of propeller rotation at n = 17.7 rps to one sample per 1.14° at n = 8.9 rps.

4.3.2.3.2 Results

Typical segments of time domain data recorded at each pressure sensor during experiments with the higher pitch ducted propeller in blocked flow are shown from Figure 4-38 to Figure 4-45. Each plot shows a record of the pressure at one sensor, with time shown on the horizonal axis and the absolute pressure on the vertical axis. A position pulse showing the angular position of the shaft is shown along the top of each figure. The

leading edge of the reference propeller blade is adjacent to the centre sensor when the pulse begins.

Figure 4-35 and Figure 4-37 illustrate the typical cavitation patterns on the back of a propeller blade and the adjacent surface of the blockage, respectively. Comparison with Figure 3-12, showing the location of the pressure sensors, gives an indication of the flow conditions in the region of each sensor. The port sensor was in variable flow conditions resulting from the vortex shed from the vertical edge of the blockage and the pressure regime associated with the passing propeller blade. The cavitation patterns shown in Figure 4-35 and Figure 4-37 indicate a cyclic variation from dominance of the shear flow in the wake of the block to dominance of the blade pressure. The middle sensor was located in the fully stalled flow of the blockage, away from the effects of flow around the edges of the blockage. Stable sheet cavitation was apparent on the blade back when a blade was adjacent to this location. The starboard sensor was also close to the edge of the blockage in an area of highly turbulent flow as indicated by the substantial amount of cloud cavitation apparent in the region.

A comparison of experimental results displayed from Figure 4-38 through to Figure 4-45 shows consistent differences in the record of hydrodynamic pressure from one sensor location to another, throughout the range of experimental conditions. In all cases the amplitudinal variation increased with rotational speed but exhibited limited sensitivity to variations in flow speed: this presents further evidence on the appropriateness of a cavitation number based on rotational speed for such work. Comparison of the tests run at an ambient pressure of $P_A/P_{ATM} = 1.08$, shown in Figure 4-38 to Figure 4-41, with those

run at reduced pressure, $P_A/P_{ATM} = 0.46$, presented in Figure 4-42 through Figure 4-45, further illustrates the dynamic effects of cavitation.

i) Effects of Position

Peak to peak differences between minimum and maximum measured pressure for a given set of conditions were lowest for the port sensor and highest for the centreline location. At a high ambient pressure, $P_A/P_{ATM} = 1.08$, and a rotational speed, n, of 8.8 rps, presented in Figure 4-38a, the maximum typical variation at the port sensor was $\Delta P = 16.0$ kPa. For the same conditions at the centreline sensor, the difference was $\Delta P = 63.7$ kPa and at the starboard sensor was around $\Delta P = 30$ kPa. Increased rotational speed resulted in an increase of peak to peak variation for all three locations. At a higher rotational speed, n = 11.8 rps, and the same ambient pressure, Figure 4-40 a, b and c show that the peak to peak differences at the port, centreline and starboard sensors were around 30 kPa, 90 kPa and 40 kPa, respectively.

Figure 4-38 illustrates the variation in the pressure at the middle sensor at a rotational speed of 8.84 rps. At the point when a blade is adjacent to the sensor, the measured pressure undergoes an abrupt drop from about 110 kPa to a minimum pressure ranging from between P = 46 kPa to P = 75 kPa. As the blade moves past the sensor, the pressure begins to rapidly increase toward the maximum level, with the rate of pressure increase slowing as the upper limit is approached. The cycle repeats with each subsequent blade pass.

The cycle remained the same as the rotational speed increased, but the pressure dropped to a lower level as the blade passed,. For a rotational speed of n = 11.8 rps, illustrated in Figure 4-40, the minimum pressure has dropped to a range between 15 kPa and 50 kPa. A further drop occurred a higher rotational speed, n = 17.1 rps, with a resulting minimum pressure of 5 kPa.

The record of pressure variation at the port sensor location showed a more erratic character with less severe peak to peak oscillations, as shown in Figure 4-38a. At n = 8.8 rps, a maximum pressure of about 110 kPa was reached at the point of blade pass. Unlike the results from the middle sensor, there was no abrupt pressure drop as the blade moves away from the sensor. Instead, there was a gradual, erratic decline in pressure to a minimum level with a mean value of about 90 kPa. Increasing rotational speed resulted in similar patterns, however as speed increased, the erratic nature of the signal increased, the average value of the minimum pressure between blade passes decreased from about 90 kPa at n = 8.8 rps to around 40 kPa at n = 17.7 rps, and an increase in the magnitude of the peak associated with blade pass was noticeable.

The pressure at the starboard measurement location showed a different trend. At n = 8.8 rps, the pressure record, shown in Figure 4-38c, displayed an erratic variation about a mean level of about P = 100 kPa between blade passes. When a blade passed, the pressure displayed an abrupt drop, to a level that ranged from 62 kPa to 80 kPa. The pressure then increased in a manner similar to that of the middle sensor until the pressure had reached the mean level of 100 kPa, about which it again began to oscillate. Increasing

rotational speed resulted in an increase in the erratic nature about the mean and an increase in the level of pressure drop associated with blade pass.

ii) Effects of Cavitation

Figure 4-42 through Figure 4-45 show representative samples of data collected during low pressure tests at similar rotational and flow speeds to those discussed above. For each set of test conditions, the effect of reduced ambient pressure was a downward shift of the mean pressure by about 63 kPa, with a minimum pressure limit around P = 1.9 kPa, near the level of vapour pressure of water. The effect of the reduced pressure was substantially increased cavitation visible on the propeller and blockage, as described in the previous section.

The limiting effect of cavitation can be clearly seen in Figure 4-44b which shows data from the middle sensor at a rotational speed of n = 11.8 rps and a speed of advance of V_A = 0.42 m/s. Above some critical pressure, P_c, near to the vapour pressure of the test water, the characteristics of the plot closely matched that of similar test conditions at high pressure, shown in Figure 4-40b. As the blade passed the sensor, the pressure abruptly dropped, but did not drop below the critical value (P_c = 5 kPa in this case). The pressure remained at that minimum level until the blade was sufficiently away from the sensor to allow the recovery of pressure to resume the same pattern as in Figure 4-40. The pressure then increased at a decreasing rate of change until the next blade approached the sensor and the cycle repeated. This is consistent with results of tests with the R-Class

open propeller, which showed that cavitation limited the maximum attainable mean block and propeller loads.

Data taken from the starboard pressure sensor during tests at high rotational speeds and low cavitation numbers showed intermittent positively directed pressure spikes. Such spikes are apparent in both Figure 4-44c and Figure 4-45c. While it is difficult to definitively explain such spikes with the data set available, they are consistent with the suggestion that collapsing cloud cavitation bubbles in the latter phase of blade pass cause microjets of water to impinge on the block surface. The result of such collapses could result in forward directed forces on the block.

Pressure on the face of the block is indicative of the load imposed on the propeller at those locations. As in the case with the open propeller, cavitation resulted in a modification of the pressure regime on the block: modifications which would be reflected on the propeller blade. Similarly, the load on the block and the propeller are related to the position of the blade with respect to the block.

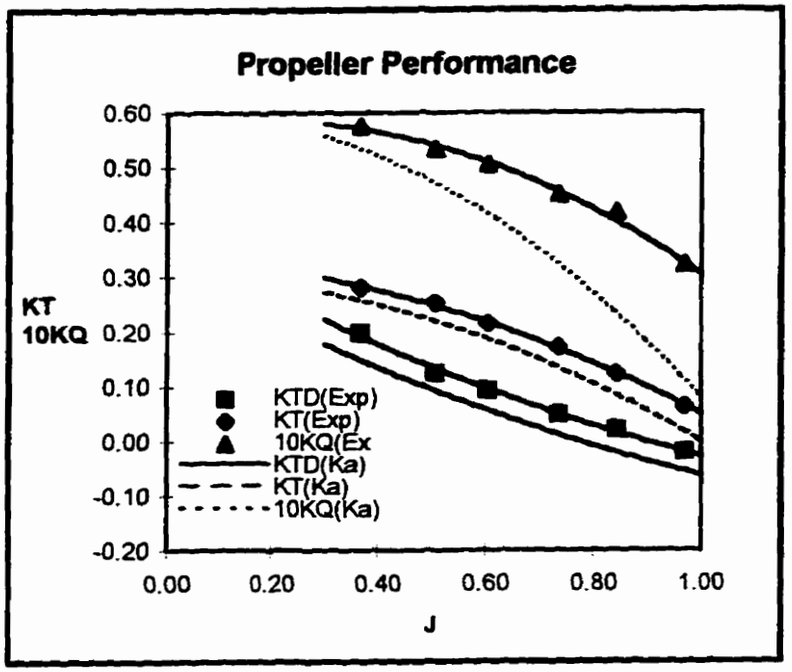

Figure 4-32 JRPA Ducted Propeller Performance, Uniform Flow

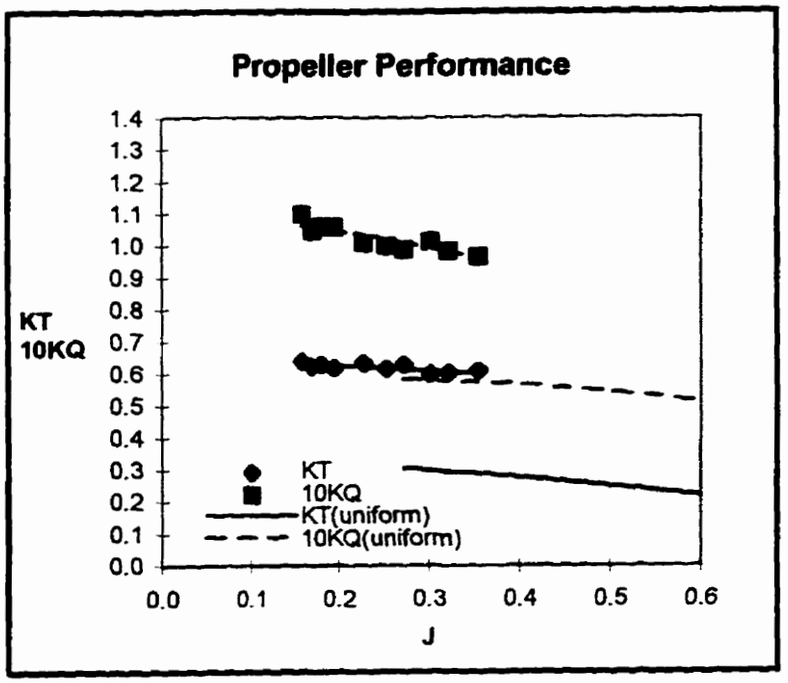

Figure 4-33 JRPA Ducted Propeller Performance, Blocked Flow

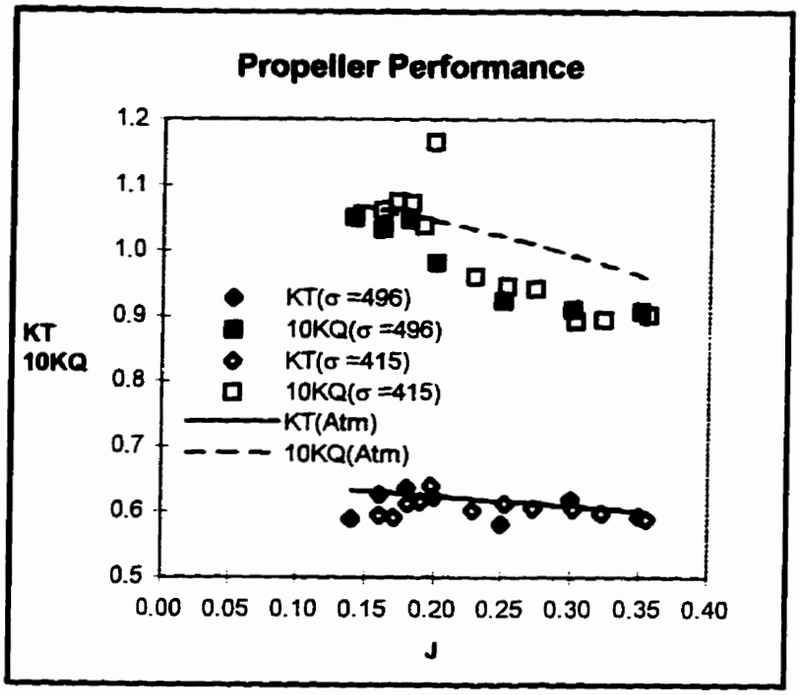

Figure 4-34 JRPA Ducted Propeller Performance, Blocked Flow

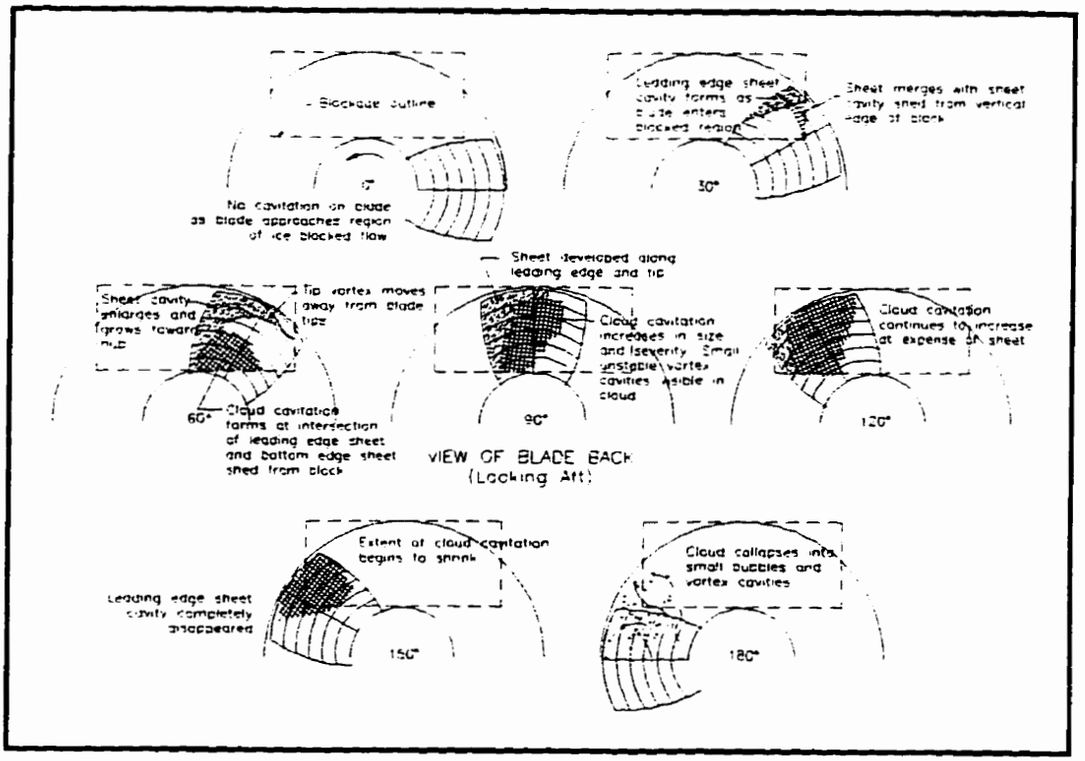

Figure 4-35 Blade Back Cavitation in Blocked Flow

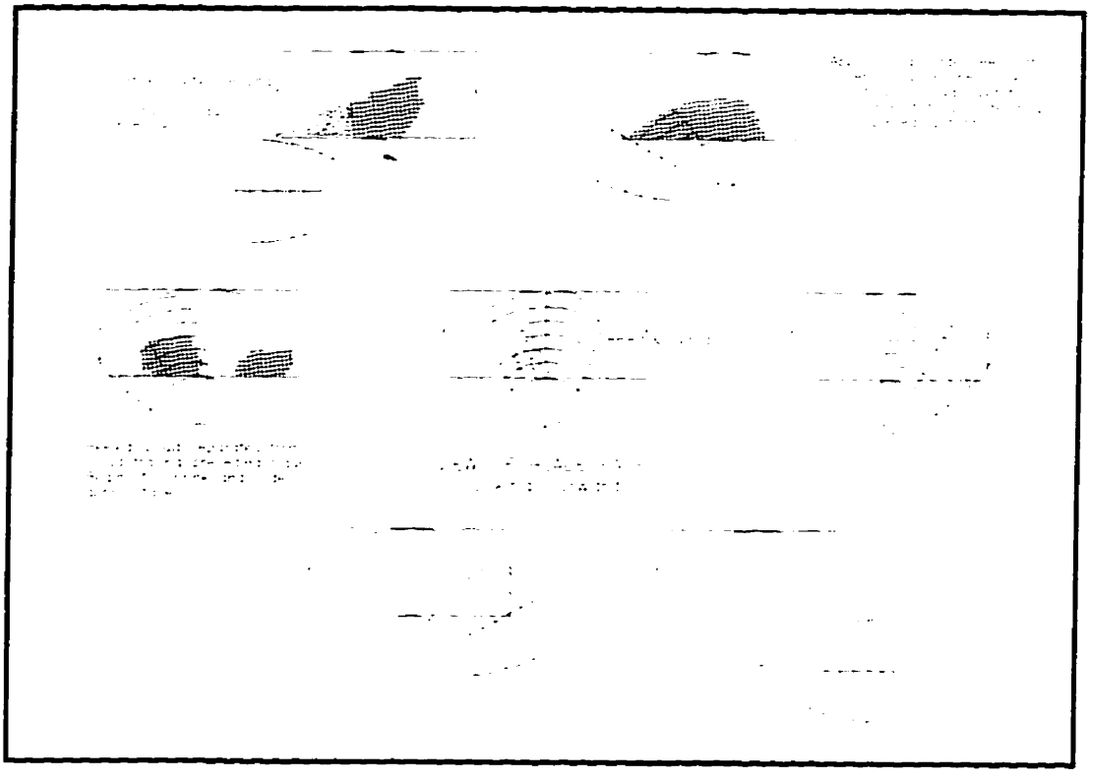

Figure 4-36 Blade Face Cavitation in Blocked Flow

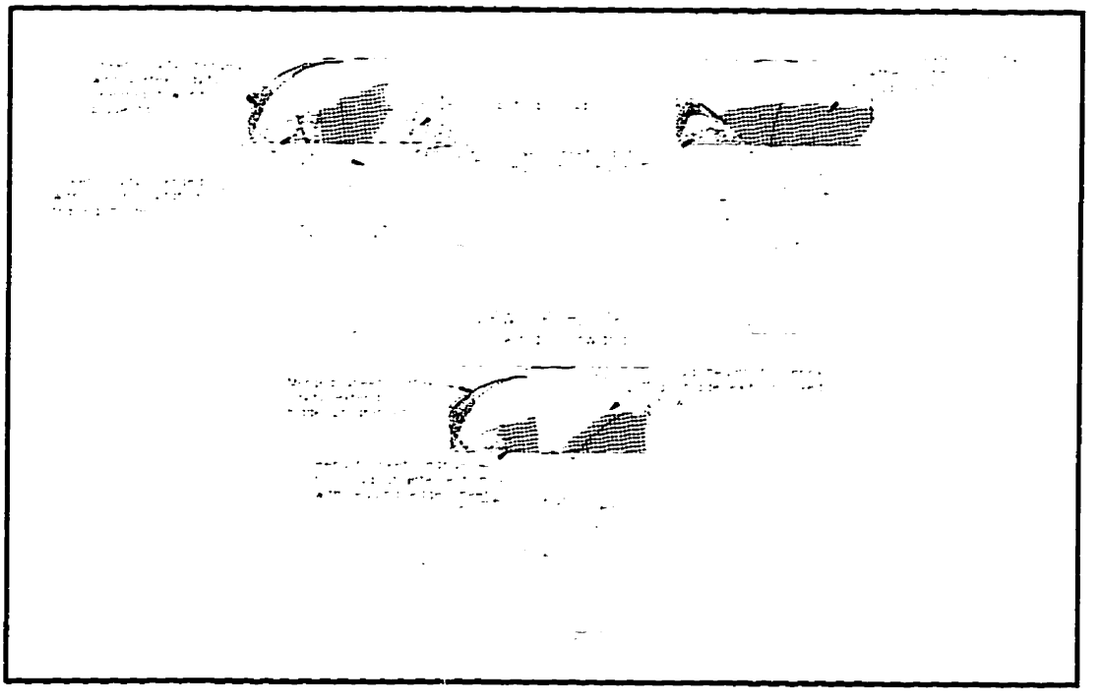

Figure 4-37 Block Face Cavitation

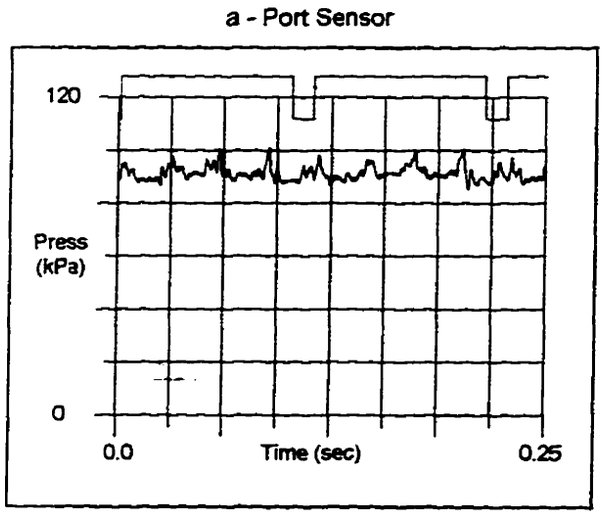

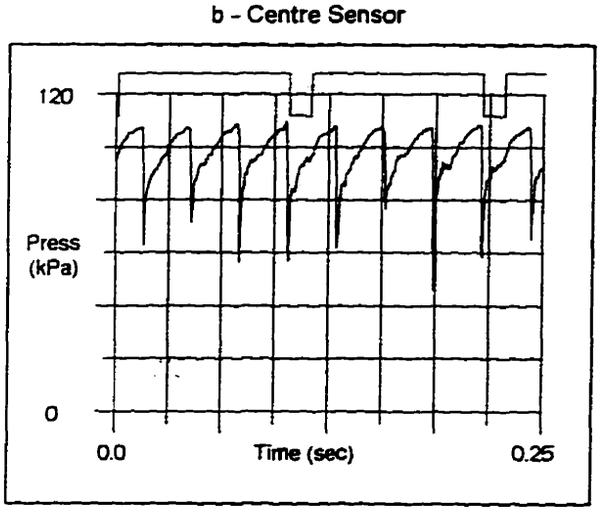

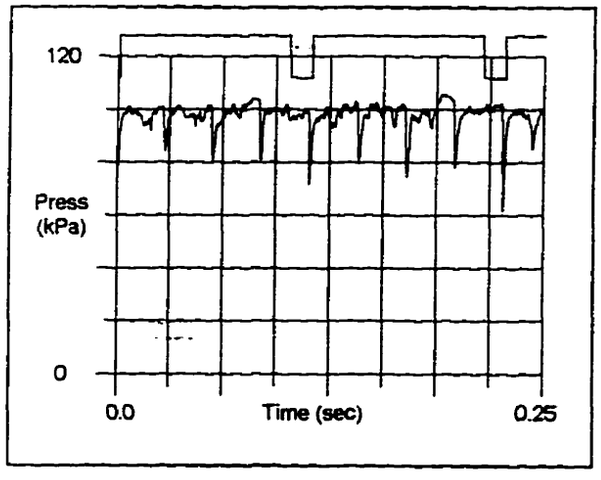

Figure 4-38 Blade Pass Pressure
8.8rps, 0.42m/s, 109kPa

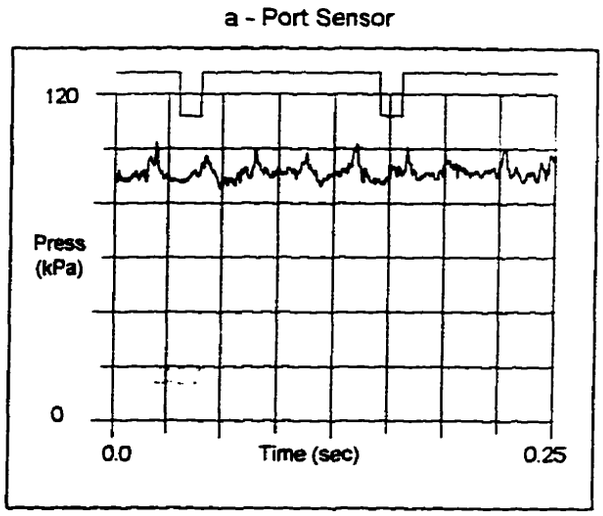

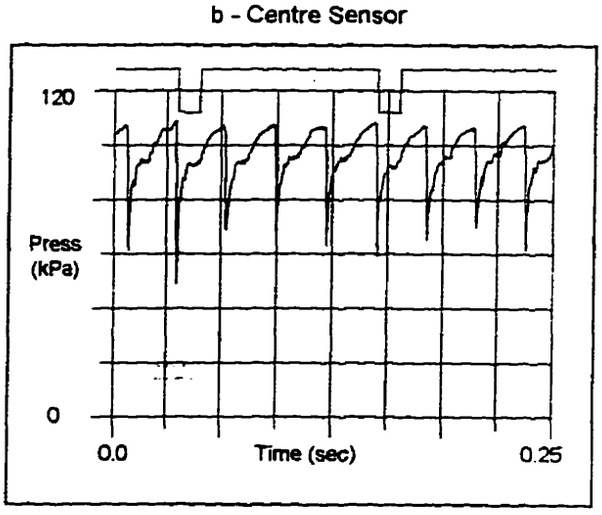

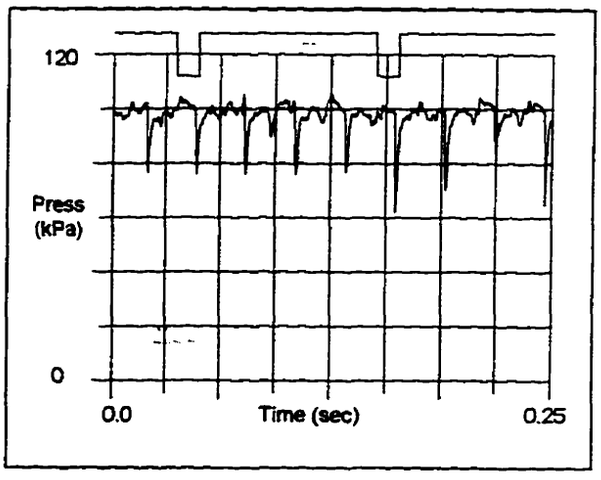

Figure 4-39 Blade Pass Pressure
8.8rps, 0.84m/s, 109kPa

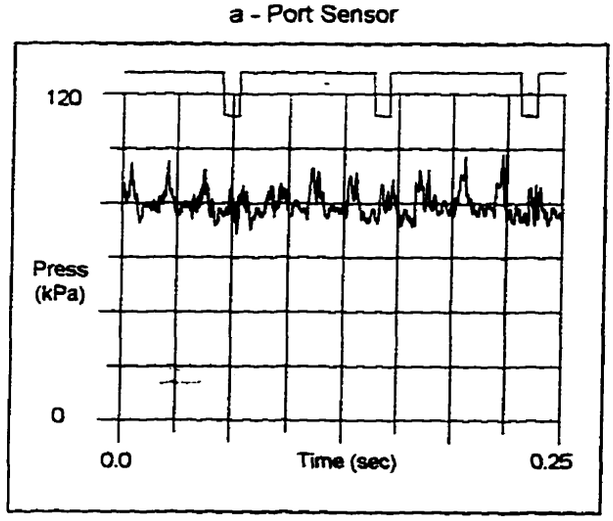

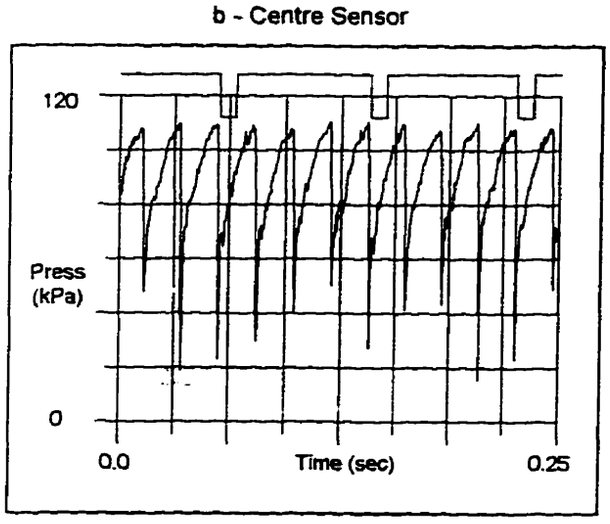

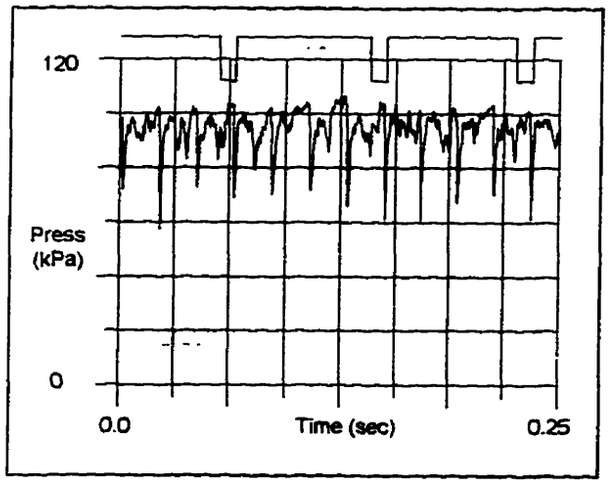

Figure 4-40 Blade Pass Pressure
11.8rps, 0.44m/s, 109kPa

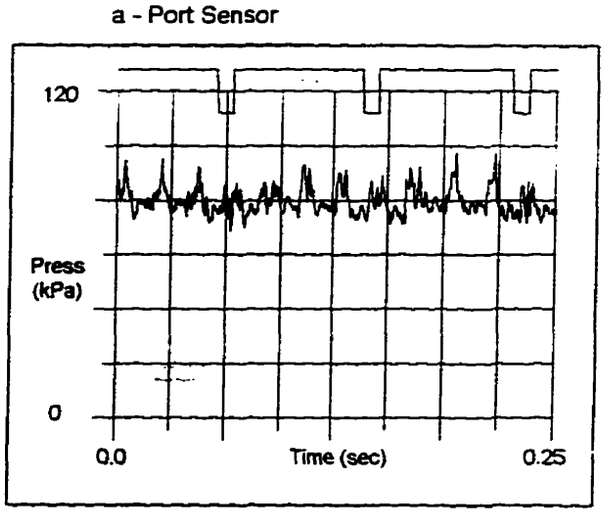

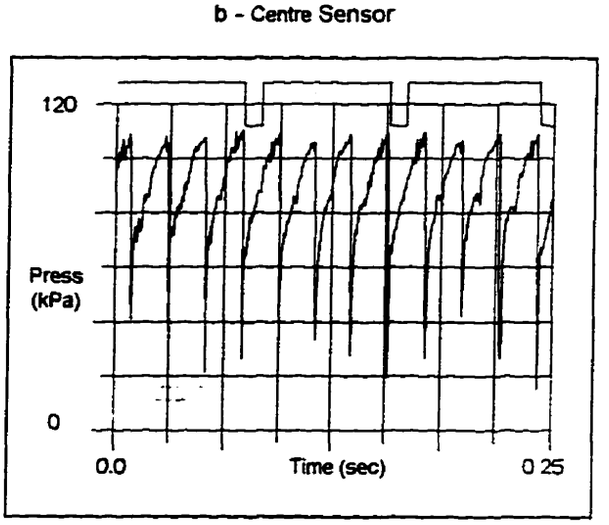

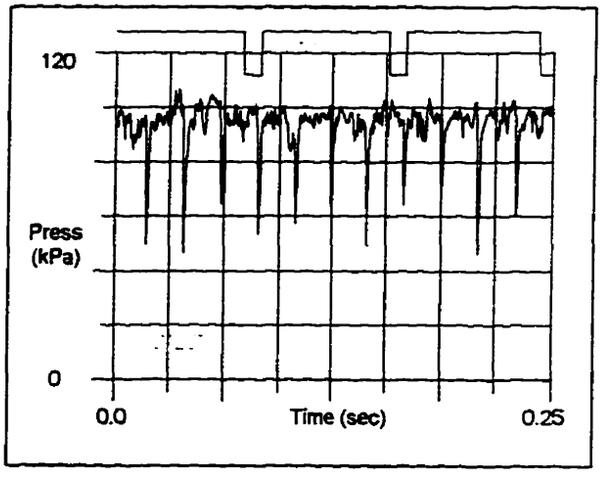

Figure 4-41 Blade Pass Pressure
11.8rps, 0.84m/s, 109kPa

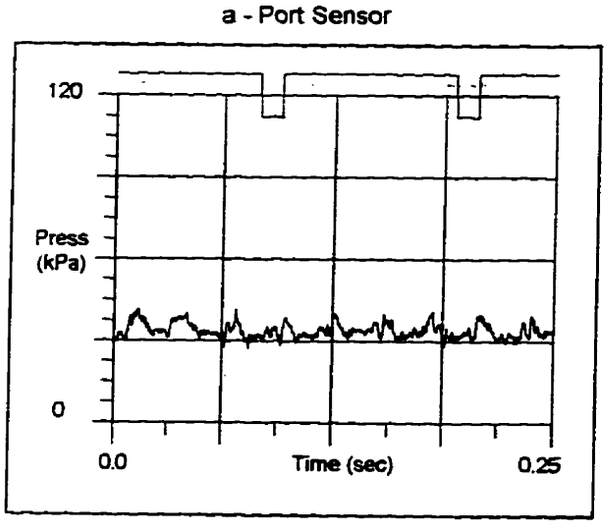

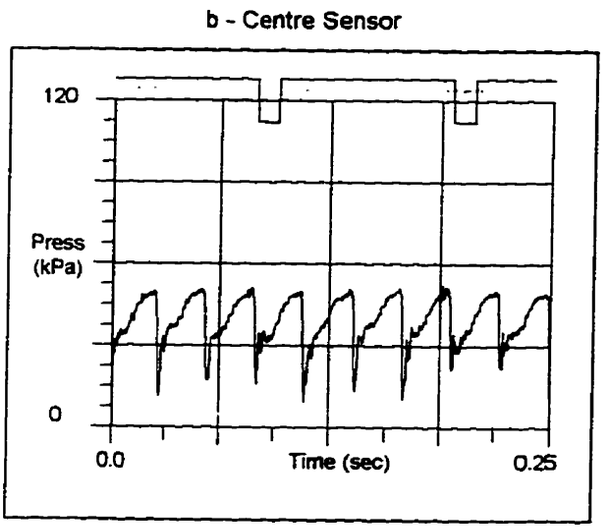

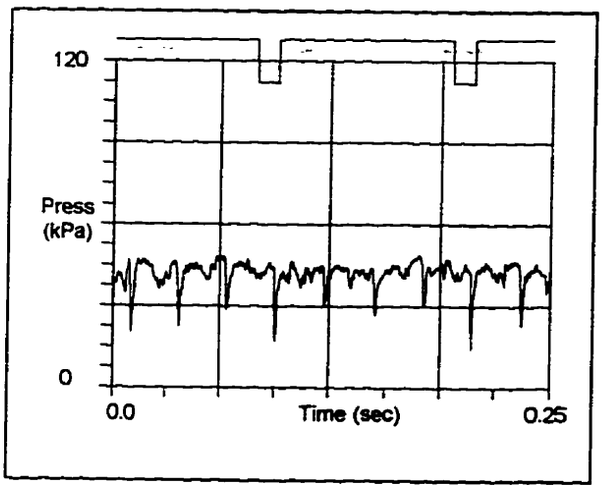

Figure 4-42 Blade Pass Pressure
9.0rps, 0.42m/s, 50kPa

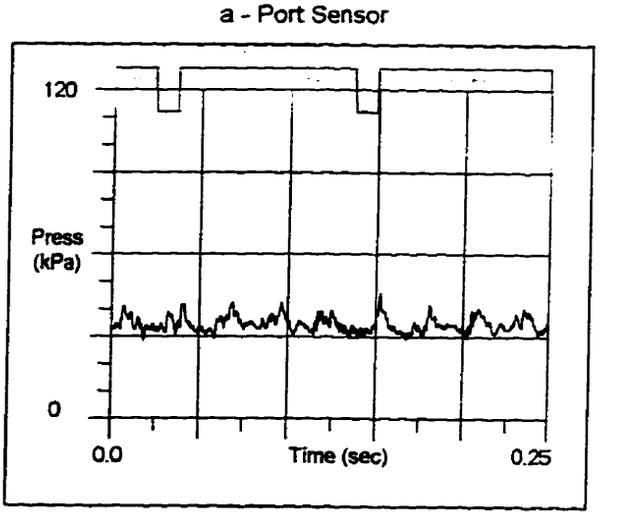

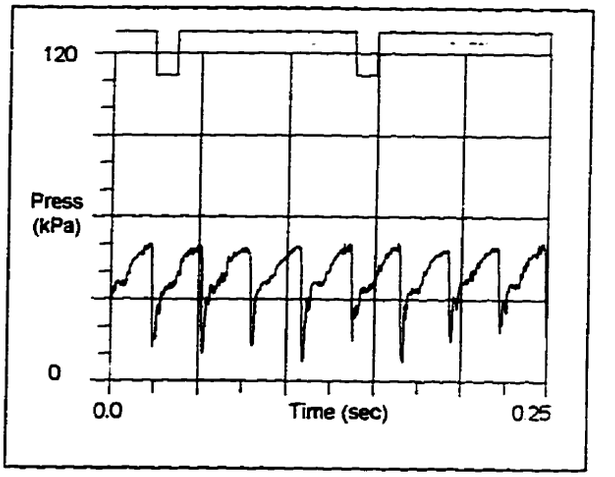

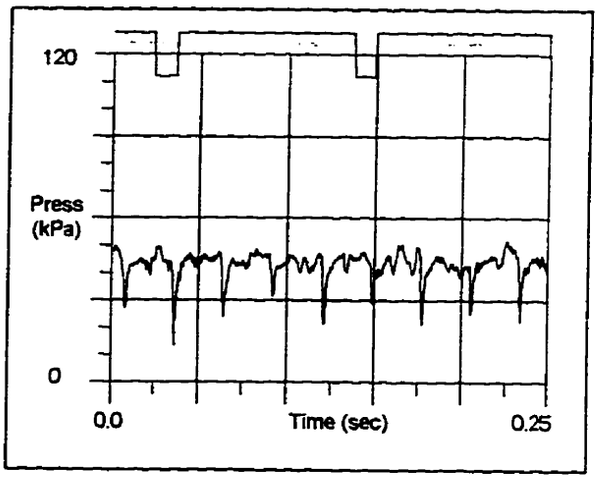

Figure 4-43 Blade Pass Pressure
8.9.rps, 0.84m/s, 50kPa

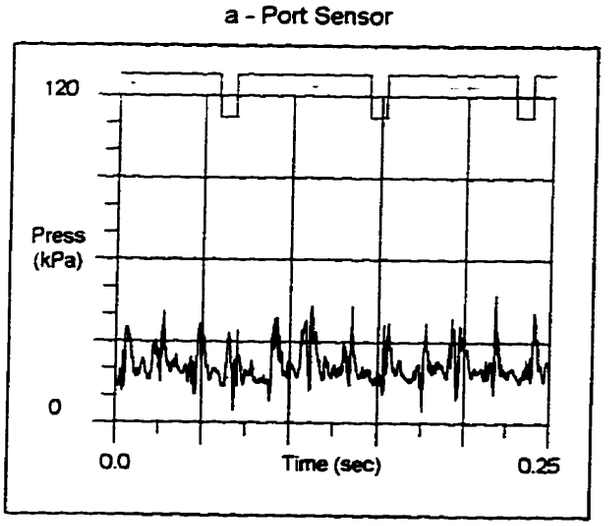

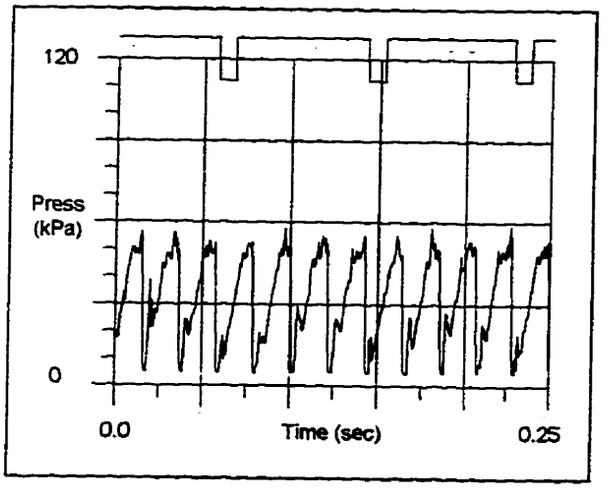

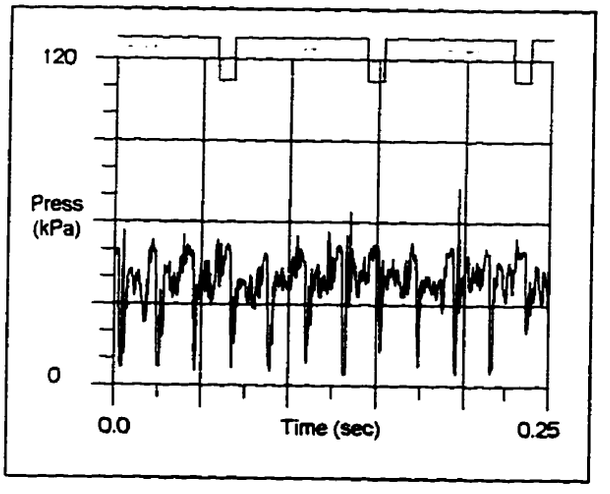

Figure 4-44 Blade Pass Pressure
11.8rps, 0.42m/s, 50kPa

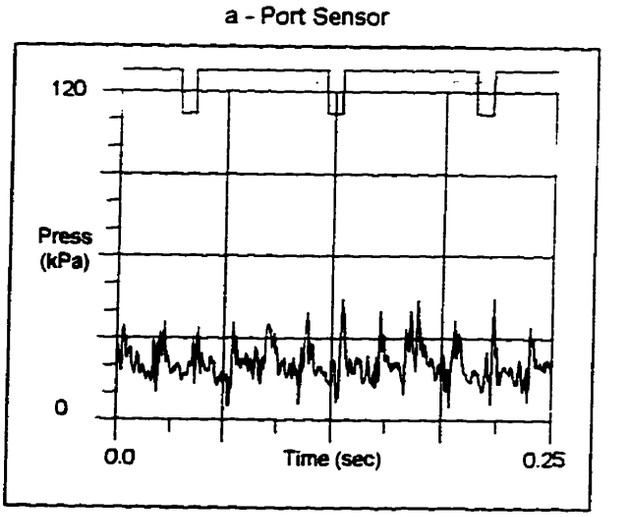

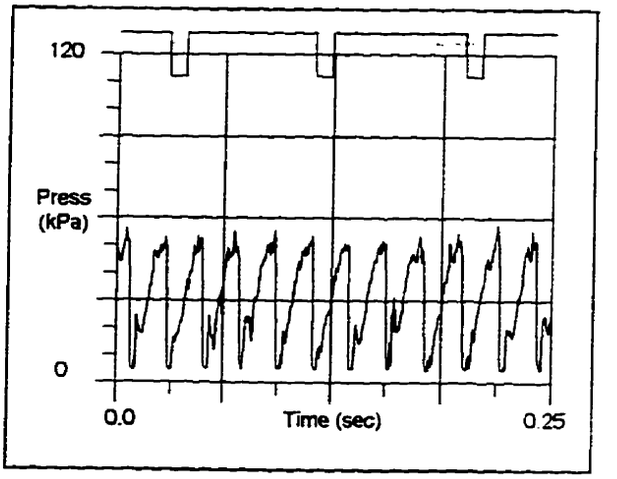

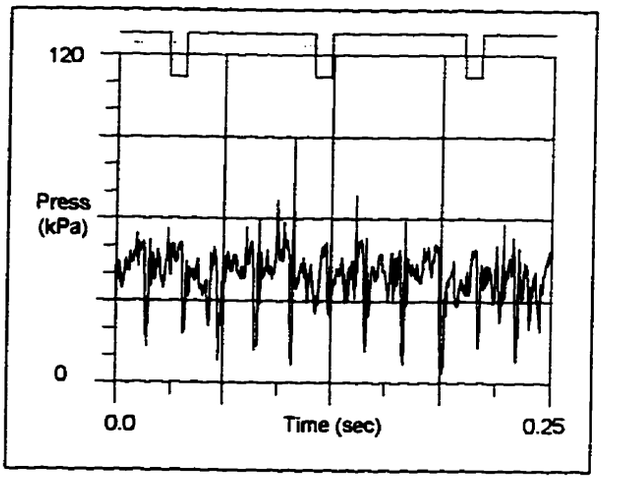

Figure 4-45 Blade Pass Pressure
11.9.rps, 0.84m/s, 50kPa

5. DISCUSSION

5.1 Average effects of blockage

When a propeller becomes blocked with a piece of ice in such a way that there is no contact between the ice piece and the propeller, mean levels of thrust and torque are dramatically increased. This was shown for all propellers examined throughout the course of the research.

Figure 4-3 shows the results from the first series of tests run with the JRPA open propeller in the cavitation tunnel at IMD. The figure shows increased levels of both thrust and torque coefficients in blocked flow, over uniform flow values, for the range of advance coefficients tested. Figure 4-10 shows similar results for the R-Class propeller when it was tested in the cavitation tunnel at the University of Tokyo. In that figure, it can be seen that the operation of a propeller at high advance coefficients, in close proximity to a milled ice piece, results in an increase of thrust by as much as three times the open water levels and an increase in torque by as much as twice the open water values. This was further corroborated by tests with the R-Class propeller in the towing tank at Memorial, as seen in Figure 4-13.

Analogous results have been produced using the ducted propellers, built for the JRPA research, and a Marin Type-37 duct installed in the cavitation tunnel at IMD. Figure 4-33 presents the results of tests that were run over a range of advance coefficients with that apparatus. The increase in thrust and torque coefficients due to blockage were even higher than for the open propellers. At an advance coefficient of about $J = 0.3$, the thrust coefficient increased by 131% from $K_T = 0.26$ to $K_T = 0.60$. At the same

conditions, the torque coefficient increased by 74%, from $K_Q = 0.057$ in uniform flow to $K_Q = 0.099$ in blocked flow.

5.1.1 Decreased Efficiency

While the previously presented figures show greater increases in thrust than torque, the increase in thrust comes with a decrease in total system thrust because of the drag load imposed by the blocking ice piece. Figure 4-24 presents the block load measured coincident with thrust and torque during the tests conducted in the University of Tokyo cavitation tunnel. Figure 4-25 presents coefficients of thrust, torque and block load for the same conditions, in addition to propulsion efficiency when the increased drag associated with block load is taken into account. The net effect was a drop in the mean performance of the system. While no measurement of block load was made during tests with the ducted propeller, a similar result would occur, since in that case it would, in fact, be the duct supporting the ice piece instead of the load cell used in the open propeller experiments.

5.1.2 Load Components

The constituent components of the increased load due to blockage was more fully investigated in the towing tank at Memorial than in the cavitation tunnel work. That work showed the average increases can be considered to be the sum of two constituent components: wake and proximity. Figure 4-14 shows that in the case of the R-Class propeller, for a propeller diameter to block gap ratio in excess of 0.05, the effect of blockage was a fixed increase in both thrust and torque: at an advance coefficient of $J = 0.4$, this increase was around 20% of the uniform flow values. At levels of gap falling

below five per cent of the propeller diameter, the proximity of the ice blockage resulted in higher levels of load, with the increments of thrust and torque up to as high as 75% of the uniform flow values.

Additionally, the measurements taken in the towing tank suggest that the increase in the thrust and torque coefficients is a function of the portion of the blade span that is blocked by the ice piece. Figure 4-11 and Figure 4-12 present the measurement of thrust and torque for blockage cut depths of 25 mm and 50 mm (equal to 12.5% and 25% of the propeller diameter) respectively. The figures show that the average increase in thrust and torque over uniform flow for a cut depth of 50 mm is approximately four times that of thrust and torque for a cut depth of half that size. That is, the increase in load was equal to the square of the spanwise increase in blockage.

5.2 Average effects of cavitation

The results discussed in the preceding sections of this chapter were recorded during tests conducted above atmospheric pressure, in which minimal cavitation was present. As the ambient pressure at the propeller is reduced to levels resulting in cavitation numbers near typical full scale values, the average measured loads are further modified. Figure 4-4 illustrates the effect of cavitation number on both the thrust and torque coefficients for tests conducted with the JRPA propeller at reduced cavitation numbers in the tunnel at IMD. Analogous results from tests in the tunnel at the Tokyo University are presented in Figure 4-15 and Figure 4-16 for the thrust and torque coefficients of the R-Class propeller, respectively. A similar effect of cavitation is seen in the three figures: cavitation reduced the mean recorded levels of both thrust and torque coefficients. For the earlier tests with the JRPA open propeller, the reductions in thrust

and torque were seen for advance coefficients less than J = 0.4. The results measured with the R-Class propeller model showed reductions over the full range of advance coefficients tested.

The principal difference between the two sets of tests was the definition of cavitation number: in the earlier work with the JRPA propeller, the cavitation number was based on flow speed and in the latter work the cavitation number was based on rotational speed. Difficulties with the experimental apparatus in the earlier work resulted in bias and precision errors which precluded quantifying the magnitude of the change of thrust and torque due to cavitation. However, in the more recent work, the figures show that over the range of advance speeds tested, the thrust coefficients dropped by an almost constant amount of approximately $\Delta K_T = 0.13$. For the same conditions, the torque coefficients dropped by around $\Delta K_T = 0.11$. Such drops represent as high as a 50% reduction in measured mean load on the propeller. Similar reductions were seen in block load, as shown in Figure 4-24.

Analogous effects of cavitation are seen in Figure 4-34 to occur with ducted propellers in blocked flow. However, due to difficulties in testing at a sufficiently high level of shaft rotational speed, the results provide only a qualitative indication of the effect on the performance of the ducted propulsion system.

5.3 Dynamic effects of cavitation

While the mean effect of increased cavitation is a reduction in the thrust and torque coefficients over the full range of advance coefficients at which a propeller might operate, the decrease in average propeller forces was simultaneous with increased oscillation of those forces about the mean value. This was first noted during tests with the JRPA open

propeller. Increased cavitation was also coincident with increased noise and vibration compared with tests at high cavitation numbers with little cavitation. Similar observations were made during tests with the JRPA ducted propellers and the R-Class open propeller.

The first quantitative evidence of the increased oscillation about the mean load was provided by the time domain results shown in Figure 4-6 and Figure 4-7. The records were taken using an instrumented stub shaft mounted to the end of the propeller shaft in the cavitation tunnel at IMD and show that the amplitude of torque measured at the lower cavitation number (Figure 4-7) were approximately twice the torque amplitudes measured from the test at the higher cavitation number.

The increase in oscillation was also seen in time domain records of block load at high and low cavitation numbers, as shown in Figure 4-29. Comparison between the two records indicate that the effect of substantial cavitation was a reduction in the mean value of block load, as seen in Figure 4-24. but an increase in the unsteady oscillation about the mean by about three times the value recorded with minimal cavitation. While the presented figure shows only the results for the highest and lowest cavitation number for one advance coefficient, the increased oscillation was progressive with decreasing cavitation number and the trend was consistent for the range of advance coefficients tested.

5.3.1 Modified Load Phase

Results presented in the time domain in Figure 4-29 are repeated in Figure 4-30 in the position domain. Figure 4-27 provides the positional frame of reference and Figure 4-23 shows the incident forms of cavitation on the R-Class propeller. Figure 4-30 shows that as cavitation increased, the phase of loading to which a propeller blade was exposed

was modified. By comparing the measured load with the angular position of those propeller blades located within the milled recess of the simulated ice blockage, it can be seen that the developed hydrodynamic load was affected by the form of cavitation developed as the blade passed behind the blockage. Cloud cavitation incident on the blade during the latter part of the blade pass was predominantly responsible for the increase in vibratory loading due to a dramatic drop in blade thrust as the blade passes through that region.

The variation of pressure, and hence blade load, with location on the block face was further verified by pressure measurements in tests with the ducted propeller. Data from the pressure measurements are presented from Figure 4-38 through to Figure 4-45. The time domain data indicates a different pressure regime was present at each location and that the mean pressure varied across the face of the block. Analogously, the incident load on the propeller blade would have varied as the blade passed across the face of the blockage.

The pressure sensor data is consistent with results of tests with the R-Class propeller. At the centreline sensor, the reduced pressure records presented in Figure 4-44b and Figure 4-45b show the limiting effect of cavitation as the pressure is prevented from dropping below the cavitation pressure, P_c. This compares well with the records presented in Figure 4-24 and Figure 4-26 which shows the mean load developed on the block by the nearby propeller was reduced as a result of cavitation. Similarly, results shown in Figure 4-44c and Figure 4-45c are consistent with results shown in Figure 4-30, where the block load is reduced during the latter part of a blade pass behind the blockage.

Positively directed spikes shown in pressure sensor records could be indicative of cloud cavitation bubble collapse, which would contribute to the decrease in block load.

5.4 The nature of cavitation

The structure of cavitation during propeller-ice interaction is presented in Figure 4-8 and Figure 4-23 for open propeller and in Figure 4-35 and Figure 4-36 for ducted propellers. As a propeller blade passes behind an obstructing ice piece, cavitation typically begins as stable sheet and vortex cavitation. Progress through the wake of the ice block results in the development of cloud cavitation in the latter stages. As described above, the phase of hydrodynamic load on the ice blockage is closely related to the change in the structure of the cavitation on the propeller blade and the development of extensive cloud cavitation is coincident with dramatically increased vibration. While no erosion tests were conducted as part of the work included in this thesis, it was apparent from tests at low cavitation numbers that the cloud cavitation incident on the propeller blades in the wake of the blockages could pose a risk of cavitation erosion to the blade. This was later substantiated for open and ducted propellers by Doucet et al. (1995) and Doucet et al. (1996), respectively.

5.5 Conclusions

While the effects of blockage and cavitation on open and ducted propellers may vary in magnitude, the nature of the hydrodynamic loads are the same. Blockage results in increased mean loads for both propeller types. Using the results from tests with the R-Class propeller as an example, increases in thrust, over open water values, ranged from

46% at an advance coefficient of J = 0.2 to 300% at J = 0.7. Analogously, torque increases ranged from 35% at J = 0.2 to 106% at J = 0.7. In the ducted propeller case, blockage at an advance coefficient of J = 0.3 resulted in an increase of thrust and torque by 230% and 175%, respectively. Cavitation results in a subsequent reduction in the mean hydrodynamic loads, but an increased oscillation about the mean loads. Again using the results from tests with the R-Class propeller as an example, mean thrust dropped by 37% and mean torque dropped by 31% as the cavitation number was reduced from $\sigma_{nD} = 13.5$ to $\sigma_{nD} = 1.8$ at an advance coefficient of J = 0.2. At the higher advance coefficient of J = 0.7, thrust and torque dropped by 48% and 33% respectively for the same range in cavitation numbers. Cavitation further alters the loading regime to which a propeller is exposed by modifying the nature of the loading: a propeller blade passing through the wake of an ice piece undergoes an unloading in the latter part of the blade pass due to the progressive development of cavitation as the blade passes behind the blockage.

This implies then that when the effects of cavitation are included, the hydrodynamic loading regime to which a propeller is exposed during interaction with ice can be defined by a strip theory model which takes into account a slight increase in the mean load when a portion of a blade is behind the wake of the ice piece, but also models the dynamic nature of the load.

The increase in mean load is approximately equivalent to the effect of the blade section working in stalled flow as outlined in Veitch (1995), since the high mean loads caused by the effects of proximity are somewhat counteracted by reductions due to cavitation. The dynamic effect can then be taken into account by superposition of a sinusoidal function on top of the mean value such that the peak forward load occurs

during the first part of blade pass and the load is, or approaches, zero in the latter part of blade pass, as was indicated by block load measurements presented in Chapter 4. Then for a given blade section i, the instantaneous values of thrust and torque can be approximated as:

$$T_i = T_b\,(1+\mathrm{Sin}(2\pi x/L))$$

and:

$$Q_i = Q_b\,(1+\mathrm{Sin}(2\pi x/L))$$

where:

T_b and Q_b are the values of segmental thrust and torque at bollard pull; L is the length between the points where the blade section enters and exits the recess and; x is the distance between the entry point and the instantaneous location of the section.

Similar to the results measured for block load, the above model results in a maximum section load of twice the section bollard thrust when the blade is one quarter across the blockage recess and a minimum load of zero at the point when the blade is three quarters across the recess. The total load for the blade can then be calculated in a manner similar to Veitch (1995), summing the individual contributions of each strip-wise segment of the blade.

The principal difference between ducted and open propellers is the manner in which the propeller is exposed to hydrodynamic loading: in the ducted propeller case, an ice piece lodged across the duct can expose the propeller to the blocked loading regime without coincident contact loads whereas in the open propeller case, the hydrodynamic loading regime associated with cavitation is coincident with contact loads. In the ducted propeller case, the hydrodynamic loads may be applied to the propeller for extended

durations since clearing the blocked duct requires operator intervention. whereas in the open propeller case, the reduction in hydrodynamic loads caused by cavitation may be coincident with milling loads, resulting in an increase in the total instantaneous loading regime to which the blade is exposed.

The effects of blockage and cavitation during propeller-ice interaction must be incorporated in the development of any design load model based on numerical simulations or model scale experimental data. Neglecting these effects in either approach will underpredict the loading regime to which the propeller is exposed. In a contact type interaction. the absence of the effects of cavitation could cause overpredictions of the developed hydrodynamic forward blade load which. when added to a contact load. will result in a reduction of the aftwards directed loading regime. In a non-contact interaction. the absence of the effects of cavitation will result in an underprediction of the oscillation of blade loads about the mean value. posing a potential fatigue risk to the propeller and associated machinery.

6. REFERENCES

Bose, N., (1993), "Fishing vessel screw propeller research - Final Report and Cavitation tunnel dynamometer", Ocean Engineering Research Centre, Report No. TR-HYD-93001, Memorial University of Newfoundland.

Bose, N., (1996), "Ice blocked propeller performance prediction using a panel method", *Transactions of the Royal Institution of Naval Architects*, (in print)

Browne, R. P., (1993) "JRPA#6 Propeller/Ice Interaction: Development of semi-empirical load models - Interim Report for 1992/1993 Fiscal Year" Institute for Marine Dynamics Technical Report CR-1993-09.

Doucet, J.M., Bose, N., Walker, D. and Jones, S.J., (1996), "Cavitation erosion in blocked flow with a ducted ice class propeller", *Proceedings the 15th International Conference on Offshore Mechanics and Arctic Engineering*, Florence, Italy, June 16-20, (in print).

Doucet, J.M., Bose, N., Walker, D. and Jones, S.J., (1995), "Cavitation erosion on a model ice class propeller in blocked flow", *Proceedings of PropCav '95: An International Conference on Propeller Cavitation*, Newcastle, U.K., May 16-18.

Doucet, M., (1992), "Operation manual for the cavitation tunnel", Ocean Engineering Research Centre, Report No. TR-HYD-92005, Memorial University of Newfoundland.

Gent, W. van and Oosterveld, M.W.C., (1983), "Ducted propeller systems and energy savings", *Proceedings of the International Symposium on Ship Hydrodynamics and Energy Saving*, El Pardo, Vol. VI, pp. 3-(1-24).

Gindroz, B., (1995), "Practical Advantages of Mastering Cavitation Nuclei", Carènes, Le Magazine du Bassin D'Essais des Carènes, No. 4, pp. 16-20.

Gorshkoff, A. (1975), "Standards for Cavitation Tests", Report of the Cavitation Committee, *14th International Towing Tank Conference*, pp. 154-159.

Harvald, Sv. Aa. (1983), *Resistance and Propulsion of Ships*, John Wiley and Sons Ltd., New York, pp. 186-198.

Jussila, M. and Soininen, H. (1991), "Interaction between ice and propeller", VTT Research Notes 1281, Technical Research Centre of Finland, Espoo, Finland, 80p.

Kannari, P. (1988), "Full scale and model tests performed with a nozzle and an open propeller similtaneously" *IAHR Ice Symposium*, Sapporo, Japan, pp. 772-781

Kato, H., Watanabe, Y., Komura, T., Maeda, M., and Miyanaga, M.,1981, "New Marine Propeller Cavitation Tunnel at the University of Tokyo. Its Design Concept and Special Features", *Journal of The Society of Naval Architects of Japan* (in japanese), vol. 150, pp. 148-157

Keinonen, A. (1991), "Theoretical Modelling of Propeller Ice Interaction",Proposal of JRPA-6. Transport Canada Report, TP-10614.

Keinonen, A. and Browne, R. (1990), "Ice propeller interaction forces". Transport Development Centre Report TP 10401E.

Koskinen, P., Jussila, M., and Soininen, H. (1996), "Propeller ice load models", VTT Research Notes 1739. Technical Research Centre of Finland. Espoo, Finland, 82 p.

Kuiper, G. (1981), "Cavitation Inception on Ship Propeller Models", Publication No. 655. Netherlands Ship Model Basin, Wageningen, The Netherlands.

Laskow, V. (1988), "Ice flow and blockage investigation of shrouded propellers", Transport Development Center Report, TP-9640E, Transport Canada.

Laskow, V., Spencer, P. and Bayly, I., (1986), "The Robert LeMeur ice/propeller interaction project: full scale data", *Marine Technology*, Vol.12, No. 4, pp. 301-319.

Lindgren, H., (1963), "Propeller Cavitation Experiments in Uniform Flow - A Note on Test Procedures, Corrections and Presentation", *Proceedings of the Tenth International Towing Tank Conference*, Teddington, U.K., pp. 114-123.

Lindroos, H. and Björkestam, H. (1986) "Hydrodynamic loads developed during ice-clogging of a propeller nozzle and means to prevent the clogging", *Proceedings of Polartech'86*. The International Offshore and Navigation Conference and Exhibition. Helsinki, Finland, pp. 1061-1092

Luznik, L., Walker, D., Bose, N. and Jones, S.J., "Effects of ice blockage size and proximity on propeller performance during non-contact propeller-ice interaction", *Proceedings of the 14th International Conference on Offshore Mechanics and Arctic Engineering*, June 18-22, 1995, Copenhagen.

Michailidis, M. and Murdey, D.C. (1981) "Performance of CCGS Franklin in Lake Melvile, 1980", *Proceedings of the Spring Meeting/Star Symposium, The Society of Naval Architects and Marine Engineers*, Ottawa, Ontario

Mironer, A., (1979), *Engineering Fluid Mechanics*. McGraw Hill Book Company, New York, pp 227 - 227.

Morino, L., Chen, L-T and Suciu, E.O., (1975), "Steady and oscillatory subsonic and supersonic aerodynamics around complex configurations", *AIAA Journal*, Vol. 13, No. 3, 368-374.

Murdey, D.C., (1980), "Resistance and propulsion experiments with model 327-1 and propellers 66L and 66R" National Research Council Canada, Division of Mechanical Engineering, Report LTR-SH-269.

Newbury, S., Browne, R. and Jones, S.J., (1994) "Experimental determination of hydrodynamic non-contact loads during propeller ice interaction", *Proceedings of the 5th International Offshore and Polar Engineering Conference, ISOPE '94*, Osaka, Japan, Vol II, pp 596-601

Newbury, S., Shih, L.Y., Browne, R.P., Revill, C.R., Kenny, S. and Zheng, Y. (1993). *Proceedings of the 2nd Canadian Marine Dynamics Conference*. Vancouver, British Columbia, Canada

Oosterveld, M.W.C., and Oossanen, P. van, (1975), "Further Computer-Analysed Data of the Wageningen B-Screw Series", *International Shipbuilding Progress*, Vol 22, p.251.

Peterson, F.B., Danel, F., Keller, A. and LeCoffre, Y (1975), "Comparative Measurement of Bubble and Particulate Spectra by Three Optical Methods", Report of the Cavitation Committee - *14th International Towing Tank Conference*, pp. 27-37.

Sánchez-Caja, A., Pylkkänen, J.V. and Koskinen, P.S., (1995), "Hydrodynamic Force On Propeller Blades Caused by Transient Loads in Icebreaking Mode of Operation", VTT Technical Report VTT VAL C81.

Shih, L.Y. and Zheng, Y., (1992), "Constricted hydrodynamic flow due to proximate ice blockage over a blade profile in two dimensions", *Proceedings of the 2nd International Symposium on Propellers and Cavitation*, Hangzhou, China, pp. 74-79.

Shih, L.Y. and Zheng, Y. (1993) "Application of 3-D BEM to time dependent potential flow over a propeller with ice blockage at proximity condition" Institute for Marine Dynamics, National Research Council of Canada. St. John's, Nfld. 25 pp.

Tamura K. and Yamaguchi, H. (1995), "An attempt to draw a scenario of ice propeller interaction", *Proceedings of the INSROP Symposium '95*, Tokyo, Japan, October 1-6, pp. I-17-(1-6).

Timco, G.W., (1986), "EG/AD/S: A new type of model ice for refrigerated towing tanks", *Cold Regions Science and Technology*, Vol 12, pp. 175-195.

van Gent, W. and Oosterveld, M.W.C. (1983), "Ducted propeller systems and energy saving", *Proceedings of the International Symposium on Ship Hydrodynamics and Energy Savings*, El Pardo, Vol VI, pp. 3-(1-24).

Veitch, B., (1995), "Predictions of Ice Contact Forces on a Marine Screw Propeller During the Propeller-Ice Cutting Process",*Doctoral Thesis. Acta Polytechnica Scandinavica Mechanical Engineering Series No. 118*, Helsinki University of Technology, 140 pp.

Veitch, B. and Laukia, K., (1993) "The propeller-ice impact process", *Proceedings of POAC '93*, Hamburg, Germany, pp. 378-389.

Walker, D., Bose, N., Yamaguchi, H. and Jones, S.J., (1996) "Effects of cavitation during propeller ice interaction", *Journal of Marine Science and Technology*, The Society of Naval Architects of Japan, (in print).

Walker, D., Bose, N., Yamaguchi, H. and Jones, S.J., (1995a) "Influence of cavitation on the performance of Canadian R-Class icebreaker propellers in blocked flows". *Proceedings of the 5th International Offshore and Polar Engineering Conference, ISOPE '95*. The Hague, June 11-16, Vol. 2, pp. 434-439.

Walker, D., Bose, N., Yamaguchi, H. and Jones, S.J.. (1995b) "Effects of cavitation during propeller ice interaction", *Proceedings of the 3rd Canadian Marine Hydrodynamics and Structures Conference*. Halifax. Nova Scotia. August 14-16. pp. 23-28.

Walker, D., Bose, N. and Yamaguchi, H., (1994). "Hydrodynamic performance and cavitation of a propeller in a simulated ice-blocked flow" *Transactions of the ASME. Journal of Offshore Mechanics and Arctic Engineering*, Vol 116, pp 185-189

Walker, D., Bose, N., and Casey, S., (1994) 'Ducted propeller cavitation in blocked flow', *Proceedings of The Second International Conference on Cavitation*, Tokyo University, Tokyo, Japan, April 3-5, pp. 421-426

Walker, D. and Bose, N., (1994) "Hydrodynamic loads and dynamic effects of cavitation on ice class propellers in simulated ice blocked flow", *Proceedings of the Propellers/Shafting '94 Symposium*, The Society of Naval Architects and Marine Engineers, Virginia Beach, Virginia, September 20-21, 19p.

Walker, D., Bose, N. and Yamaguchi, H., (1993). "Cavitation and hydrodynamic performance of a propeller in a simulated ice-blocked flow" *Proceedings of the 12th International Conference on Offshore Mechanics and Arctic Engineering*, Glasgow. Scotland, Vol.1, pp. 378-389.

Williams, F.M., Spencer, D., Mathews, S.T. and Bayly, I. (1992) "Full scale trials in level ice with Canadian R-Class Icebreaker". *Transactions of the Society of Naval Architects and Marine Engineers*, V100, 18 pp.

Yamaguchi, H. (1993) "Investigation on propeller performance in uniform and blocked flow for the open propellers used in IMD ice tank and cavitation tunnel experiments-Investigation from propeller lifting surface calculations", Institute for Marine Dynamics Technical Report LM-1993-11.

Yamaguchi, H. (1988) "Hydrodynamic characteristics of a two dimensional foil or cascade in steady incompressible uniform flow with boundary layer effects taken into account". internal software.